

Electronic Theses and Dissertations, 2004-2019

2015

Development of human and rodent based in vitro systems toward better translation of bench to bedside in vivo results

Bonnie Berry
University of Central Florida

 Part of the [Biology Commons](#)

Find similar works at: <https://stars.library.ucf.edu/etd>

University of Central Florida Libraries <http://library.ucf.edu>

This Doctoral Dissertation (Open Access) is brought to you for free and open access by STARS. It has been accepted for inclusion in Electronic Theses and Dissertations, 2004-2019 by an authorized administrator of STARS. For more information, please contact STARS@ucf.edu.

STARS Citation

Berry, Bonnie, "Development of human and rodent based in vitro systems toward better translation of bench to bedside in vivo results" (2015). *Electronic Theses and Dissertations, 2004-2019*. 5155.
<https://stars.library.ucf.edu/etd/5155>

DEVELOPMENT OF HUMAN AND RODENT BASED *IN VITRO* SYSTEMS TOWARD
BETTER TRANSLATION OF BENCH TO BEDSIDE *IN VIVO* RESULTS

by

BONNIE JEANNE BERRY
B.S. University of Central Florida, 2005
M.S. University of Central Florida, 2008

A dissertation submitted in partial fulfillment of the requirements
for the degree of Doctor of Philosophy
in the Department of Biomedical Sciences
in the College of Medicine
at the University of Central Florida
Orlando, Florida

Fall Term
2015

Major Professor: James J. Hickman

© 2015 Bonnie Jeanne Berry

ABSTRACT

Prospective medicinal compounds progress through multiple testing phases before becoming licensed drugs. Testing of novel compounds includes a preclinical phase where the potential therapeutic is tested *in vitro* and/or in animal models *in vivo* to predict its potential efficacy and/or toxicity in humans. The failure of preclinical models to accurately predict human drug responses can lead to potentially dangerous compounds being administered to humans, or potentially beneficial compounds being kept in development abeyance. Moreover, inappropriate choice in model organism for studying disease states may result in pushing forward inappropriate drug targets and/or compounds and wasting valuable time and resources in producing much-needed medications. In this dissertation, models for basic science research and drug testing are investigated with the intention of improving current preclinical models in order to drive drugs to market faster and more efficiently. We found that embryonic rat hippocampal neurons, commonly used to study neurodegenerative disease mechanisms *in vitro*, take 3-4 weeks to achieve similar, critical ion-channel expression profiles as seen in adult rat hippocampal cultures. We also characterized a newly-available commercial cell line of human induced pluripotent stem cell-derived neurons for their applicability in long-term studies, and used them to develop a more pathologically relevant model of early Alzheimer's Disease *in vitro*. Finally, we attempted to create an engineered, layered neural network of human neurons to study drug responses and synaptic mechanisms. Utilization of the results and methods described herein will help push forward the

development of better model systems for translation of laboratory research to successful clinical human drug trials.

This work is dedicated to mom and dad. For all your love, sacrifice, and support.

TABLE OF CONTENTS

| | |
|--|-----|
| LIST OF FIGURES..... | ix |
| LIST OF TABLES..... | xix |
| CHAPTER 1 – GENERAL INTRODUCTION..... | 1 |
| CHAPTER 2 – THE COMPARISON OF NMDA AND AMPA CHANNEL EXPRESSION AND FUNCTION BETWEEN EMBRYONIC AND ADULT NEURONS UTILIZING MICROELECTRODE ARRAY SYSTEMS..... | 8 |
| Introduction..... | 8 |
| Materials and Methods | 11 |
| Embryonic rat hippocampal dissociated cell culture | 11 |
| Adult rat hippocampal dissociated cell culture..... | 11 |
| Immunocytochemistry and Laser Scanning Confocal Microscopy | 13 |
| MEA Plating and Culture Maintenance | 14 |
| Experimental Procedure..... | 15 |
| Evaluation and statistics..... | 15 |
| Results | 17 |
| Spontaneous activity of Adult and Embryonic Neurons | 17 |
| NMDA and AMPA channel activity and expression in adult and embryonic neurons | 18 |
| Discussion | 20 |
| CHAPTER 3 – MORPHOLOGICAL AND FUNCTIONAL CHARACTERIZATION OF HUMAN INDUCED PLURIPOTENT STEM CELL-DERIVED NEURONS (ICELL NEURONS) IN DEFINED CULTURE SYSTEMS..... | 33 |
| Introduction..... | 33 |
| Materials and Methods | 37 |
| Surface modification | 37 |
| Cell culture and maintenance..... | 37 |
| Cell viability and neuritic outgrowth analysis..... | 38 |
| Immunocytochemistry..... | 38 |
| Patch-clamp electrophysiology | 40 |
| Statistical analysis | 41 |
| Results | 42 |

| | |
|--|-----------|
| Cell purity and neuritic outgrowth analysis | 42 |
| Cell survival and viability over 28 day culture period | 43 |
| Characterization of neuronal phenotype | 44 |
| Electrophysiology | 45 |
| Discussion | 49 |
| CHAPTER 4 – PHYSIOLOGICAL Aβ CONCENTRATIONS PRODUCE A MORE BIOMEMETIC REPRESENTATION OF ALZHEIMER’S DISEASE PHENOTYPE IN CULTURED HUMAN NEURONS..... | 62 |
| Introduction..... | 62 |
| Materials and Methods | 65 |
| Cell culture..... | 65 |
| Surface modification | 65 |
| Amyloid- β oligomer preparation | 66 |
| Oligomer characterization | 66 |
| MTT assay | 67 |
| Immunocytochemistry..... | 67 |
| Patch-clamp electrophysiology | 68 |
| Statistical analysis | 69 |
| Results | 71 |
| Cell morphology and viability..... | 71 |
| Electrophysiological function | 71 |
| Immunocytochemical analysis of tau expression levels..... | 73 |
| Discussion | 74 |
| CHAPTER 5 – FEED-FORWARD NETWORK PATTERNING OF HUMAN IPSC-DERIVED NEURONS; TOWARDS THE DEVELOPMENT OF A LAYERED MODEL OF THE HUMAN CORTEX..... | 86 |
| Introduction..... | 86 |
| Materials and Methods | 90 |
| Human iPSC culture | 90 |
| Astrocyte cultures..... | 90 |
| Surface preparation | 91 |
| Extracellular MEA recordings | 92 |

| | |
|-------------------------------------|-----|
| PDMS Microtunnels | 93 |
| Results | 94 |
| Discussion | 98 |
| CHAPTER 6 – GENERAL DISCUSSION..... | 104 |
| REFERENCES | 111 |

LIST OF FIGURES

Figure 2-1. Adult and embryonic MEA culture and life cycle. Adult neurons: Mature terminally differentiated adult neurons were extracted from the hippocampus of adult rats and plated onto DETA cover slips. After 4 days the neurons were passaged from these cover slip(s) onto MEAs that had been coated with PDL / laminin (for cell adhesion). Embryonic neurons: Neurons from the hippocampus of embryonic day 18 rat fetuses were extracted and plated directly on MEAs that had been coated with PDL / laminin. Electrical recordings of spontaneous neuronal activity were performed for up to 3 months. In addition, ion channel receptor antagonists were introduced and their effects were measured against baseline electrical activity. 64-channel axion biosystems MEAs were used. 24

Figure 2-2. Phase contrast images of cultures on MEAs after 3 DIV and 30 DIV. Neurons were applied between 500 to 1000 cells / mm². Cells attached and regenerated on the PDL / laminin surface covering the MEAs, seen in the dense collection of cells covering the electrodes. Each 64-Channel MEA is arranged in an 8 x 8 array of electrode 30 μm in diameter and spaced 200 μm apart. The MEA was sampled 25,000 times per second, at 16 bits of depth. Scale bar = 50 μm. 25

Figure 2-3. MEA data processing: The spontaneous activity of embryonic and adult neurons was recorded for 3 minutes each day over the study period. Each 3 minute dataset was processed in a 3-step method. This method allowed inactive or noisy channels to be excluded. After processing, the following parameters

were extrapolated: “active channels” – a number from 0 to 64. Channels with less than 7.5 APs per minute were treated as inactive. “AP Frequency” – number of total measured APs divided by recording time. The mean and stdev of that number is independent from active channels. “AP Activity” – is 1 divided by the time between two subsequent APs, or frequency 1/s. “Burst” – where more than 1 AP occurs within 1 ms. “average burst frequency” – 1 divided by the time-difference between two subsequent bursts. “In-burst frequency” – amount of APs within a burst divided by the duration of that burst. “Non-burst frequency” – like the activity, but considers on APs that are not associated with bursts. “Burst duration” – time-interval from the first AP in a burst to the last AP in a burst..... 26

Figure 2-4. Basic firing patterns of embryonic and adult hippocampal neurons on MEAs over time. The spontaneous activity of embryonic and adult neurons was recorded for 3 minutes each day over the study period. The activity data from each day was processed to filter out inactive channels. (A) Number of active channels. (B) Frequency of APs. (C) Average activity, or 1 divided by the time between two subsequent APs (frequency 1/s). (D) Burst frequency. (E) In-burst frequency. MEA number to plating date: Embryonic: MEA 23 – 3/14, MEA 29 – 3/14, MEA 30 – 3/14, MEA 31 – 3/14, MEA 21 – 2/14, MEA 26 – 2/14, MEA 27 – 2/14. Adult: MEA 22 – 1/31, MEA 28 – 2/17, MEA 25 – 2/17, MEA 24 – 2/17, MEA 40 – 3/21, MEA 33 – 3/21, MEA 34 – 3/21, MEA 36 – 3/21, MEA 37 – 3/21, MEA 38 – 3/21. Gaps in graphs indicate activity was not recorded on that day. 28

Figure 2-5. Comparison of the impact on adult or embryonic spontaneous activity from addition of synaptic antagonists. Active channels (A,B) or AP frequencies (C,D)

were evaluated in adult or embryonic hippocampal neuron MEA systems on either 14 or 30-60 DIV in the presence of D-AP5 (25 μ M), CNQX (25 μ M), or Bicuculline (50 μ M) in culture medium. Adult neurons showed significantly decreased active channels and AP frequency due to D-AP5 in both early 14 DIV cultures as well as older 30-60 DIV cultures. This drop in activity was significantly different from embryonic 14 DIV, where fewer active channels were lost and activity increased in the remaining channels. The AMPA-channel antagonist CNQX also caused a decrease in spontaneous activity. The drop in activity between adult and embryonic cultures was, however, only reflected in the loss of more active channels in the adult system. AP frequency declines were consistent between the two culture systems. Bicuculline had limited effect on spontaneous activity in both embryonic and adult neurons..... 29

Figure 2-6. Expression of presynaptic proteins and postsynaptic channel subunits in embryonic and adult neurons *in vitro*: NR2A, NR2B, or GluR2/3 (red); synaptophysin (green); neurofilament-M (far-red); and DAPI (blue) expression after 2, 14, and 36 DIV. NMDAR2A (A) and NMDAR2B (B) were not expressed in embryonic neurons on 2 DIV and were not strongly expressed on 14 DIV (when compared to channel expression in adult neurons). After 36 DIV, the channels were expressed by the embryonic neurons at similar levels to the adult neurons. The AMPA receptor subunits GluR2/3 (C) were expressed by embryonic neurons by 14 DIV. These postsynaptic channel subunits were all found in adult neurons from 2 – 36 DIV. Synaptophysin and Neurofilament-M expression grew stronger

as both the embryonic and adult neurons recovered and regenerated *in vitro*.

Scale bars 17 μm 32

Figure 3-1. Human iPSC-derived cells thrive on both DETA and biopolymer surfaces.

(A) Cells were cultured in MM on laminin, MM on DETA, HSL1 on DETA and HSL1 on laminin through a 28-day period (B) Immunological analysis for neural markers MAP2 (green) and GFAP (red) and the nuclear marker DAPI (blue). Images are representative of 7 DIV (top) and 28 DIV (bottom) of both panels. (C) Cells which stained positive for MAP2 were quantified at 7 and 28 DIV. Error bars represent SEM. Scale bar = 20 μm 55

Figure 3-2. Neurite analysis of hiPSC-derived neurons. (A) The longest neurite length

was measured at 1, 3, and 7 DIV across all culture combinations of MM and HSL1 media and DETA and laminin surfaces. (B) Representative phase images of cells grown on laminin (left) and DETA (right) in MM at 1 DIV. Significant differences were observed between surface types at 1 DIV and between both medium and surface types at 3 and 7 DIV, * $p < 0.001$, ** $p < 0.001$, *** $p < 0.001$. Error bars represent SEM. Scale = 30 μm 56

Figure 3-3.. Viability of hiPSC-derived neurons over 28 DIV using different culture

parameters. Cells were counted per mm^2 and normalized to day 1 counts to account for culture variability and ease comparisons between conditions. No discernable differences in survival trends were observed across all conditions examined over the first 10 days in culture. After 28 DIV, HSL1 on laminin promoted a significantly higher level of survival (* $p < 0.001$), whereas cells

cultured in MM on DETA had significantly fewer viable cells (**p < 0.001). Error bars represent SEM..... 56

Figure 3-4. Human iPSC-derived neurons express lower layer cortical pyramidal phenotypic markers. Cells were stained for CTIP2 (green), SATB2 (red), and DAPI (blue) at 7 DIV in maintenance medium (A, B) and in HSL1 (C,D) on laminin (A,C) and on DETA (B,D) to assess potential layer identity. No cells stained positive for SATB2 in any condition. (E) Intact nuclei stained positive for DAPI but were not CTIP2 positive were quantified to estimate a percentage of CTIP2-positive neurons. Error bars represent SEM. Scale bar = 20 μ m. 57

Figure 3-5. Representative electrophysiological recordings of hiPSC-derived neurons. Patch-clamp recordings were taken at 7 (A) and 28 (B) DIV. (Top) Voltage-clamp recording of inward sodium and outward potassium currents (-70 mV holding potential, 10 mV steps). (Middle) Neurons were not likely to fire repeatedly in response to depolarizing current injections at a -70 mV holding potential at 7 DIV versus 28 DIV. (Bottom) A single AP was generated using a 3 ms depolarizing current pulse of 1-2 nA. D. (Inset) Phase contrast image of patched neuron. Scale = 20 μ m. 58

Figure 3-6. Patch-clamp data collected from hiPSC-derived neurons grown in the four different culture conditions. The resting membrane potential (A), AP amplitude (B), peak inward current (C), and peak outward current (D) are represented at 28 DIV. (E) The proportion of cells which repetitively fired APs in response to depolarizing current injections at a -70 mV across all time points evaluated. HSL1/laminin cultures had significantly higher resting membrane potentials (A,

***p = 0.02) and peak inward currents (C, **p ≤ 0.005). Peak inward (C) and outward currents (D) were significantly lower when grown in MM on DETA (*p ≤ 0.001 and *p ≤ 0.001, respectively). Rates of repetitive fire showed a generally increasing trend over time across all conditions (*p ≤ 0.005) with significant increases across conditions from 7 to 14 DIV and again from 21 to 28 DIV (*p ≤ 0.001), indicating the improved functional performance of cells over this culture period. Error bars represent SEM..... 59

Figure 3-7. Full width half max and rise time comparison of 7 and 28 DIV cultures in various conditions. Values of FWHM (A) and AP rise time (B) were calculated for each condition at both 7 and 28 DIV. Cells cultured in HSL1/DETA showed a significant reduction in AP duration corresponding to a decrease in FWHM from 7 to 28 DIV. This reduction in FWHM resulted in values similar to HSL1/laminin, the condition which exhibited the shortest FWHM time. All cultures grown in MM, regardless of surface, were unable to reach AP duration times similar to those grown in HSL1 at 28 DIV. AP rise times were unaffected by culture medium or surface conditions. *p < 0.05. Error bars represent SEM..... 60

Supplemental Figure 3-8. Immunostaining of human and embryonic rat neurons. Only two human iPSC-derived neurons out of all conditions examined stained positive for GFAP (green) (A). No human iPSC-derived neurons positively stained for the marker SATB2, whereas positive control embryonic rat hippocampal cultures stained positive for both SATB2 (red) and CTIP2 (green) (B). Scale bar = 20 μM. 61

Supplemental Figure 3-9. Patch-clamp data collected from hiPSC-derived neurons grown in various conditions. The resting membrane potential (A), peak AP amplitude (B), peak inward current (C), and peak outward current (D) are represented across all time points evaluated. Error bars represent SEM. 61

Figure 4-1. Treatment of hiPSC derived neurons with physiological doses of A β does not appear to effect gross cell morphology or viability. A) Representative phase contrast images of hiPSC-derived neurons comparing untreated, chronic, and acute A β treated cells at 30 DIV. Scale = 50 μ m. B) Viability of hiPSC-derived neurons determined by MTT assay at 30 DIV following treatment with A β . Acute 5 μ M treatment significantly reduced cell viability ($P < 0.05$) whereas acute and chronic 10 nM treatments had no significant effect on cell survival. 79

Figure 4-2. Representative electrophysiological recordings of untreated and A β -treated hiPSC-derived neurons. Patch-clamp recordings were taken between 28-30 DIV in control (column A), 10 nM chronic (column B), and 5 μ M acute (column C). Recordings from cells acutely treated with 10 nM A β were also taken but are represented by control data here as there were no significant differences between the two conditions ($p > 0.05$). (Top row) Voltage-clamp recording of inward sodium and outward potassium currents (-70 mV holding potential, 10 mV steps). (Second row) Neurons fired repeatedly in response to depolarizing current injections at a -70 mV holding potential. (Third row) A single AP was generated using a 3 ms depolarizing current pulse of 1-2 nA. (Bottom row) Gap free recordings were performed for up to 5 m to measure spontaneous activity of patched cells. (Inset) Phase contrast image of patched neuron. Scale = 20 μ M. 80

Figure 4-3. Changes in electrophysiological characteristics of hiPSC-derived neurons treated with A β . The resting membrane potential (A), peak inward current (B), peak outward current (C), maximum APs fired in response to depolarizing current injections at -70 mV (D), and peak action AP (E) are represented at 28 DIV. Whereas the resting membrane potential, membrane resistance, peak outward current, and AP amplitude was maintained across all conditions, inward sodium currents and maximum APs fired were significantly reduced in acute, 5 μ M treated cultures ($p < 0.05$). Treatment with 5 μ M of A β resulted in an even more significant drop in spontaneous neural firing activity ($p < 0.01$). Time to peak AP and AP duration, and represented by rise time (F) and FWHM (G) respectively was significantly increased in 5 μ M treatment of A β ($p < 0.05$). 10 nM A β acute treatment did not have a significant effect on spontaneous APs fired during gap-free recordings (H) but chronic 10 nM A β resulted in a significant drop in the spontaneous activity of these cultures ($p < 0.05$). Error bars represent SEM. 82

Figure 4-4. Tau protein is upregulated in hiPSC-derived neurons treated with higher-than-physiologic concentrations of A β . (A) Cells were fixed at culture endpoints (28-30 DIV) and stained for beta-III tubulin (red), tau (green), and DAPI (blue). Scale bar = 20 μ m. (B) Image analysis of tau protein intensity was analyzed relative to control tau positive staining while accounting for differences in cell viability ($p = 0.057$). 82

Supplemental Figure 4-5. XPS analysis of laminin on glass vs. laminin on DETA. XPS analysis of laminin on DETA-modified glass and unmodified glass. The carbonyl

peak, which is indicative of protein for these samples, is smaller on glass than on DETA-modified glass relative to the underlying substrate (Si)..... 84

Supplemental Figure 4-6. Amyloid beta oligomerization gel electrophoresis and coomassie blue stain. Pure oligomerized samples of A β were run on 10-20% tris-tricine gels and stained to visualize protein bands. Only low molecular weight bands were present. 85

Figure 5-1. Schematic of feed-forward chemical pattern architecture for MEAs. Purple areas correspond to areas with cell-attracting chemical treatment. Small blue dotted background corresponds to chemically treated areas which are not favorable for cell growth. Grey circles indicate positions of microelectrodes (not to scale and not part of pattern). Reservoirs for cellular attachment are 100 μ m tall and span the length of the entire microelectrode area. Axonal tracts (thin connecting lines, 2.5 μ m wide) direct axonal growth in the indicated direction and extend to within 20 μ m of the connecting reservoir where there are breaks to prevent backward axonal growth. 101

Figure 5-2. Time-lapse phase-contrast images of hiPSCs grown on DETA/13F feed-forward patterns on glass coverslips. Human iPSCs were plated at 1000 cells/mm² onto patterned glass coverslips and monitored over 4 DIV for pattern adherence. Scale = 50 μ m..... 101

Figure 5-3. Successful patterning of hiPSCs arranged over a MEA at 7 DIV. Cells were plated onto DETA/13F feed-forward patterned MEAs where they exhibited accurate pattern conformity. Scale = 200 μ m. 102

Figure 5-4. PDMS microtunnels on MEAs. Cells were plated on either side of μm by 3 μm microtunnels that bisected the field of electrodes and created two separate culture populations. PDMS barriers (not shown) were also placed on one side of the microtunnels on for some cultures to allow one cell population to extend axons to synapse on the other side for unidirectional flow of APs from one population to the other. Scale = 100 μm 103

LIST OF TABLES

| | |
|--|----|
| Table 3-1. Composition of HSL1 medium..... | 60 |
| Table 4-1. HSL1 medium, detailed below, was designed to promote the long-term survival and maturation of hippocampal neurons <i>in vitro</i> | 83 |

CHAPTER 1 – GENERAL INTRODUCTION

Medical advancements in developed countries, coupled with a greater public awareness of health issues (smoking, drinking, diet, exercise etc.) means people are living longer than they were 40 years ago [1]. US residents born in 1970 were expected to live 70.8 years on average. By 2008, the average life expectancy of an American resident rose to 78 years. With this ageing population, comes a significant increase in the incidence rate of neurological disorders, since most neurodegenerative conditions are age related. In 2000, there were 4.5 million US residents with Alzheimer's Disease (AD). By the year 2050, this number is expected to almost triple to 13.2 million [2]. For such a severe problem facing aging populations there is a serious lack of effective treatments or therapies. As of 2015, there are only 5 FDA-approved drugs for treatment of AD. These 5 drugs treat the symptoms of AD but their capacity for preventing further damage is debated [3]. Currently, the production of better drugs for AD prevention and symptom alleviation is prohibited by the poor availability of suitable models of the complex human central nervous system (CNS) for both drug screening and disease modeling purposes.

Drug development, from identification of new chemical entities (NCEs) to commercialization of an FDA licensed treatment, is a long and costly process; current estimates suggest the complete procedure can cost up to \$1.2 billion per drug over a 10 to 12 year period [4-6]. Drug attrition from development protocols (due to safety concerns, lack of significant observed benefit, etc.) drives this cost up. The market analysis firm Frost & Sullivan has estimated the price of failure at \$50-70 million per

drug, with about 90% of candidate compounds failing at pre-clinical development stages [7]. Unfortunately, a significant number of compounds that progress to clinical trials also fail. Only 1 in 5 compounds entering clinical trials ever typically reaches the market [4, 5, 8]. Although some of this failure can be attributed to poor clinical trial design, patient drop out etc., safety pharmacology concerns remain the major cause of drug attrition during clinical development and validation of NCEs (responsible for about 30% of all drug attritions) [9]. The fact that so many potentially dangerous compounds are not selected out during preclinical development highlights an inability for current preclinical techniques to adequately predict compound efficacy and/or toxicity in humans.

The gold standard for preclinical evaluations is a combination of *in vitro* analysis and animal testing. Small animal (mouse and rat) studies are incredibly useful as predictors of human development and tissue responses. Rodent models have significant advantages for their use in that they are genetically similar to humans, have a relatively short life span for rapid assessment, and can be inbred to be more genetically consistent from one sample to the next. However, such models have been repeatedly shown to be poor predictors of human responses to drugs [10].

Murine and other animal models are poor predictors of human drug responses for many reasons. For example, gene expression responses to multiple inflammatory pathways are similar in humans, whereas in mice, different pathways are triggered during inflammation events [11]. In the referenced study, results from non-correlative tests performed in mouse models were used to screen pre-clinical drug candidates for their ability to block inflammatory responses in humans. Of the nearly 150 clinical trials

testing compounds that were prescreened in this manner, not one succeeded in clinical trial.

Moreover, though animal models have their place in basic biological research and predictive drug screening, these animals can be used at inappropriate, underdeveloped stages which fail to reflect advanced development. In the case of studying neurodegenerative disease *in vitro*, early-stage embryonic rat tissue is often used to study disease mechanisms which implicate ion channels not yet maturely expressed (discussed in further detail in Chapter 2). Results obtained from such studies may generate misleading data and exacerbate the issue in translating results from animal models to successful clinical results in humans.

Furthermore, for rare conditions, such as Huntington's Disease (HD), the animal models which exist do not replicate the symptoms of the disease in just one organism or species [12]. Multiple models must be utilized in order to begin to elucidate potential therapeutic targets for HD treatment. Both small rodent models and large animal models, such as pig, sheep, and monkeys, have been developed to begin to mimic the disease state.

Other animal models do not account for human variability. Amyotrophic lateral sclerosis (ALS) is hugely heterogeneous where most cases are sporadic and only about 10% are familial. Superoxide dismutase 1 (SOD1) mutations found in familial ALS patients only accounts for a small percentage of patient mutations, and has been found to have over 150 pathogenic variations [13, 14]. As such, standard SOD1 mouse models of ALS fail

to recapitulate the complexity and genetic variability of this disease, severely limiting the translational relevance of data obtained using this model [15, 16].

As an alternative to *in vivo* testing, the *in vitro* analysis of single human cells and monolayers removes issues with non-correlating data between species [17]. Furthermore, such assays are useful for the study of cellular behavior and phenotype without the complication of tissue-tissue interplay and whole body metabolic dynamics. Using standard culture systems, the metabolic and functional development, as well as drug responses, of individual cells and tissues can be analyzed in isolation. The development of human induced pluripotent stem cell (hiPSC) technologies in recent years has served to increase the availability of human cell types for such analyses [18]. Human iPSCs can be derived from multiple sources including skin fibroblasts [19], extra-embryonic tissues from umbilical cord and placenta [20], blood cells [21], and urine-derived cells [22, 23]. A variety of different methods have also been developed to improve the efficiency of iPSC generation, including viral and lentiviral integration, non-integrating viral vectors, and protein- and small molecule-based reprogramming [24]. These cells have also greatly increased the potential for *in vitro* preclinical screens to predict human responses to drugs and to accurately model genetic variability between patients [25, 26]. Since hiPSCs cells can be isolated and transformed from a specific patient into a cell type of interest, it has been suggested that patient-specific modeling could aid physicians in recommending effective, non-toxic drug treatment to patients in the near future.

However, despite the potential of hiPSC technologies to improve preclinical screening methods, issues with maturity, a lack of structural organization (particularly for well-ordered tissues such as CNS), and an inability to effectively model interactions between supporting cell types has so far reduced the utility of these human cell cultures for such applications [27, 28]. Typically, *in vitro* cell-based models function with only a fraction of *in vivo* performance levels, which reduces the ability for such assays to accurately predict functional responses. For example, skeletal muscle and cardiac models usually exhibit reduced contractile functionality compared with native tissues [29-31]. Similarly, neuronal models often display altered spike burst activity [32]. Finally, as is the case for certain animal models, observed compound effects *in vitro* have not correlated closely with *in vivo* outcomes [33].

There is a clear need for a better preclinical model. Body-on-a-chip technologies hold potential for improving preclinical assessment of NCE efficacy, as well as absorption, distribution, metabolism, and excretion (ADME) in human systems. Interconnected organ-on-a-chip microdevices, which mimic tissue structure and function, enable the detailed assessment of compound, complex effects, and facilitate study of tissue-tissue metabolic cross-talk in a controlled and fully-defined system. The successful development of these systems is predicated on the development of suitable cell culture environments. Such environments must be capable of maintaining stable and phenotypically mature cell populations in configurations that enable physiologically-relevant assessment of functional changes in response to chemically, physically, or pathologically induced stress.

Over the past decade, substantial progress has been made in the development of bioengineered culture platforms that offer more accurate representations of a variety of human tissues. Such models include representations of human heart, lung, skeletal muscle, liver, gastrointestinal tract, kidney, and CNS. However, none of the published platforms have so far have been adopted as standardized models for the tissue they are emulating. This is due to a number of factors including cost of fabrication, reliability, suitability for commercial requirements, and complexity. The major factor limiting market penetration of these models, however, is that very few have demonstrated an ability to develop structural, metabolic, and functional phenotypes that adequately recapitulate that of the native tissue. Without this ability, such models are likely to be incapable of providing accurate data in terms of predicting drug effects in humans, over and above what is possible with conventional cell culture methods.

The widespread adoption of more advanced cell culture models is therefore predicated on a capacity to demonstrate engineered tissue development that closely mimics what is observed *in vivo* in a cost-effective and reliable way. Such systems not only hold the potential to revolutionize the drug development process, but also hold the key to improving our ability to study tissue development, maintenance, and breakdown in disease.

Specifically, the pathophysiological mechanisms of many neurodegenerative disorders are not fully understood, which makes their effective treatment difficult. In order to better understand the causes of neurodegenerative disease, and so identify suitable targets for therapeutic treatment, improved models of early disease stages are required. To this

end, these dissertation studies were developed to attempt to address current limitations in the *in vitro* modeling of neural tissue in both healthy and diseased states. In order to focus the project, the following four specific aims were addressed:

- 1) Examine the differences in ion channel expression and network connectivity in adult vs. embryonic rat hippocampal cells by measuring network connectivity on MEAs in response to ion channel drug challenges as a means to assess model maturity.
- 2) Characterize the functional competence of human stem-cell derived pyramidal “hippocampal-like” neurons and characterize their development and maturation in different culture conditions *in vitro*.
- 3) Determine effects of amyloid beta on the electrical properties of human stem-cell derived pyramidal “hippocampal-like” neurons (from Aim 2) *in vitro*.
- 4) Build a layered brain model using human stem-cell derived pyramidal “hippocampal-like” neurons with specific focus on the establishment of chemical or electrical stimulation parameters to induce and maintain Long-Term Potentiation (LTP) on MEAs.

CHAPTER 2 – THE COMPARISON OF NMDA AND AMPA CHANNEL EXPRESSION AND FUNCTION BETWEEN EMBRYONIC AND ADULT NEURONS UTILIZING MICROELECTRODE ARRAY SYSTEMS

Note: The contents of this chapter, with minor changes, was also submitted in partial fulfillment of Darin Edwards's dissertation in Summer 2011.

Introduction

A common limitation of neuronal MEA systems as well as neuroscience research in general has been the reliance upon neurons derived from embryonic tissue [34-36]. While neurons derived from embryonic sources are fully differentiated, they are developmentally immature, with transcriptional profiling indicating two-thirds of genes are only expressed postnatally and >95% of the expressed genes showing highly significant changes during postnatal development [37]. When evaluating the machinery responsible for synaptic transmission, AMPA channel expression is limited at birth, only increasing postnatally [38]. The gene expression for the NMDA channel subunits NR2A and NR2B was not detected until near birth at E21-22, with expression not peaking until P20 [39]. *In vitro*, NR2A/B channels are detected at only very low levels until after 2 weeks in embryonically derived neurons [40]. Gene expression for the axonal sodium transporter subunit 1 begins around P15, then increasing until P30 [41, 42]. *In vitro*, expression patterns for all genes, specifically axonal and synaptic channels responsible for signal transmission, is similar to that seen *in vivo*, with gene expression showing significant changes over the course of weeks [39-41, 43-45]. While embryonic rat tissue

is relatively easily obtainable and easy to culture and maintain, the usefulness of these developmentally immature neurons for studies of neuronal electrical activity and synaptic transmission is restricted by the limited expression or lack of expression of certain channels responsible for synaptic transmission in the adult brain. In addition, using these developmentally immature neurons in studies of neurodegenerative diseases or drug discovery can yield results that are difficult to correlate with the function or action of mature neurons in adult brain tissue. In fact, because of this lack of NMDA expression the utilization of embryonic or neonatal neurons yield promising *in vitro* epilepsy models [46, 47].

We have developed a long-term hybrid *in vitro* system utilizing mature, terminally differentiated neurons derived from adult rat hippocampal tissue in dissociated culture [48, 49]. Whereas most electrophysiological studies rely upon patch-clamp electrophysiology [50, 51], a method which is labor-intensive, requires specialized training, and cannot be used to monitor neuronal function over more than a few hours at a time, we utilized microelectrode arrays (MEAs). MEAs are innovative tools used to perform electrophysiological experiments for the *in vitro* study of both neuronal activity and connectivity in populations of neurons [35, 52] for extended time periods (days – months) [53-56].

We concurrently measured spontaneous network activity from both embryonic and adult neurons on MEAs in the presence/absence of synaptic transmission antagonists against NMDA and AMPA channels. In addition, we evaluated both embryonic and adult neurons for NMDA channel subunit expression and AMPA channel subunit expression

over 36 days *in vitro* (DIV). Adult neurons cultured in defined medium *in vitro*, displayed expression patterns consistent with mature neurons *in vivo*, were electrically active, and formed functional synaptic connections [57]. Our results indicate that neurons derived from embryonic tissue did not express mature synaptic channels for several weeks, and consequently their response to synaptic antagonists was significantly different than that of neurons derived from adult tissue sources. These results establish the usefulness of this unique hybrid system derived from adult hippocampal tissue for drug discovery and fundamental research. Moving toward using a high-throughput hybrid *in vitro* system will expand and improve drug testing and basic research by providing a viable, easily manipulatable alternative to expensive, resource intensive *in vivo* testing. Uses for these systems include studies into the mechanisms of learning and memory formation [58] and investigations into drug discovery, neurodegenerative diseases, and biosensor applications [34, 53, 54].

Materials and Methods

Embryonic rat hippocampal dissociated cell culture

All research was approved by the Institutional Animal Care and Use Committee at the University of Central Florida and conformed to NIH guidelines. Embryonic hippocampal neurons were cultured using a protocol described previously [59, 60]. Pregnant rats, 18 days in gestation, obtained from Charles River were euthanized with carbon dioxide and the fetuses were collected in dissecting medium made with ice-cold Hibernate E (BrainBits) supplemented with B27 (2%), Glutamaxtm (2 mM), and antibiotic-antimycotic (1%) (Invitrogen). Each fetus was decapitated and the whole brain was transferred to fresh ice cold dissecting medium. After isolation, the hippocampi were enzymatically digested at 37°C for 10 minutes with papain (2 mg/mL, Worthington 3119), Hibernate-E without calcium (BrainBits) and 2 mM Glutamax (Invitrogen). Hippocampi were quickly transferred to fresh dissection medium to halt enzymatic digestion. Hippocampal neurons were dissociated by triturating the tissue using a fire-polished Pasteur pipette. After centrifugation (300 x g, 4°C), cells were resuspended in culture medium (Neurobasal Medium (Gibco)/B27/Glutamaxtm/antibiotic-antimycotic) and plated on MEAs (see below).

Adult rat hippocampal dissociated cell culture

Adult neurons were extracted, dissociated, cultured, and maintained using a protocol and medium similar to a protocol described previously [49, 61]. Briefly, the hippocampus of adult rats (Charles River, age 6-12 months) were dissected and homogenized into

small tissue fragments in cold medium (~4°C) consisting of Hibernate-A (HA, BrainBits) supplemented with B27 (2%), Glutamaxtm (2 mM), and antibiotic-antimycotic (1%). The tissue was digested for 30 minutes at 37°C in calcium-free Hibernate-A (BrainBits) containing papain (2 mg/mL). Following digestion, the tissue was washed three times with cold HA media to remove any active enzyme. Next, the tissue was suspended in dissociation medium, (Hibernate-A Brain Bits (HA) supplemented with B27 (2%, Gibco 17504-044), Glutamax (2mM, Gibco 35050-061), Antibiotic / Antimycotic (1%, Gibco 15240-096), Z-Asp(OMe)-Gln-Met-Asp(OMe) fluoromethyl ketone (4mM, Sigma C0480), Z-Val-Ala-Asp fluoromethyl ketone (5mM, Sigma C2105), Dextrose-coated Cerium Oxide Nanoparticles (100nM, a gift from Dr. Manuel Perez), and (±)-6-Hydroxy-2,5,7,8-tetramethylchromane-2-carboxylic acid (Trolox, 70nM, Sigma 238813)) and broken apart into individual cells through mechanical dissociation with fire-polished Pasteur pipettes. The dissociated cells were suspended in plating medium, Neurobasal-A Medium with osmolarity adjusted to 295 mOsm (Gibco, 10888-022), B27 (2%), Glutamax (2 mM), antibiotic-antimycotic (1%), Recombinant Human Brain-Derived Neurotrophic Factor (20 ng/ml, Cell Sciences CRB600B), NT-3 (20 ng/ml, Cell Sciences CRN500B), bFGF (5 ng/ml, Invitrogen 13256-029), Insulin-like Growth Factor (20 ng/ml, Sigma I2656), Dextrose-coated Cerium Oxide Nanoparticles (100 nM), Trolox (70 nM, Sigma 238813), and then deposited onto DETA (N-1 [3-(trimethoxysilyl) propyl]-diethylenetriamine, United Chemical Technologies Inc., Bristol, PA, T2910KG) coated glass cover slips, according to published protocols [62, 63]. After 30-45 minutes, the cover slips were washed with warm HA by gently swirling the medium to remove tissue debris. Following this washing step fresh plating medium was applied and remained for

the first 3 DIV. On 3 DIV the medium was removed and replaced by maintenance medium (composed of all components of plating medium except Trolox and Dextrose-coated Cerium Oxide Nanoparticles) supplemented with 5 μ M Roscovitine (Rosco, Sigma, R7772) to halt cell division. After 4 DIV, the adult hippocampal neurons on the DETA cover slips were passaged to MEAs. Briefly, neurons were dislodged from the DETA with trypsin (0.05% trypsin / EDTA in HBSS, Gibco, 25200). Trypsin inhibitor (trypsin inhibitor, soybean, Gibco, 17075-029) in Dissociation Medium at 0.5 mg/mL deactivated the trypsin. The dislodged neurons were collected and spun at 500 x g for 5 minutes. The supernatant of deactivated trypsin in HBSS was discarded, and the neuronal cell pellet was suspended in 1 ml plating medium for culturing.

Immunocytochemistry and Laser Scanning Confocal Microscopy

To prepare cells for immunocytochemical characterization, cover slips were rinsed twice with Phosphate Buffered Saline (PBS). Cells were fixed with 4% paraformaldehyde for ten minutes at room temperature, and subsequently rinsed three times with PBS. Cells were permeabilized for five minutes with 0.5% Triton X-100 in PBS, and were then blocked for two hours in 5% normal goat serum (Gibco) in PBS. Anti-neurofilament-M (Chemicon, AB5735, 1:500), anti-synaptophysin (Chemicon, MAB368, 1:300), and either anti-NMDAR2A (Chemicon, AB1555P, 1:200), anti-NMDAR2B (Chemicon, AB15557P, 1:200), or anti-glutamate receptor 2/3 (Chemicon, AB1506, 1:50) were added in blocking solution for 12 hr at 4°C. After 3 washes with PBS, fluorescently labeled secondary antibodies (Invitrogen, A11011 (594 nm), A21449 (647 nm), and A11029 (488 nm), in blocking buffer were applied (1:200) for two hours. Vectashield

mounting medium with DAPI (H1200, Vector Laboratories, Burlingame, CA) was used to mount the cover slips onto slides. Fluorescent images were acquired with the UltraView spinning disc confocal system (PerkinElmer) with AxioObserver.Z1 (Carl Zeiss) stand, and a Plan-Apochromat 40x/1.4 Oil DIC plan-apochromat objective with 26 μm resolution. Z-stack projections of the scanned images were generated and modified within the Volocity image processing program (PerkinElmer).

MEA Plating and Culture Maintenance

The MEA chips (Axion Biosystems) provided 64 platinum-black coated gold-electrodes with a diameter of 30 μm , organized in an 8 by 8 array with 200 μm pitch. Clean MEAs were sterilized with 70% alcohol and then incubated with 1 ml poly-L-lysine (100 $\mu\text{g}/\text{ml}$) for 30 minutes. An area just large enough to cover all electrodes was additionally coated with 3 μl laminin (2 $\mu\text{g}/\text{ml}$) over night. Embryonic rat hippocampal neurons were plated directly on MEAs at a density of 500 cells/ mm^2 . Adult rat hippocampal neurons were first cultured on DETA coated cover slips for initial recovery and removal of debris. Embryonic tissue did not require this pre-plating step as there is very little debris generated from the culturing process. After 4 days on DETA cover slips, the adult neurons were passaged onto MEAs at a density of 500 cells/ mm^2 (Figure 2-1). Every 2-3 days, half the medium was replaced with fresh maintenance medium supplemented with 2 μM Rosc. Supplementing the adult neurons with 25 μM glutamate (N-Acetyl-L-glutamic acid, Aldrich, 855642) at 2 DIV increased the electrical activity of the adult neurons [48].

MEAs were incubated with their covers off to allow gas exchange but covered upon removal from the incubator to reduce contamination, media evaporation, and gas exchange. The head stage of the recording system (Axion Biosystems) was pre-heated to 37 °C before MEAs with adult or embryonic hippocampal cultures were investigated.

Experimental Procedure

The activity of neuronal networks was recorded at 25 kHz using the software *Axion's Integrated Studio* (AXIS). Signal amplitudes 6 times larger than the standard deviation of the base line were detected as action-potential (AP) spikes. The spike data was then imported into Matlab 2010b (The MathWorks) for further processing. Baseline spontaneous activity in adult and embryonic neurons was recorded for 3 minutes on 5 consecutive days per week, starting at 7 DIV. The synaptic antagonists D-(-)-2-Amino-5-phosphonopentanoic acid (D-AP5, 25µM, Tocris Bioscience, 0106) and 6-Cyano-7-nitroquinoxaline-2,3-dione disodium (CNQX, 25µM, Tocris Bioscience, 1045) were separately administered to both adult and embryonic neurons on 14 DIV and at various time points between 30 and 60 DIV. Three minute recordings were made to quantify the effect from these antagonists on spontaneous activity. If necessary, additional baselines were recorded prior to the administration of antagonists. After MEA measurements were recorded, the antagonists were washed from the neurons with an entire media change; 24 hours later, the activity of the neurons had returned to baseline levels.

Evaluation and statistics

Data analysis was performed off-line using unpublished Matlab functions to evaluate spike files created during each MEA recording. In brief, each 3 minute dataset was

processed to extract the following parameters: “active channels” (a number from 0 to 64); “AP frequencies” (reciprocal inter-spike intervals); “Burst” (where at least 10% of the active channels showed more than 1 AP with 1 ms); “Burst duration” (time-interval from the first AP in a burst to the last AP in a burst); “Average burst frequency” (the reciprocal time-difference between two subsequent bursts); “In-burst frequency” (amount of APs within a detected burst divided by the duration of that burst); “Non-burst frequency” (reciprocal inter-spike intervals between APs that were not associated with bursts). In about 25% of the adult cultures and 14% of the embryonic cultures, portions of the neuronal networks detached from the substrate over time and especially after about 6 weeks. In order to accommodate the different numbers of active channels between MEAs all values were corrected for the amount of active channels on an MEA. For each of the 3 minute recordings, a representative results chart was produced as shown in figure 2-3. Effects from synaptic antagonists were measured as the percent of active channels or AP frequency of treated embryonic or adult cultures versus the baseline activity of the same cultures recorded before administration of the antagonist.

Results

Dissociated neuronal cultures from adult and embryonic sources recovered on MEAs and formed networks on MEAs at a density of 500 cells / mm² (Figure 2-1). Three-minute recordings of spontaneous activity were taken of each MEA, 5 times per week, for up to 70 DIV. Phase-contrast pictures of the MEAs were taken after each recording for a daily assessment into the condition of the cells as well as verification of physical contact between cells and electrodes (Figure 2-1). Neurons, both adult and embryonic, were stable and electrically active on MEAs for up to 90 DIV (data not shown).

Spontaneous activity of Adult and Embryonic Neurons

Spontaneous firing activity started in both the adult and embryonic neurons between 7–10 DIV. Movement of MEAs from the incubator to the heated recording stage and the subsequent 3 minute recording period did not significantly affect the pH or temperature of the medium, represented by consistent baseline activity. However, brief increases in baseline neuronal activity were observed as a result of medium changes. Over the more than 2 month culture period, embryonic MEAs ($n = 6$) consistently displayed a higher number of active channels, with an average of 37 ± 8 channels active per MEA versus 15 ± 5 channels in adult MEA cultures ($n = 9$). Action potential (AP) firing frequencies in embryonic cultures with approximately 2 - 4 Hz were higher than in adult cultures with AP firing frequencies of 1 - 2 Hz. Spontaneous bursting occurred about one week earlier in adult cultures as opposed to embryonic cultures. The burst development over the first 6 weeks was consistent between the two types of neuronal networks (Figure 2-3A).

After the 6th week, however, bursts in the adult cultures appeared less often, whereas the burst frequency in the embryonic cultures increased further. For both embryonic and adult cultures, the duration of bursts decreased over the time span of 10 weeks (Figure 2-3B). The bursts of embryonic cultures were on average 3 - 5 times longer as opposed to bursts in adult cultures. While burst durations in the embryonic cultures were consistently variable (about ± 1 s) over the 10 weeks of experimentation, bursts in the adult cultures decreased in length. This focusing of bursts in adult cultures was accompanied by a steady increase of the in-burst firing frequencies over time (Figure 2-3C). The in-burst frequencies of adult cultures recovered within the first 2 weeks, whereas embryonic cultures recovered slower and reached mature in-burst levels after about 6 weeks. The non-burst firing frequencies (APs not related with bursts) were consistent over the entire time for the adult cultures, but decreased steadily in the embryonic cultures (Figure 2-3D). Overall, the burst activity focused and matured earlier and more consistently in adult cultures on MEAs, whereas embryonic cultures showed a slower, more chaotic maturation.

NMDA and AMPA channel activity and expression in adult and embryonic neurons

Antagonists were administered to embryonic and adult cultures on MEAs in separate experiments: 25 μ M D-AP5 (NMDA channel antagonist) and 25 μ M CNQX (AMPA channel antagonist). D-AP5 (25 μ M) caused a significant decrease in the number of active channels in both adult and embryonic MEA cultures (Figure 2-4 A,B). Adult cultures lost a greater percentage of channel activity (90 ± 6 % on 14 DIV, 82 ± 6 % on 30-60 DIV) versus embryonic cultures (65 ± 4 % on 14 DIV, 36 ± 7 % on 30-60 DIV).

Changes in the AP frequency also varied with lower frequencies in adult cultures ($76\pm 8\%$ on 14 DIV, $82\pm 17\%$ on 30-60 DIV) which were significantly different from the measured effect on embryonic cultures (Figure 2-4 C,D). On 14 DIV, the firing rate of embryonic neurons increased $90\pm 6\%$, while in 30-60 day old cultures the firing rate decreased $70\pm 7\%$. While NMDA channels were expressed at low levels in embryonic neurons on 14 DIV, the level of expression was not nearly as high as in adult neurons on 14 DIV (Figure 2-5 A,B). The difference in NMDA channel expression (NR2A and NR2B subunits) in adult and embryonic neurons *in vitro* likely caused the contrasting reaction to D-AP5 in the two populations of neurons. Because adult neurons expressed a greater number of NMDA channels, their reaction to the competitive NMDA antagonist D-AP5 was much more pronounced.

Addition of CNQX caused the activity of far fewer channels to be lost in both adult and embryonic MEA cultures as compared to D-AP5 (Figure 2-4 A,B). Adult cultures lost a greater percentage of channel activity ($52\pm 3\%$ on 14 DIV, $24\pm 5\%$ on 30-60 DIV) versus embryonic cultures ($23\pm 5\%$ on 14 DIV, $0\pm 7\%$ on 30-60 DIV). Changes in AP frequency in both the adult and embryonic cultures were not affected by CNQX after 14 DIV (Figure 2-4D). The activity of the neurons was only slightly decreased in both embryonic and adult cultures between 30 to 60 DIV ($31\pm 6\%$ drop in adult MEAs, $47\pm 5\%$ drop in embryonic MEAs). While expression of the AMPA channel subunits GluR2/3 was not observed in embryonic neurons on 2 DIV, expression had increased to mirror adult levels by 14 DIV (Figure 2-5 C).

Discussion

The results demonstrated that adult neurons cultured from the hippocampus of rats recovered functionally and had the capacity to fire spontaneously on MEAs over 60 DIV. Additional culture techniques were used to allow adult neurons to recover from initial plating trauma and reduce debris before being densely deposited on the MEAs and to improve recovery of electrical activity *in vitro*. Adult cells were first pre-cultured at a low-density and then were passaged and deposited onto MEAs at 500 cells / mm², a density high enough to allow the formation of multiple synaptic connections. This step allowed for the removal of debris from the cultures and allowed recovery after dissociation to enable high survival in MEA cultures. The application of a pre-plating step along with the supplementation of glutamate in the culture medium promoted elevated electrical activity in the adult neurons [48]. After 7 to 10 DIV, sporadic spontaneous firing activity was detected, and stable reliable recordings were evident after this point.

Since neuronal MEA systems have typically relied upon neurons derived from embryonic tissue [34-36, 53-55], we compared our novel adult hippocampal MEA system to traditional embryonic MEA systems. Recording from both adult and embryonic MEAs were made daily through 90 DIV (data not shown) and fully characterized out to 60 DIV. Embryonic MEAs consistently displayed higher numbers of active channels, with an average of 40 channels active versus 20 active on adult MEAs. The majority of other parameters, including AP frequency, activity, average burst frequency, and average in-burst frequency, all displayed similar characteristics between

the adult and embryonic MEA systems. This new adult MEA system, at its core, exhibited similar firing characteristics to the more traditional embryonic MEA systems. However, the adult cultures developed the capability of synchronized bursting about one week earlier than the embryonic cultures. Bursting in neuronal networks is usually seen as an indicator for maturity [64]. Spontaneous periodic synchronized bursting during formation of mature patterns of connections in cortical cultures [65]. While embryonic neurons regenerate, fire APs and eventually develop synchronized bursts on MEAs, the developmental maturity of these neurons had not been robustly established. In the hippocampus of embryonic rats, neural progenitors differentiate into neurons between E15-E18 [37, 43, 66]. While these cells obtained from embryonic rats are fully differentiated, they are developmentally immature, with transcriptional profiles showing two-thirds of genes are only expressed postnatal and >95% of expressed genes show highly significant changes during postnatal development [37]. When examining the machinery responsible for synaptic transmission, gene expression for the NMDA channel subunits NR2A and NR2B was not detected until near birth on E21-22, with expression not peaking until P20 [39]. During this developmental period, NR2B was predominantly expressed in the early postnatal brain while NR2A expression increased to eventually outnumber NR2B, with each subunit lending different kinetics of excitotoxicity, neurotoxicity, and plasticity [67]. *In vitro*, NR2A/B channels are detected at only very low levels until after 2 weeks in embryonic neurons [40]. AMPA channel expression is also limited at birth, only increasing postnatally [38]. Gene expression for the axonal sodium transporter subunit 1 begins around P15, increasing till P30 [41, 42]. *In vitro*, expression patterns for all genes, specifically axonal and synaptic channels

responsible for signal transmission, is similar to that seen *in vivo*, with gene expression showing significant changes over the course of weeks [39-41, 43-45]. The importance of these dynamics of neuronal maturation highlights the need for gene and protein expression in study population of neurons to mirror that in mature adult neurons *in vivo*. If embryonic neurons do not express the same machinery responsible for electrical activity or signal propagation in adult neurons, then their response to neurotoxic agents or drug therapies may not be correlative to responses in the mature adult brain.

Our method of culturing adult neurons resulted in a system where NMDA and AMPA channel subunits were expressed throughout the lifespan of the culture. NMDA channel subunits NR2A and NR2B as well as AMPA channel subunits GluR2/3 were expressed on and after 2 DIV. This contrasted greatly from neurons derived from embryonic tissue, with delayed NMDA and AMPA channel expression until 14 DIV and later. Responses of neurons to NMDA and AMPA channel antagonists were found to be significantly different in embryonic neurons as compared to adult neurons, with each antagonist decreasing activity in adult neurons to a greater degree than in embryonic neurons. Our results show that embryonic neurons in culture develop a mature profile of ion channel subunits after 3-4 weeks. Therefore, embryonic neurons should not be employed for experiments until they have fully matured in culture, especially in studying neurodegenerative diseases such as Alzheimer's where synaptic protein profiles may play a critical role in the process of synaptic failure [68-72].

In comparison to embryonic MEA systems, our method of using adult hippocampal neurons on MEAs, is more appropriate to acquiring data with mimics the adult brain.

While preparation of these MEAs was slightly more complicated than embryonic neuronal MEAs, the end result yielded a long-term screen methodology that is more biomimetic of the synaptic machinery responsible for critical synaptic function required in learning and memory [73-76]. Additionally, due to the earlier development of bursts and general maturation, this system can facilitate quicker, more reliable, and more correlative investigations into drug discovery, neurotoxic agents, and neurodegeneration. Finally, this method can be used in the future to allow for the adult human neuronal networks cultured on MEAs.

In conclusion, we have demonstrated critical differences between adult and embryonic neurons and their respective synaptic connections which could be highly relevant in neurodegenerative disease research. By demonstrating the similarities and differences between adult and embryonic neurons and the response of each to synaptic antagonists, the value of this adult neuron culture system has been established for application in neuronal regeneration and drug discovery studies. The significance of this finding is that most *in vitro* neuronal research utilizes embryonic hippocampal neurons for periods of less than 7-11 weeks. By incorporating adult neurons into an MEA system, a long-term system has been created to enable the screening of a large number of cells and the study of pathogen and drug effects on the same population of cells over an extended period of time. This screen could find important applications in pharmaceutical drug development by providing an *in vitro* test platform for investigations into neurodegenerative disease, traumatic brain injury, stroke, drug discovery, and fundamental research.

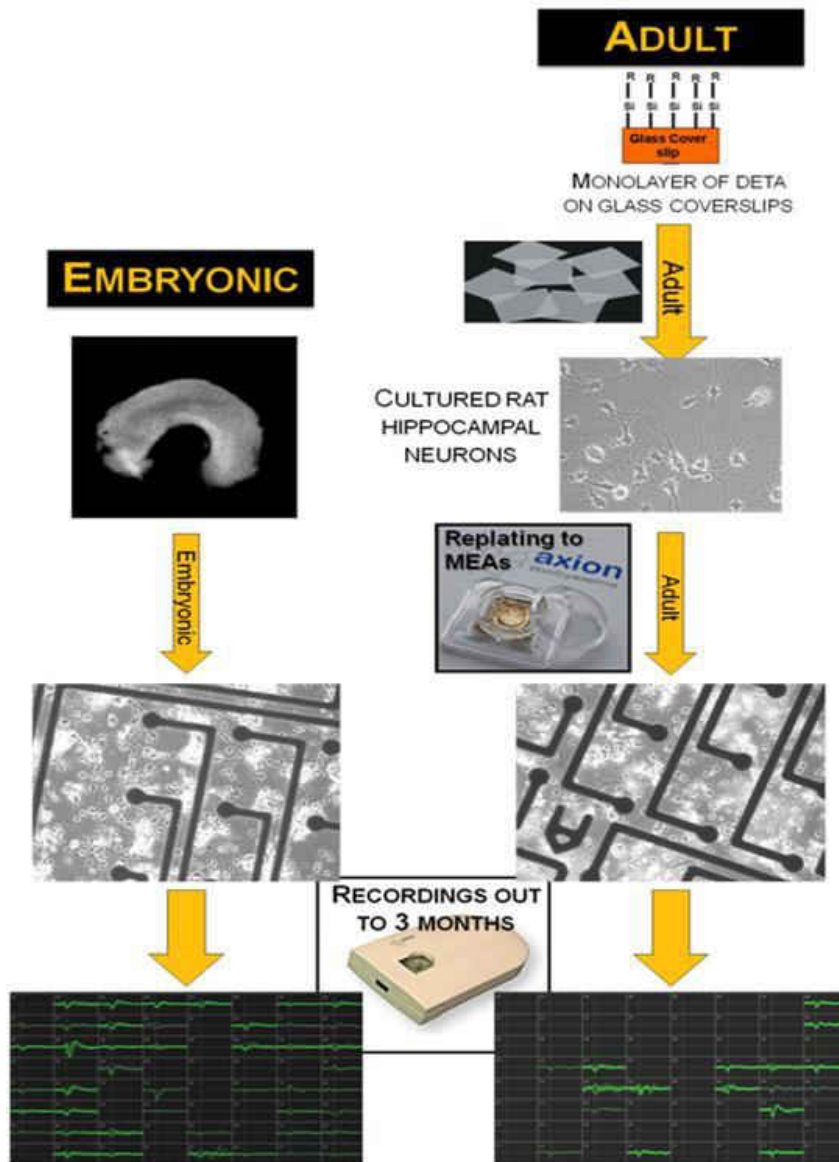


Figure 2-1. Adult and embryonic MEA culture and life cycle. Adult neurons: Mature terminally differentiated adult neurons were extracted from the hippocampus of adult rats and plated onto DETA cover slips. After 4 days the neurons were passaged from these cover slip(s) onto MEAs that had been coated with PDL / laminin (for cell adhesion). Embryonic neurons: Neurons from the hippocampus of embryonic day 18 rat fetuses were extracted and plated directly on MEAs that had been coated with PDL / laminin. Electrical recordings of spontaneous neuronal activity were performed for up to 3 months. In addition, ion channel receptor antagonists were introduced and their effects were measured against baseline electrical activity. 64-channel axion biosystems MEAs were used.

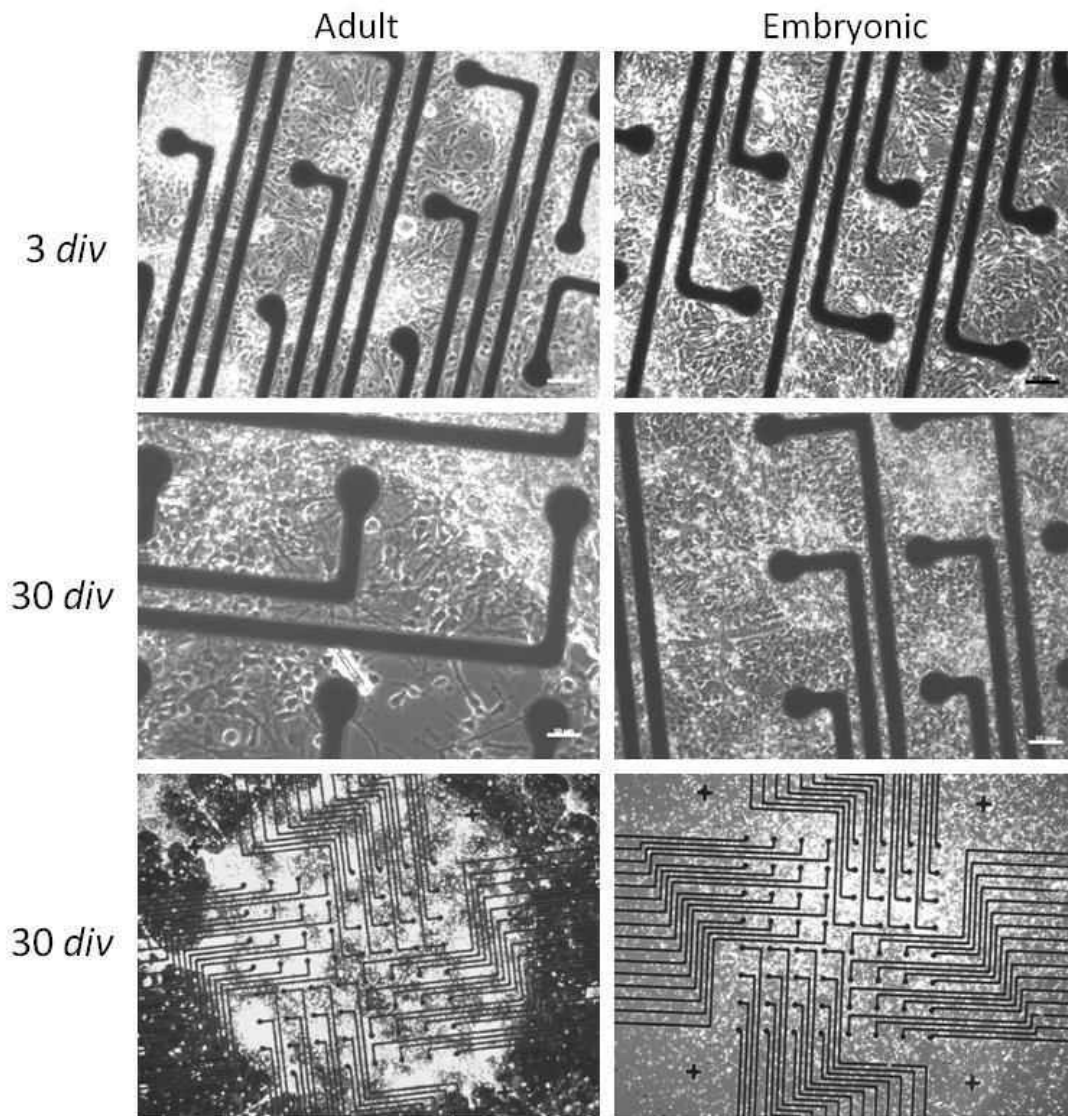


Figure 2-2. Phase contrast images of cultures on MEAs after 3 DIV and 30 DIV. Neurons were applied between 500 to 1000 cells / mm². Cells attached and regenerated on the PDL / laminin surface covering the MEAs, seen in the dense collection of cells covering the electrodes. Each 64-Channel MEA is arranged in an 8 x 8 array of electrode 30 μM in diameter and spaced 200 μM apart. The MEA was sampled 25,000 times per second, at 16 bits of depth. Scale bar = 50 μm.

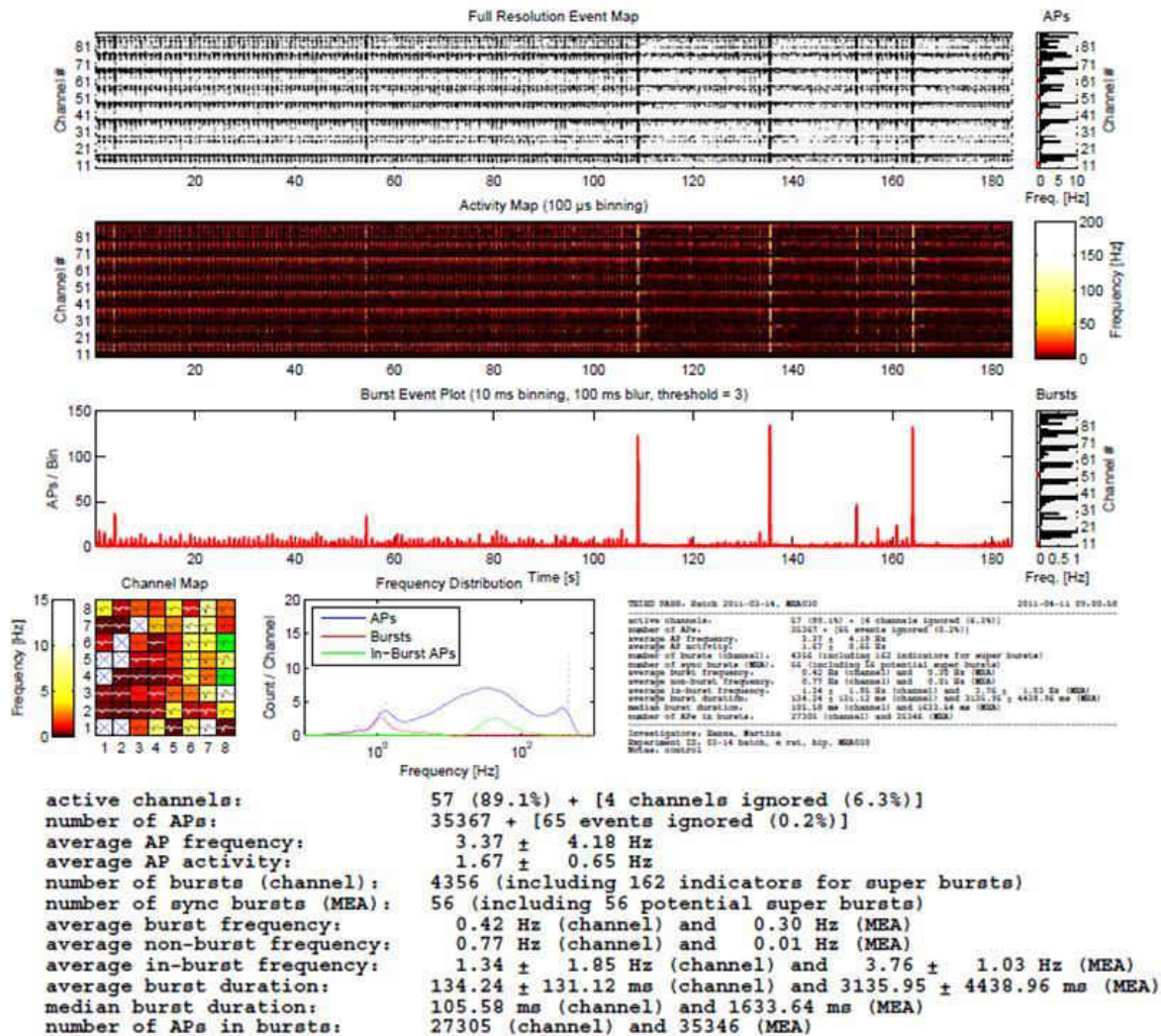
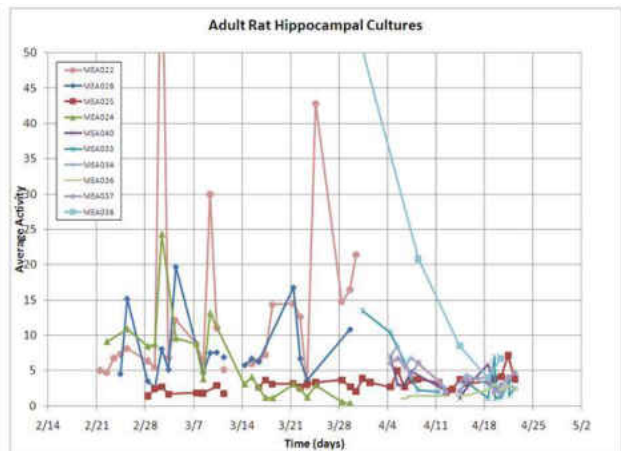
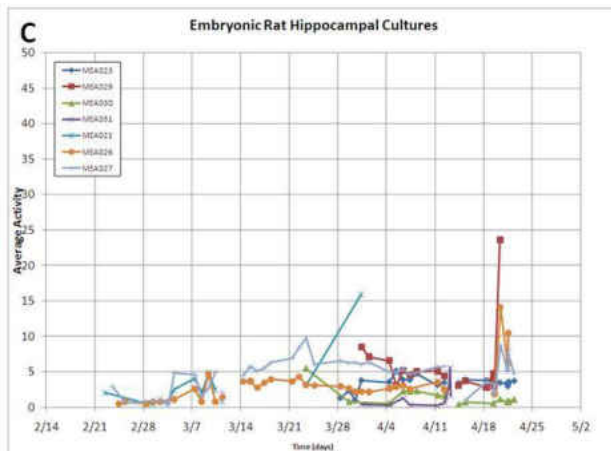
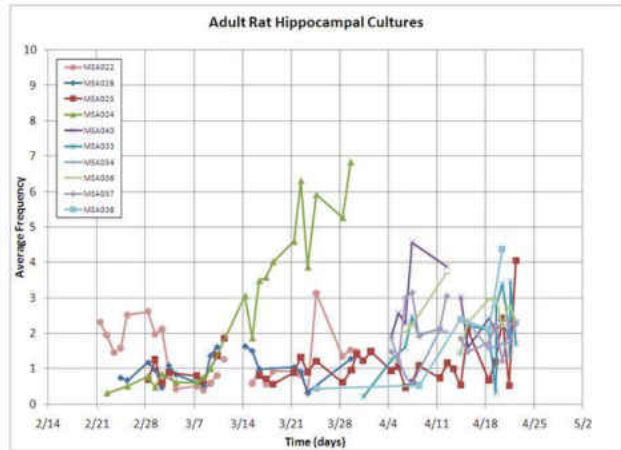
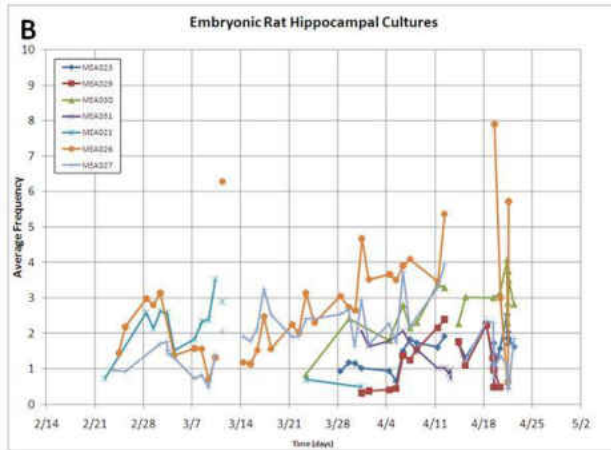
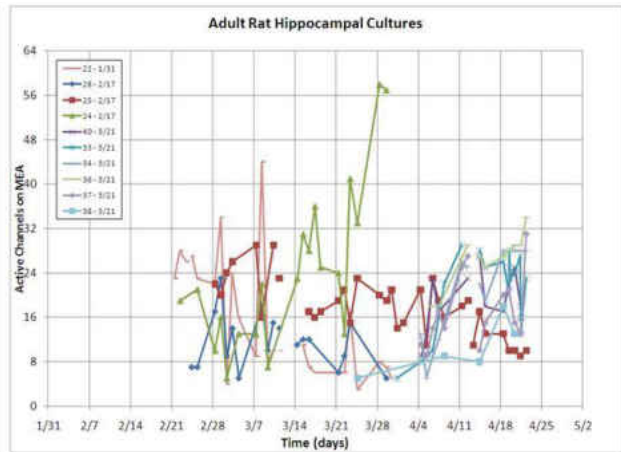
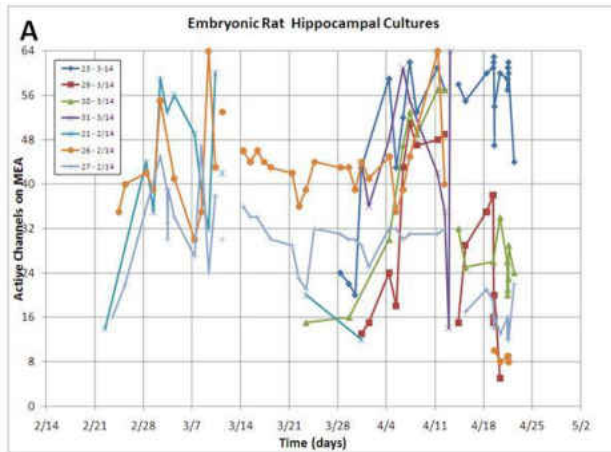


Figure 2-3. MEA data processing: The spontaneous activity of embryonic and adult neurons was recorded for 3 minutes each day over the study period. Each 3 minute dataset was processed in a 3-step method. This method allowed inactive or noisy channels to be excluded. After processing, the following parameters were extrapolated: “active channels” – a number from 0 to 64. Channels with less than 7.5 APs per minute were treated as inactive. “AP Frequency” – number of total measured APs divided by recording time. The mean and stdev of that number is independent from active channels. “AP Activity” – is 1 divided by the time between two subsequent APs, or frequency 1/s. “Burst” – where more than 1 AP occurs within 1 ms. “average burst frequency” – 1 divided by the time-difference between two subsequent bursts. “In-burst frequency” – amount of APs within a burst divided by the duration of that burst. “Non-burst frequency” – like the activity, but considers on APs that are not associated with bursts. “Burst duration” – time-interval from the first AP in a burst to the last AP in a burst.



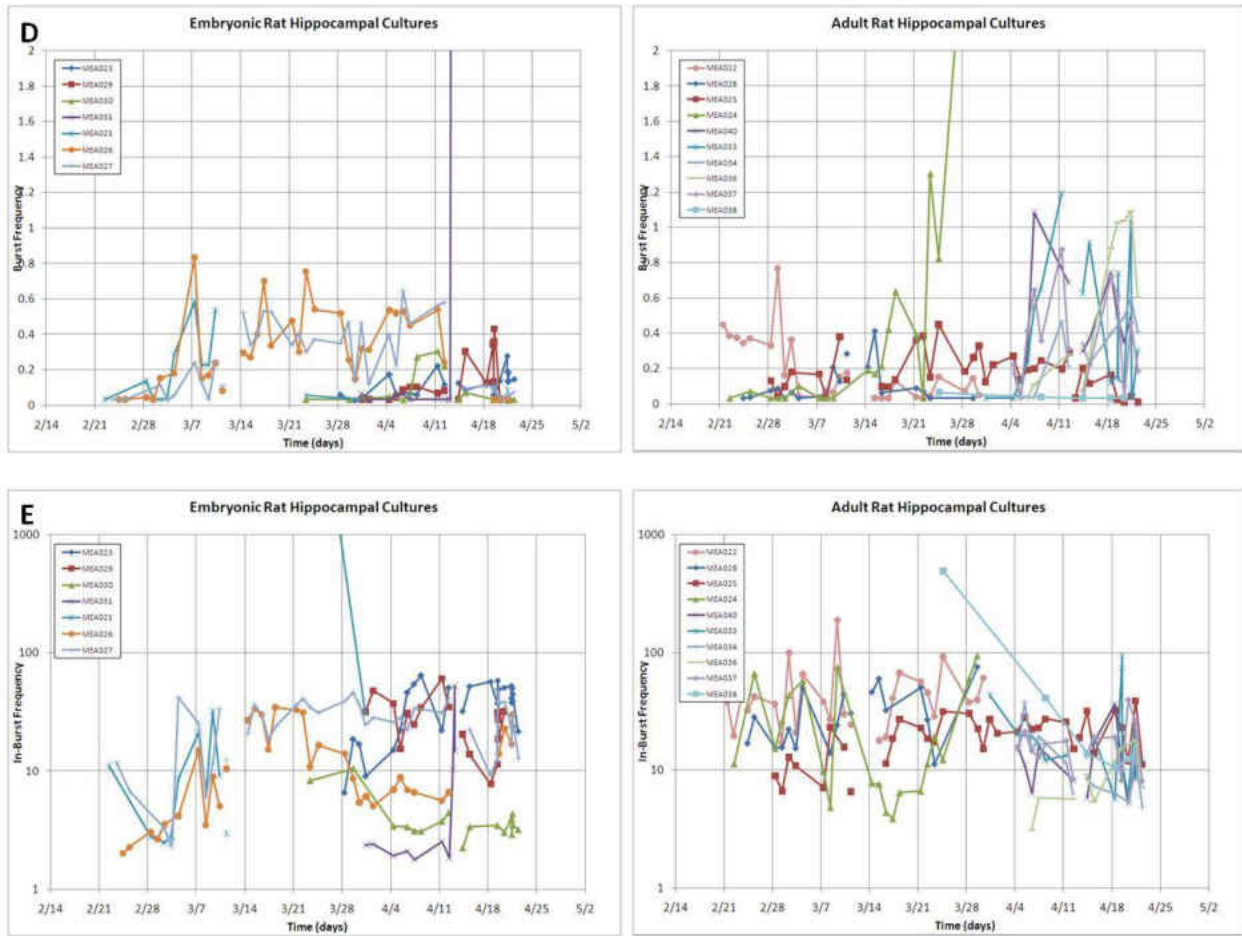


Figure 2-4. Basic firing patterns of embryonic and adult hippocampal neurons on MEAs over time. The spontaneous activity of embryonic and adult neurons was recorded for 3 minutes each day over the study period. The activity data from each day was processed to filter out inactive channels. (A) Number of active channels. (B) Frequency of APs. (C) Average activity, or 1 divided by the time between two subsequent APs (frequency 1/s). (D) Burst frequency. (E) In-burst frequency. MEA number to plating date: Embryonic: MEA 23 – 3/14, MEA 29 – 3/14, MEA 30 – 3/14, MEA 31 – 3/14, MEA 21 – 2/14, MEA 26 – 2/14, MEA 27 – 2/14. Adult: MEA 22 – 1/31, MEA 28 – 2/17, MEA 25 – 2/17, MEA 24 – 2/17, MEA 40 – 3/21, MEA 33 – 3/21, MEA 34 – 3/21, MEA 36 – 3/21, MEA 37 – 3/21, MEA 38 – 3/21. Gaps in graphs indicate activity was not recorded on that day.

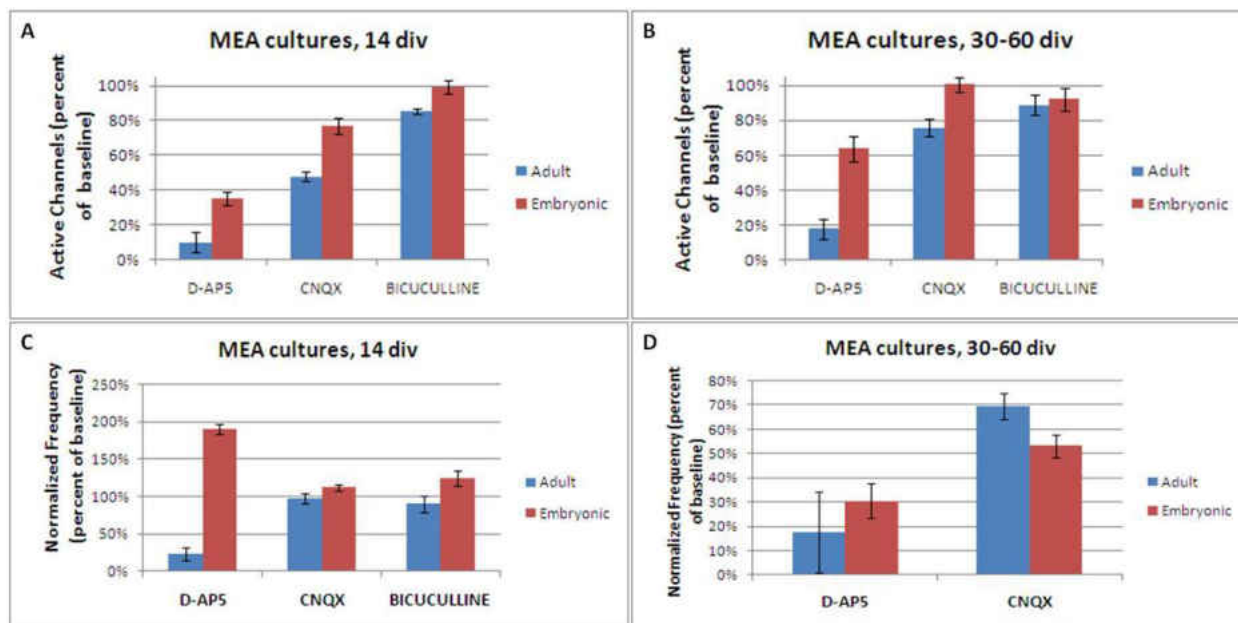
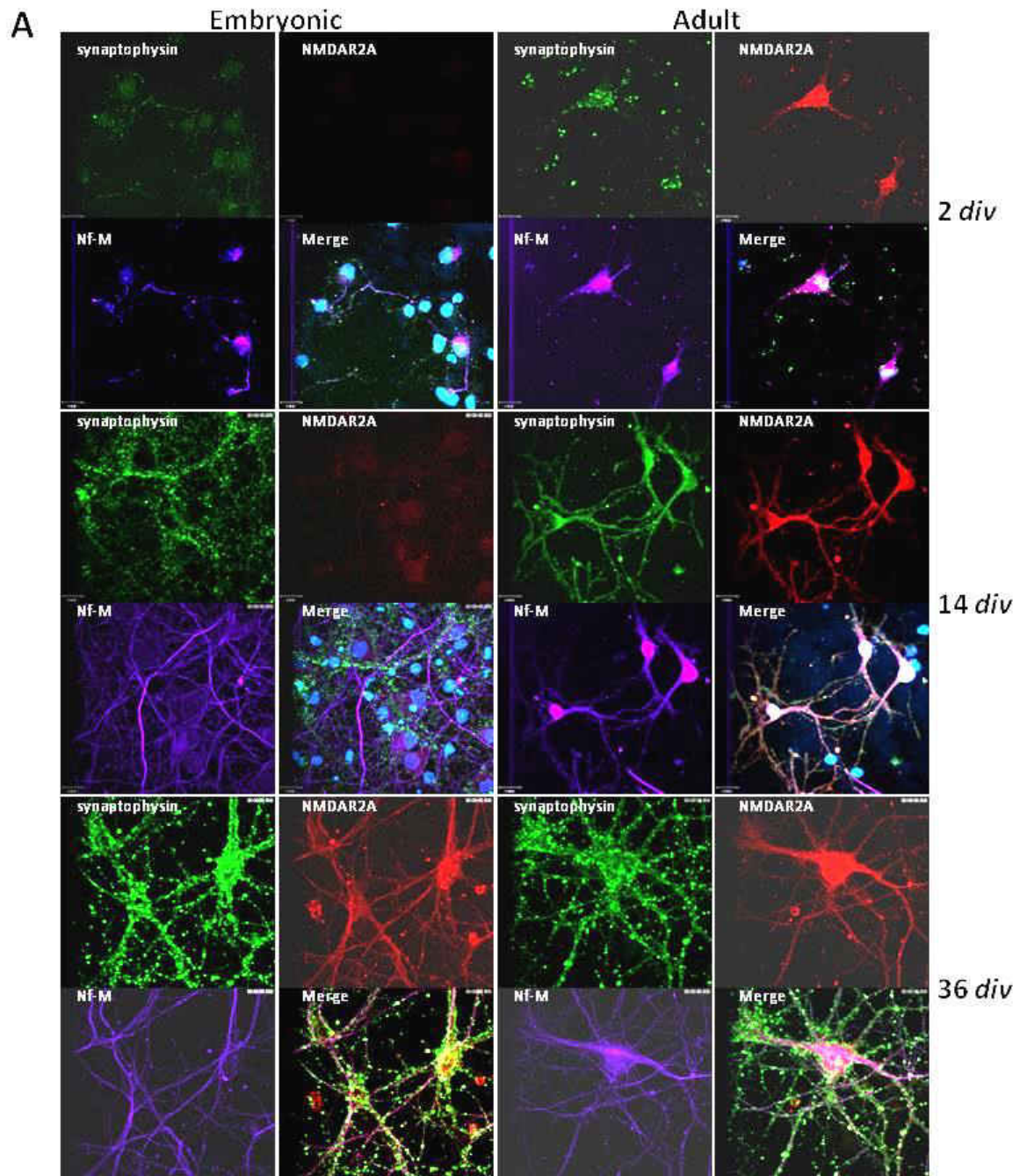
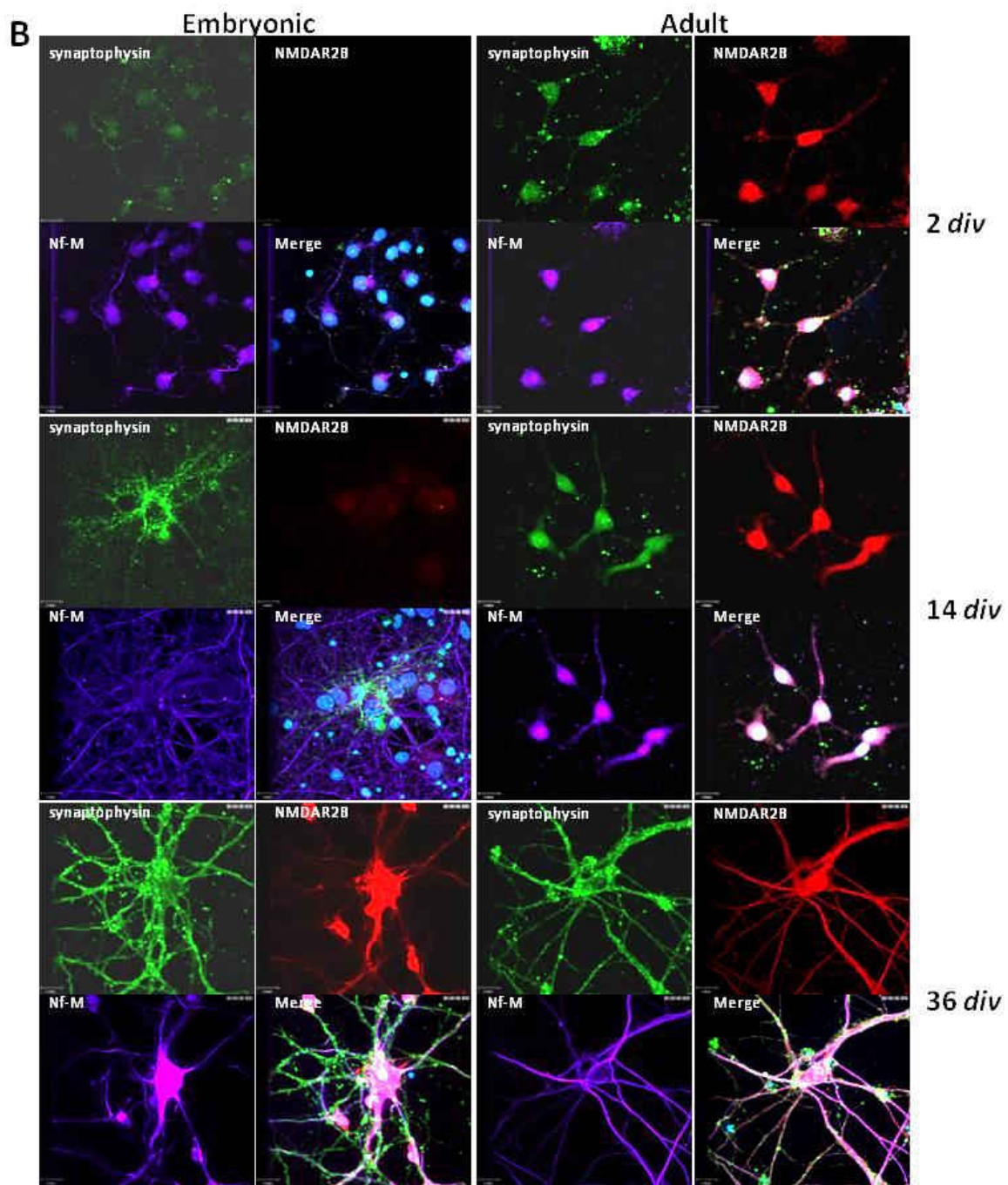


Figure 2-5. Comparison of the impact on adult or embryonic spontaneous activity from addition of synaptic antagonists. Active channels (A,B) or AP frequencies (C,D) were evaluated in adult or embryonic hippocampal neuron MEA systems on either 14 or 30-60 DIV in the presence of D-AP5 (25 μ M), CNQX (25 μ M), or Bicuculline (50 μ M) in culture medium. Adult neurons showed significantly decreased active channels and AP frequency due to D-AP5 in both early 14 DIV cultures as well as older 30-60 DIV cultures. This drop in activity was significantly different from embryonic 14 DIV, where fewer active channels were lost and activity increased in the remaining channels. The AMPA-channel antagonist CNQX also caused a decrease in spontaneous activity. The drop in activity between adult and embryonic cultures was, however, only reflected in the loss of more active channels in the adult system. AP frequency declines were consistent between the two culture systems. Bicuculline had limited effect on spontaneous activity in both embryonic and adult neurons.





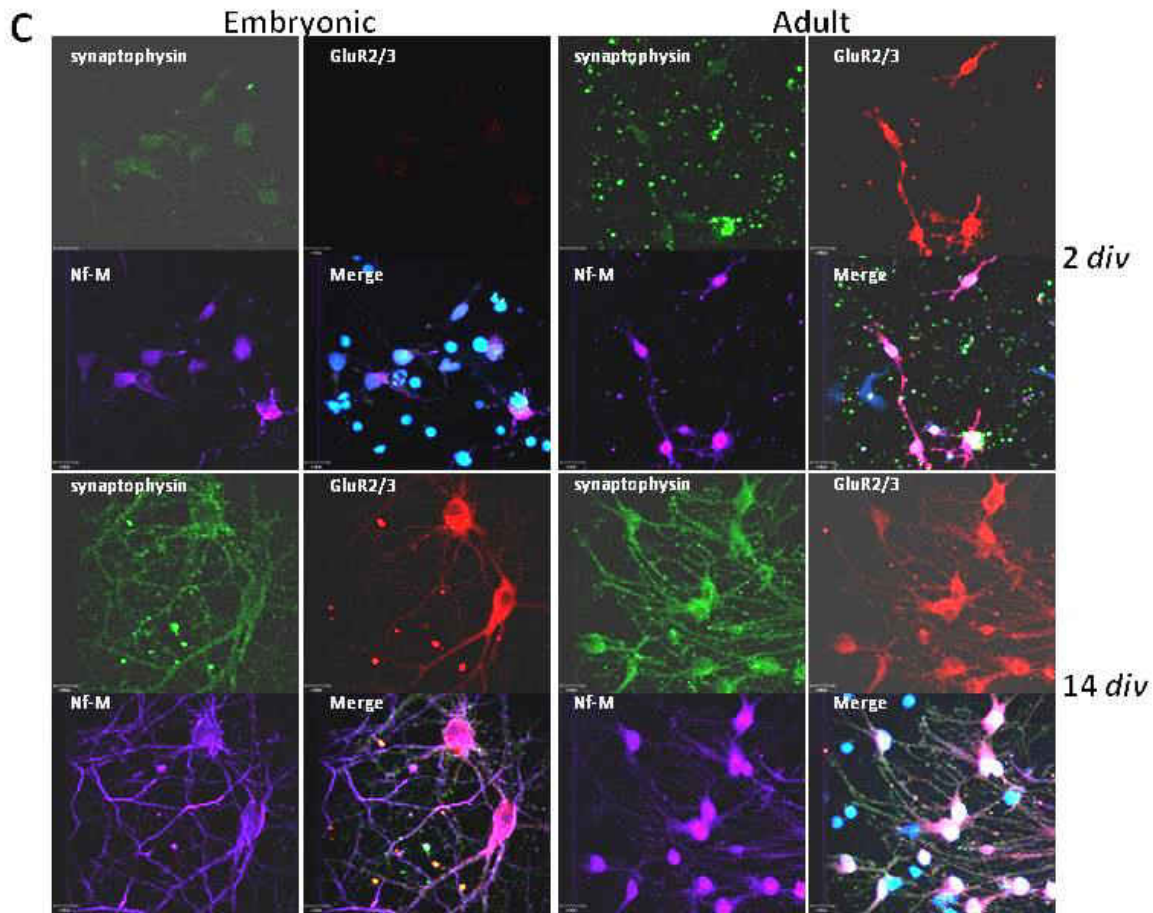


Figure 2-6. Expression of presynaptic proteins and postsynaptic channel subunits in embryonic and adult neurons *in vitro*: NR2A, NR2B, or GluR2/3 (red); synaptophysin (green); neurofilament-M (far-red); and DAPI (blue) expression after 2, 14, and 36 DIV. NMDAR2A (A) and NMDAR2B (B) were not expressed in embryonic neurons on 2 DIV and were not strongly expressed on 14 DIV (when compared to channel expression in adult neurons). After 36 DIV, the channels were expressed by the embryonic neurons at similar levels to the adult neurons. The AMPA receptor subunits GluR2/3 (C) were expressed by embryonic neurons by 14 DIV. These postsynaptic channel subunits were all found in adult neurons from 2 – 36 DIV. Synaptophysin and Neurofilament-M expression grew stronger as both the embryonic and adult neurons recovered and regenerated *in vitro*. Scale bars 17 μ m.

CHAPTER 3 – MORPHOLOGICAL AND FUNCTIONAL CHARACTERIZATION OF HUMAN INDUCED PLURIPOTENT STEM CELL-DERIVED NEURONS (ICELL NEURONS) IN DEFINED CULTURE SYSTEMS

Introduction

It is necessary to determine the system requirements for human stem cells for long-term *in vitro* culture. Current efforts to streamline and accelerate established drug screening protocols and body-on-a-chip device development [77-80] are predicated on the development of robust and fully-functional human cell types derived from both embryonic and induced pluripotent (iPSC) stem cells. To this end, the characterization of competent sources of terminally-differentiated human pyramidal neurons is necessary for the development of neuronal network models for these devices and for high throughput single cell assay systems. In addition, the utilization of neurons derived from iPSCs enables the *in vitro* study of neurodegenerative conditions, such as Alzheimer's disease, derived directly from patient populations. Baseline characterization of a stable cell source is a necessary first step for pre-clinical drug testing applications, as well as for the establishment of personalized drug development protocols utilizing these patient-specific stem cells.

Neurons derived from hiPSCs by Cellular Dynamics International (CDI, Madison, WI), termed iCell Neurons, offer one commercial source for such cells. These hiPSC-derived populations are composed of GABAergic and glutamatergic post-mitotic neurons which rapidly regenerate post-thaw. Previous data obtained from these cells using culture

parameters established by the manufacturer indicates their functional characterization over two weeks *in vitro*, including evidence for their ability to generate three major voltage-dependent currents (Na_v , Ca_v , and K_v) [81]. However, analysis of neuronal performance over a two week period in a single culture environment is insufficient if these cells are to be considered for incorporation into chronic drug evaluation studies *in vitro* [82, 83]. Careful assessment of maturation end points and cell survival over an extended time-course is necessary to justify incorporation of CDI's hiPSC-derived neurons into body-on-a-chip and other devices for chronic drug toxicity and efficacy studies.

The development of complex *in vitro* systems requires the establishment of reproducible surface modifications, medium formulations and cell propagation protocols [84]. Assessment of effective culture parameters is necessary in order to evaluate the best system for developing controlled neuronal networks for *in vitro* drug evaluation protocols. The chemical silane N-1(3-[trimethoxysilyl]propyl)-diethylenetriamine (DETA), can be used to create a cytophilic culture surface, providing a fully-defined and reproducible alternative to biopolymer coatings [85]. Previously, DETA has been used in conjunction with cytophobic surfaces to successfully culture as well as pattern cells into controlled configurations [86], providing the means to develop *in vitro* engineered cell networks for a variety of advanced culture applications [87, 88]. Furthermore, previous work has demonstrated that DETA is capable of promoting the survival and maturation of primary neurons in culture for extended periods [61, 83, 89]. DETA, an analogue of spermine, has been shown to promote neuron survival *in vitro* through interactions with

NMDA-receptor complexes, and is also known to promote increased longevity in a number of model organisms by reducing the overproduction of harmful reactive oxygen species and autophagy regulation [90-92]. For these reasons, DETA is an ideal surface modification for use in the establishment of complex, multi-organ *in vitro* platforms for drug-evaluation protocols. The medium composition is also a key variable in establishing a defined culture system. The development of fully-defined, serum-free systems is critical for the generation of reliable pre-clinical data, as serum-containing medium comprises unknown, variable factors which may confound results, thereby limiting the ability to draw robust conclusions from such studies [18].

In this study, the survival, purity and electrophysiological development of hiPSC-derived neurons over a one month culture period was evaluated under various controlled conditions. Cells maintained in the manufacturer's culture conditions were compared with those kept in a fully-defined, serum-free cell culture environment that was developed to promote the long-term survival of primary adult hippocampal neurons [61, 83]. The collected data demonstrate that these hiPSC-derived neurons can be grown on both biopolymer and chemically-defined surfaces for at least one month. During this time, the cells maintained a consistent neuronal population and underwent electrophysiological maturation, characterized by evaluation of the number of repetitively firing neurons in culture, changes in major voltage currents, and decreased action potential (AP) duration. These cells maintain a high level of viability consistently for at least 28 days. A subset of the cultured cells expressed markers specific to layer 5 cortical neurons, indicating a degree of neuronal sub-type heterogeneity within the

population. The collected electrophysiological and biochemical data indicate these cells possess a pyramidal phenotype and increasingly mature over one month *in vitro* [93]. However, differences in functional maturity and survivability were noted over the conditions examined. Based on these findings, these hiPSC-derived neurons present an excellent source of human pyramidal-like neurons for use in novel *in vitro* applications such as body-on-a-chip platform development or for use in functional high throughput screening systems.

Materials and Methods

Surface modification

Glass coverslips (Thomas Scientific 1217N81, 18 mm, no. 1.5) were cleaned using an oxygen plasma cleaner (Harrick PDC-32G) for 10 min at 100 mTorr. The N-1(3-[trimethoxysilyl]propyl)-diethylenetriamine (DETA, United Chemical Technologies Inc., Bristol, PA, T2910KG) self-assembled monolayers were produced by reaction of plasma-cleaned glass with a 0.1% (v/v) mixture of the DETA in freshly distilled toluene (Fisher T2904) as described by Ravenscroft et al. (1998).[88] The DETA-coated coverslips were heated to just below the boiling point of toluene (70°C), thoroughly rinsed with toluene, reheated to 70°C, and then oven dried. Surfaces were validated prior to use in cell culture using contact angle measurement and X-ray photoelectron spectroscopy as described previously.[94]

Cell culture and maintenance

Human hiPSC-derived neurons were obtained from CDI in frozen vials containing at least 2.5 million cells (catalogue number: NRC-100-010-001). Cells were handled according to the manufacturer's user's guide. Briefly, cells were removed from liquid nitrogen storage (-196°C) and thawed for 3 minutes in a 37°C water bath. Cells were gently transferred to a 50 ml Falcon tube where 1 ml of CDI's Complete Maintenance Medium (MM) was added drop-wise to the cell suspension. Cells were swirled gently to minimize osmotic stress and an additional 8 ml of medium was slowly added. Cells were plated at a density of 700 cells per mm² on DETA or poly-L-ornithine (PLO)/laminin

(0.01% PLO and 3.3 µg/ml respectively) coated coverslips and placed in an incubator set to 37°C and 5% CO₂. PLO/laminin surfaces will be referred to as “laminin surfaces” throughout the text. Cells were given complete medium changes after 24 hours in vitro, as per the manufacturer’s instructions, and were subsequently fed every 3-4 days with half changes of the medium. Hybrid Systems Laboratory medium 1 (HSL1) was prepared as described by Edwards et. al, with the exception of the inclusion of bFGF (See Supplemental Table 1).[83] This medium was originally developed as a maintenance medium for the long-term support in culturing of adult rat hippocampal neurons. CDI MM is proprietary and therefore cannot be detailed herein, but is commercially available.

Cell viability and neuritic outgrowth analysis

In order to assess the ability of hiPSC-derived neurons to survive in different combinations of medium and surface compositions, cells were grown in MM and HSL1 on DETA and laminin-coated surfaces. Phase contrast images were taken with an inverted microscope (Zeiss Axiovert) after 1, 3, 7, 10, 14, 21, and 28 DIV, counted and normalized to day 1 cell counts for each culture. The longest neurite from a minimum of 75 cells per condition was measured (ImageJ; National Institutes of Health, Bethesda, MD) from phase contrast images taken at 1, 3, and 7 DIV.

Immunocytochemistry

Cells were fixed using 4% paraformaldehyde for 20 min, rinsed with and stored in phosphate-buffered saline (PBS) at 4°C until they were used for immunocytochemical analysis. Cells were then permeabilized for 20 min with 0.2% Triton X-100 in PBS and

incubated at room temperature for 2 hrs in blocking buffer (2.5% donkey serum, 2.5% goat serum, and 0.5% BSA) to prevent non-specific antigen binding. Primary antibodies (chicken anti-microtubule associated protein 2 (anti-MAP2) polyclonal (abcam, ab5392, 1:1000), rabbit anti-glial fibrillary acidic protein (GFAP) polyclonal (Millipore, AS5804, 1:1,000), rat anti-CTIP2 monoclonal (abcam, ab18465, 1:100), and mouse anti-SATB2 monoclonal (abcam, ab51502, 1:100)) were diluted in blocking buffer then added to the permeabilized cultures. Cells incubated with primary antibody solutions were maintained overnight at 4°C. Cells were then rinsed four times with PBS and incubated with their respective secondary antibodies diluted in blocking serum: goat anti-chicken Alexa 488 (A11039), goat anti-chicken Alexa 568 (A11041), donkey anti-rat Alexa 488 (A21208), donkey anti-mouse Alexa 568 (A10037), and donkey anti-rabbit Alexa 568 (A10042) at 1:200 (Molecular Probes) for 2 hrs at room temperature. After rinsing four times in PBS, cells were mounted with Vectashield hard-set mounting medium with DAPI (HI500, Vector Laboratories, Burlingame, CA) onto glass slides and allowed to dry before imaging. The cells were photographed using a Zeiss LSM 510 confocal microscope. Expression of the respective antibodies was then quantified manually to compare the effects of medium and surface on the proportion of cells staining positive for CTIP, SATB2, GFAP, and MAP2. Positive and negative controls were run to ensure secondary antibodies were not significantly contributing to background staining and that primary antibodies were functioning as anticipated (Supplemental Figure 3-8). Only cells with intact nuclei staining positive for DAPI were counted and cumulative frequency analysis was performed to ensure enough cells were qualified to appropriately represent

the mean. A minimum of 75 cells per condition per replicate were counted from three separate cultures.

Patch-clamp electrophysiology

Whole-cell patch clamp recordings were performed in a chamber on the stage of an upright microscope (Axioscope FS2, Carl Zeiss, Göttingen, Germany). The chamber was filled with the same medium as utilized for cell culture (+10 mM HEPES buffer). The osmolarity was approximately 296 mOsm and 233 for the HSL1 and MM respectively. The intracellular solution composition was: 140 mM K-gluconate (Sigma, G-4500), 4 mM NaCl (Fisher, S642-212), 0.5 mM CaCl₂ (Fisher, C70-500), 1 mM MgCl₂ (Sigma, 63068), 1 mM EGTA (Fisher, 02783-100), 5 mM HEPES acid (Fisher, BP310-100), 5 mM HEPES base (Fisher BP410-500), 5 mM Na₂ATP (Fisher, BP413-25). Osmolarity was adjusted to between 25-40 mOsm less than extracellular solutions. The near-physiological pH of the medium was monitored with phenol red indicator. Borosilicate glass patch pipettes (BF150-86-10; Sutter, Novato, CA) were prepared using a Sutter P97 pipette puller. A pipette resistance of 4–10 MΩ was used for all intracellular patch clamp recordings. Voltage clamp and current clamp experiments were performed with a Multiclamp 700B amplifier (Axon Instruments, Foster City, CA, USA). Signals were filtered at 2 kHz and digitized at 20 kHz with an Axon Digidata 1322A interface. To generate a single action potential (AP), a 3 ms depolarizing current pulse of sufficient intensity (1-2 nA) was applied. Inward and outward currents were evoked by a series of 250 ms depolarizing steps from -70 to +170 mV with +10 mV increments. Before seals (1 GΩ) were made on cells, offset potentials were nulled. Capacitance subtraction was

used in all recordings. Data recording and analysis were performed using pClamp 10 software (Axon Instrument, Foster City, CA, USA).

Statistical analysis

To determine significant differences in cell viability, expression levels of neuronal markers, and rates of repetitive AP firing, Chi-Squared Goodness of Fit tests were performed across surface treatments and medium compositions at each time point examined. Multiple regression analyses were also performed on repetitive firing data to assess temporal trends. Longest neurite measurements were calculated from a minimum of 75 cells per condition using image analysis software (ImageJ; National Institutes of Health, Bethesda, MD). Longest neurite and electrophysiology data were log-transformed where necessary to reduce variation and/or normalize data before running two-way ANOVA followed by Tukey's test for multiple comparisons; one-way ANOVAs were run to compare day 7 and 28 data for full width half max (FWHM) and AP rise time. For each experiment, data was collected from a minimum of three independent cultures and all electrophysiological measurements were averaged from a minimum of 15 cells. For all data analyzed, a P value of less than 0.05 was considered significant. Data is presented as mean \pm standard error of the mean.

Results

Human iPSC-derived neurons were maintained on DETA or laminin coated coverslips for 28 days DIV. Cells established on these surfaces were either maintained in CDI Complete Maintenance Medium (MM) or a serum-free medium developed by the Hybrid Systems Laboratory (HSL1) optimized for the maintenance of primary adult rat hippocampal neurons [83]. Electrophysiological and biomolecular analysis of these cells was performed at various time-points throughout the culture period in order to fully evaluate cell viability, morphology, identity and functional maturity over time *in vitro*.

Cell purity and neuritic outgrowth analysis

The commercially-available iCell neurons are known to be relatively pure neuronal populations; however, as culture conditions were changed from what was recommended by the manufacturer, cell purity was reevaluated. In order to ascertain the neuronal purity of the cultures maintained in the different conditions, cells were fixed and stained for the neuron-specific marker MAP2 and the glial marker glial fibrillary acidic protein (GFAP) following 7 and 28 DIV (Figure 3-1). Cells stained at a rate of close to 100% positive for MAP2 whereas almost no positive staining (only two cells across all conditions; Supplemental Figure 3-8A) was observed for GFAP in any culture system combination, indicating the high degree of neuronal purity of the iCell Neurons.

In order to assess the effect of surface and media compositions on neuritic outgrowth, the longest process from a minimum of 75 cells was measured for each condition at 1, 3 and 7 DIV. Analysis of the collected data indicated that a significant difference in neuritic

extension existed between cells maintained on laminin and DETA surfaces and between those fed with MM and HSL1 ($p < 0.001$, Figure 3-2). Biopolymer coated surfaces promoted a greater level of neurite growth over 7 DIV than did DETA treated surfaces. Similarly, medium composition had a significant effect on process development. On laminin surfaces, cells maintained in MM had an average neurite length of $123.60 \mu\text{m}$ (± 1.65) after 7 DIV. Cells maintained in HSL1 were significantly shorter after 7 DIV ($p < 0.001$), with a mean length of $103.65 \mu\text{m}$ (± 5.59). On DETA surfaces, cells grown in MM for 7 DIV had an average neurite length of $55.87 \mu\text{m}$ (± 1.67) which was significantly shorter than cells maintained in HSL1 which possessed an average neurite length of $79.03 \mu\text{m}$ (± 2.55). Although both medium and surface conditions had a significant effect on neurite outgrowth, the effect of surface treatment was substantially greater than that of medium composition, with laminin promoting roughly 40% longer neurites than DETA after 24 hours in culture.

Cell survival and viability over 28 day culture period

Phase contrast images of cultured cells were collected at 1, 7, 10, 14, 21 and 28 DIV and then counted in order to assess viability across all surface types and media compositions. The number of cells per mm^2 was calculated and normalized to results from day 1 to ascertain whether cell number per unit area increased or decreased in relation to the cell numbers present at the time of plating across different culture parameters (Figure 3-3).

In all culture conditions examined, cell survival was found to drop over the 28 day culture period at a rate of 0.8% cells per day in HSL1 and 1.6% cells per day in MM; this

difference in rate of cell death was statistically significant ($p = 0.04$). Cell survival was significantly improved when cells were maintained in HSL1 ($p < 0.001$), where the cultures indicated a 40% improvement in cell viability at 28 DIV. The disparity observed between DETA cultures using different media indicates an important interplay between surface and medium composition for maintaining cells *in vitro*. The best conditions for promoting long-term cell survival was HSL1 on DETA surfaces, which promoted significantly greater survival over 28 DIV than all other conditions ($p < 0.001$). As these hiPSC-derived cells are non-proliferative and the factors added to the HSL1 medium are not known to induce cell proliferation, the fact that no significant increase in cell number was observed at any time in any culture condition reiterates that cell division was not occurring in these cultures regardless of medium compositions or surfaces tested.

Characterization of neuronal phenotype

Characterization experiments were conducted using immunocytochemical analysis to identify whether the neurons expressed markers for specific cortical layers following 7 DIV. All cultures examined were negative for the upper cortical layer marker SATB2 (embryonic rat hippocampal cultures served as positive controls; Supplemental Figure 3-8B), but a subpopulation was positive for the deep layer V marker of subcortically projecting neurons, CTIP2 (Figure 3-4). No significant differences in CTIP2 immunostaining were observed between different culture parameters, with all conditions containing roughly 44% CTIP2 positive cells.

Electrophysiology

Electrophysiological maturity of cells maintained under different culture conditions was assessed after 7, 14, 21 and 28 DIV. Representative recordings from cells at 7 DIV and 28 DIV reveal general trends in electrophysiological maturation: increased inward and outward current (Figure 3-5, top), increased capacity for repeat firing (Figure 3-5, middle), and ability to fire robust APs (Figure 3-5, bottom)..

Detailed analysis of electrophysiological data obtained from endpoint (28 DIV) studies indicated significant differences in the properties of cells maintained with the medium and surface combinations utilized in this study (Figure 3-6). Laminin surfaces in combination with HSL1 ($-54 \text{ mV} \pm 1$, $n = 21$) produced cells with significantly higher resting membrane potentials than laminin with MM ($-51 \text{ mV} \pm 2$, $n = 16$, $p = 0.02$), DETA with MM ($-46 \text{ mV} \pm 1$, $n = 15$, $p = 0.001$) and DETA with HSL1 ($-49 \text{ mV} \pm 2$, $n = 16$, $p < 0.001$). Similarly, laminin with HSL1 cultures produced significantly greater peak inward currents than all other culture conditions investigated ($-1513 \text{ pA} \pm 177$, $p < 0.005$). DETA with MM cultures produced significantly smaller peak inward ($-454 \text{ pA} \pm 44$, $p < 0.001$) and outward ($522 \text{ pA} \pm 77$, $p = 0.001$) currents than all other experimental conditions, suggesting this combination of medium and surface type is less capable than others investigated for promoting functional maturation of iCell Neurons. However, no significant differences were observed in AP peak amplitudes from cells maintained in different conditions, indicating that even the poorer culture conditions investigated were able to support robust electrical function in these cells. Analysis of iCell Neurons electrophysiological properties over time in culture (Supplementary Figure 3-9) indicates

the relative functional stability of these cells over this 28 day culture period. Some variability is apparent between culture conditions, with MM/ DETA producing consistently poorer inward and outward currents over time, supporting the observations made from 28 day analysis discussed above. However, the collected data suggest all investigated parameters were capable of maintaining functional performance of these cells *in vitro* over the time course investigated.

Assessment of rates of repetitive firing of APs across all conditions highlighted a trend toward increased incidences over time *in vitro* ($p = 0.004$, Figure 3-6E). Rates of repetitive fire increased significantly across conditions from 7 to 14 DIV and again from 21 to 28 DIV ($p < 0.001$), indicating the improved functional performance of cells over these time periods. The fact that further maturation of electrophysiological profiles occurred after the 2 week culture period previously examined^[81] highlights the importance of long-term evaluation of cells in order to identify appropriate experimental end-points for future studies. The majority of patched cells fired repetitively at 28 DIV, with the exception being those maintained in MM on DETA where only 40.0% of patched cells displayed such behavior. This observation correlates with cell viability data for this culture condition, which indicated the largest decrease in cell numbers at this time point, and highlights the unsuitability of this surface and medium combination for maintaining long-term cultures of these iPSC-derived neurons *in vitro*. Additionally, the medium used had a significant effect on the number of cells capable of repetitive firing ($p = 0.03$), with an increase of approximately 15% of the total cells repetitively firing in HSL1 medium versus MM. The surface on which the cells were grown was not

a significant contributor to the ability of the cells to repetitively fire ($p = 0.15$). The highest rate of repetitive firing was 81.3% of patches seen in cells maintained in HSL1 on DETA at 28 DIV. Cells in MM or HSL1 on laminin had repetitive firing rates of 62.5% and 66.7% respectively at this time point. Given this high level of functional maturity at this late stage, the data suggests 28 DIV as a suitable sampling time-point for end point analysis of these *in vitro* cultures.

The maturation of AP waveforms between 7 and 28 DIV were investigated in cells maintained across all described conditions. Results indicate that cells cultured in HSL1/laminin conditions exhibited the shortest AP FWHM after 7 days ($4.77 \text{ ms} \pm 0.42$), and maintained this short FWHM to 28 DIV ($4.77 \text{ ms} \pm 0.31$, Figure 3-7A, $p < 0.05$). Although HSL1/laminin showed no maturation of AP waveform between 7 and 28 days (as measured by FWHM), its performance at 7 days was already significantly improved over other conditions ($p < 0.05$). This result therefore suggests that HSL1/laminin culture conditions promote rapid maturation of AP waveform, which is then maintained up to 28 DIV. Notably, HSL1/DETA promoted improvement of FWHM between 7 ($10.14 \text{ ms} \pm 1.69$) and 28 DIV ($5.98 \text{ ms} \pm 0.70$) ($p < 0.05$), but the data recorded at 28 DIV was not significantly different from that recorded from cells in the HSL1/laminin condition. The significant difference between HSL1/DETA and HSL1/laminin at 7 days ($p < 0.05$) suggests maturation was slower on DETA than on laminin in this medium. All cultures grown in MM, regardless of surface treatment, were unable to reach AP duration times similar to those grown in HSL1 at 28 DIV ($p < 0.05$). There were no significant

differences in any medium or surface combination that significantly effected AP rise time (Figure 3-7B, $p < 0.05$).

Discussion

The ability to use mature, fully functional human neuronal tissue *in vitro* can be a vital tool in the development of high-throughput drug test-beds that mimic *in vivo* biocomplexity. Development of robust assays using hiPSC-derived neurons however could give a higher level of statistical homogeneity when translating bench-top research to clinical studies, and may uncover new options for personalized medicine in neurodegenerative disease, psychiatric disorders, and stroke recovery. Establishment of such cell lines is predicated on the full characterization of molecular markers and electrophysiological function to allow accurate comparison to relevant clinical and pre-clinical data.

This study highlights that commercially available hiPSC-derived neurons demonstrate variable viability, neuritic development and functional maturation depending on the combination of medium and culture surface to which they are exposed. The cultured cells were found to be almost a pure neuronal population, as indicated by consistent MAP2 marker expression and lack of significant GFAP expression across all experimental conditions and time points examined. Between 7 and 28 DIV, the number of neurons, as a percentage of the cultured cell population remained constant, suggesting the absence of proliferative neuronal precursor cell types. This stability is important for body-on-a-chip devices where stable populations are necessary to facilitate long-term assessment of drug effects [77-80].

Typical neuronal morphology was observed across all biological and chemically-modified surfaces and media types examined. However, differences in neurite outgrowth were observed across examined culture surface and medium combinations. Laminin-treated substrates promoted a 40% increase in neurite extension compared with DETA counterparts after 24 hours, and this difference persisted across the subsequent 6 days analyzed. This observation correlates with previous data highlighting the role of laminins in promoting neuritic development both *in vivo* and *in vitro* studies [95, 96]. Control over extensive neuritic outgrowth could be advantageous for body-on-a-chip applications since laminin proteins could be deposited in areas where outgrowth is necessary over prolonged distances. While this attribute has its advantages, use of laminin in body-on-a-chip devices as a culture substrate may cause neurite tracks to extend beyond desired targets. While it is true that physical barriers may be utilized to control neuronal architecture, this is not always a feasible option where intricate nano- or micro-scale features may be destroyed by the addition of such barriers. Restrained neuritic development, such as that observed on DETA-treated surfaces, may be advantageous for chip-based technologies since multi-organ biomimetic devices require the manipulation of surface cues at key areas to aid efforts in directing neuritic development to reach target cell types. Such cues can be altered to suit the complex architecture of chip based devices and be tailored to suit specific experimental parameters.

Significant differences in neurite growth rates were likewise observed between media types investigated in this study. MM showed a significant improvement over HSL1 for

promoting neurite outgrowth from cells cultured on laminin surfaces. Conversely, HSL1 promoted significantly greater outgrowth on cells maintained on DETA. This disparity indicates a level of synergistic effect between surface and medium on cellular development *in vitro*. Since HSL1 was developed for use with DETA surfaces, and the MM was similarly optimized for laminin substrates, it seems logical that these combinations would perform better than their counterparts (MM/DETA and HSL1/laminin). However, it also points out the danger from simply substituting one variable in a culture system and expecting positive results.

Human iPSC-derived neurons grown in MM have been assessed over short (2 week) time courses [81]. Cell viability data from this study highlights that while MM is likewise capable of promoting high levels of cell survival over 4 week culture periods, HSL1 medium promotes significantly greater cell survival over the same period. This is not surprising, since HSL1 medium was specifically developed for promoting the long-term survival and development of hippocampal neurons in culture [61, 83]. The observed differences in cell survival highlight the importance of medium optimization for specific experimental protocols in order to ensure detected changes are due to experimental variables rather than unoptimized culture conditions.

RT-PCR and immunocytochemical analysis of iCell Neurons as reported by CDI demonstrate the culture as mixed populations primarily of GABAergic and Glutamatergic neurons. Further gene expression analysis indicates the iCell neurons are representative of a forebrain identity as evidenced by regional expression of genes such as LHX2, FOXG1, OTX2, GBX2, and EN1 (private conversation with CDI).

However, further understanding of neuronal cell type specificity is important for assessing whether these cells are applicable to specific assays and drug toxicology experiments. Positive staining for the layer 5 specific pyramidal marker, CTIP2, indicates that roughly 44% percent of the cell population possesses a deep layer cortical phenotype in all tested culture conditions. All cultures examined were negative for the upper layer marker, SATB2, suggesting the remaining cells did not possess an upper layer cortical phenotype. The presence of a significant number of upper and lower level pyramidal markers which are stable in culture would be beneficial for investigators looking to model complex layered brain architecture such as that of the CA1 region of the hippocampus [97, 98]. However, given that the examined cultures were almost 99% positive for MAP2 but only 44% positive for CTIP2, there remains some ambiguity as to the specific neuronal identity of a significant proportion of these iCell neurons. Further in-depth characterization of these neurons would be useful for a complete understanding of the phenotypic origin of the cell sub-populations.

Data from patch-clamp experiments indicated that these hiPSC-derived neurons reach electrical functionality at early time points. By 7 DIV, hiPSCs are able to fire robust APs with peak amplitudes relatively similar to those seen in mature slice cultures of postnatal Wistar rats (reported as $91.35 \text{ mV} \pm 3.36$)[99] and macaque monkeys (reported as $83.1 \text{ mV} \pm 1.6$) [100] (Supplemental Figure 3-9). However, they continue to undergo functional maturation as evidenced by the increased inward and outward currents (Supplementary Figure 3-9), increased rates of repetitive firing over 28 DIV (Figure 3-6), and, in some cases, a reduction in FWHM. When examining the rate of development of

repetitive firing cells on different surfaces, it is apparent that laminin promoted a more rapid maturation of cultured neurons. By 14 DIV, laminin treated cultures already possessed repetitive firing behavior in roughly 54% of patched cells, compared with less than 40% in DETA treated cultures. The rate of repetitive fire on laminin surfaces levelled off in later time points whereas DETA cultures improved, suggesting a slower rate of maturation on these surfaces, but supporting earlier claims of the suitability of DETA for maintaining functional cultures in long-term systems. Regardless of surface/medium composition, all conditions reached numbers of cells capable of repeat APs firing similar to male guinea pig slice cultures where the number of cells repetitively firing was 38 – 59%, depending on the CA3 subregion of the hippocampus [101].

In developing cortical neurons, APs become larger and shorter in duration as a result of changes in expression of voltage-activated Ca^{2+} channels and rectifying K^+ channels [102]. Therefore, shortening of FWHM in cultured neurons is an important indicator of cellular maturation. Cells cultured in HSL1 medium exhibited an AP duration profile closer to that seen in mature rat and mouse slices [103, 104], indicating improved electrophysiological function in these cells. In HSL1 medium, cells on DETA surfaces exhibited improved FWHM between 7 and 28 DIV (Figure 3-7A). However, laminin surfaces already possessed short FWHM values by 7 days, indicating faster AP waveform maturation on this surface. This observation supports the repetitive firing data discussed above, and suggests that laminin surfaces promotes more rapid maturation of neuronal electrophysiological function. Interestingly, although AP duration was affected by medium composition and surface type, AP rise time was unaffected (Figure

3-7B). This result could indicate incomplete maturation that is not promoted by the culture conditions tested, or more likely that these cells already exhibit a mature sodium conductance profile capable of producing rapid AP rise times.

This study highlights the importance of considering surface characteristics and medium composition in terms of their likely effect on experimental parameters. Although these cells are functional at early time points, investigators should consider the maturation of electrical properties as cells may function differently at earlier vs. later time points in different culture conditions. This is especially important when investigating neurodegenerative diseases or any condition where functional performance is expected to change over time or a more mature functional phenotype is required.

The ability for hiPSC-derived neurons to survive in various culture conditions is necessary since complex body-on-a-chip devices require compatibility with different platforms, media types, and environments other than those defined by the manufacturer. Our results indicate that hiPSC-derived neurons display typical neuronal morphology and remain mitotically stable and differentiated for extended periods. Moreover, their ability to respond to chemical cues makes them an ideal candidate for *in vitro* modeling of complex neural architecture for body-on-a-chip applications. However, these cells exhibit significant variance in the development of electrophysiological performance over 28 DIV, and their ability to develop fully functional phenotypes is heavily influenced by culture conditions. The collected data therefore highlights the need to assess cellular performance under different culture conditions (e.g. surface and media type) in order to achieve optimal cellular development and maturation and for

integration of human-based *in vitro* systems for next-generation drug-screening applications.

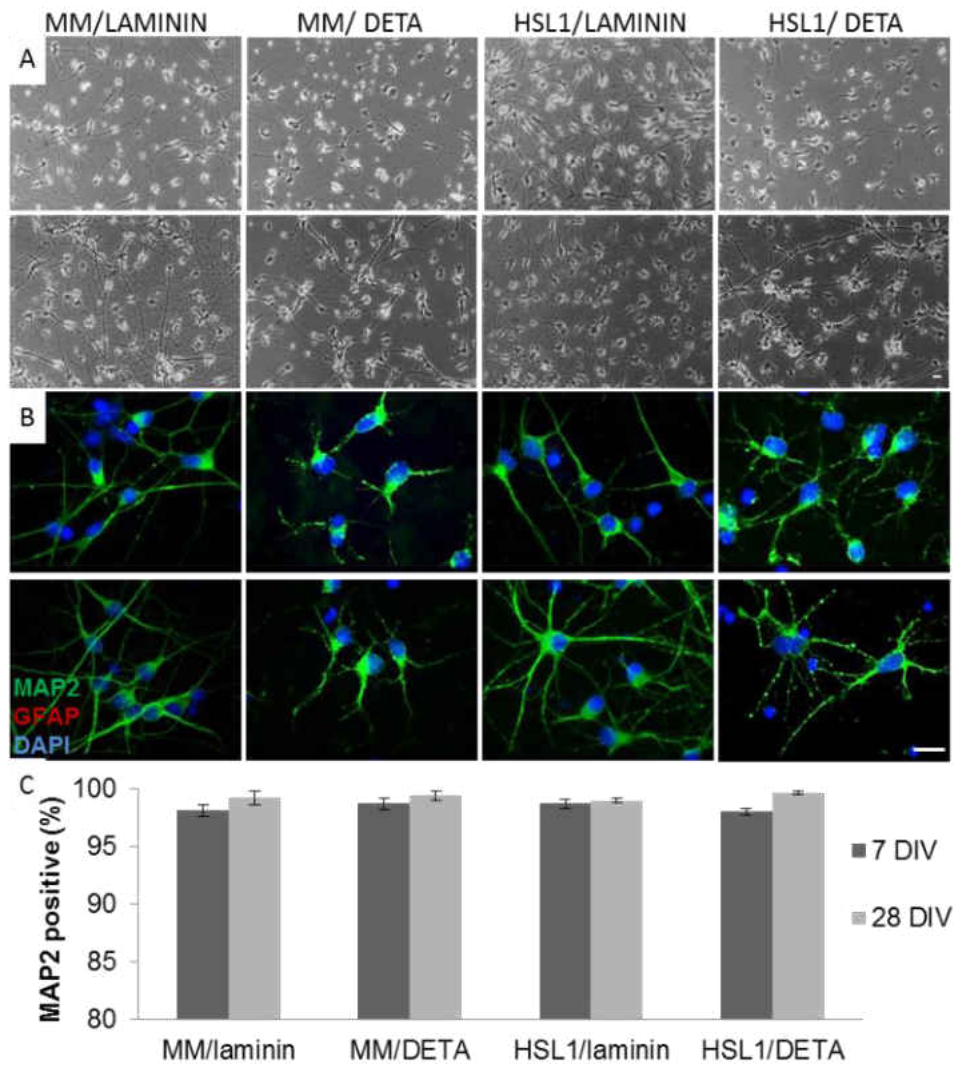


Figure 3-1. Human iPSC-derived cells thrive on both DETA and biopolymer surfaces. (A) Cells were cultured in MM on laminin, MM on DETA, HSL1 on DETA and HSL1 on laminin through a 28-day period (B) Immunological analysis for neural markers MAP2 (green) and GFAP (red) and the nuclear marker DAPI (blue). Images are representative of 7 DIV (top) and 28 DIV (bottom) of both panels. (C) Cells which stained positive for MAP2 were quantified at 7 and 28 DIV. Error bars represent SEM. Scale bar = 20 μ m.

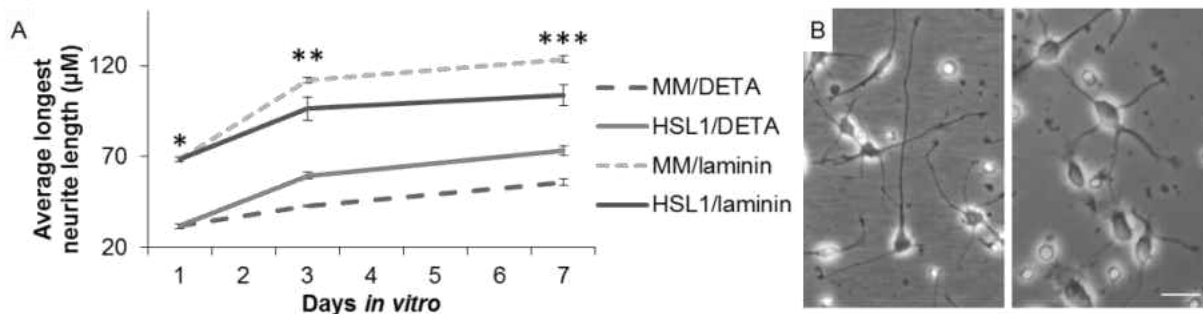


Figure 3-2. Neurite analysis of hiPSC-derived neurons. (A) The longest neurite length was measured at 1, 3, and 7 DIV across all culture combinations of MM and HSL1 media and DETA and laminin surfaces. (B) Representative phase images of cells grown on laminin (left) and DETA (right) in MM at 1 DIV. Significant differences were observed between surface types at 1 DIV and between both medium and surface types at 3 and 7 DIV, * $p < 0.001$, ** $p < 0.001$, *** $p < 0.001$. Error bars represent SEM. Scale = 30 µm.

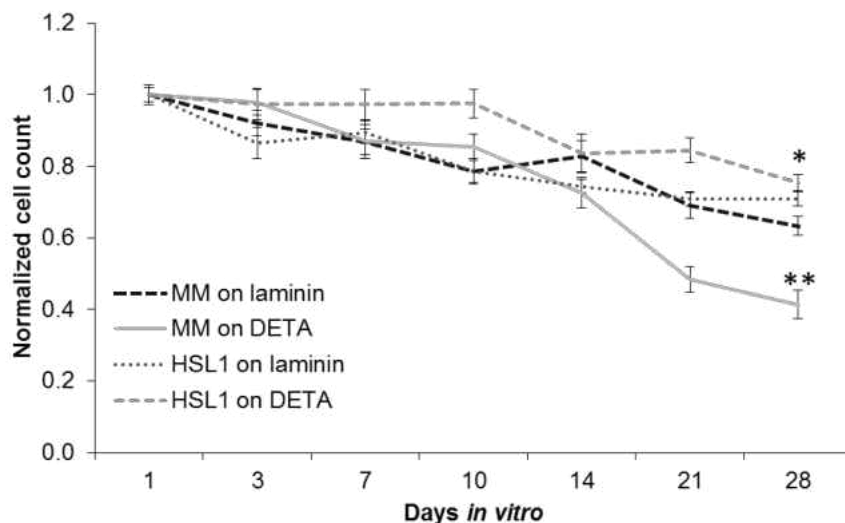


Figure 3-3. Viability of hiPSC-derived neurons over 28 DIV using different culture parameters. Cells were counted per mm^2 and normalized to day 1 counts to account for culture variability and ease comparisons between conditions. No discernable differences in survival trends were observed across all conditions examined over the first 10 days in culture. After 28 DIV, HSL1 on laminin promoted a significantly higher level of survival (* $p < 0.001$), whereas cells cultured in MM on DETA had significantly fewer viable cells (** $p < 0.001$). Error bars represent SEM.

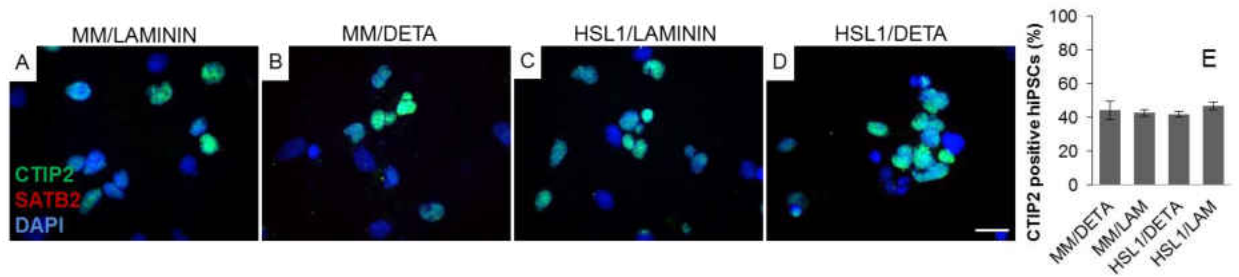


Figure 3-4. Human iPSC-derived neurons express lower layer cortical pyramidal phenotypic markers. Cells were stained for CTIP2 (green), SATB2 (red), and DAPI (blue) at 7 DIV in maintenance medium (A, B) and in HSL1 (C,D) on laminin (A,C) and on DETA (B,D) to assess potential layer identity. No cells stained positive for SATB2 in any condition. (E) Intact nuclei stained positive for DAPI but were not CTIP2 positive were quantified to estimate a percentage of CTIP2-positive neurons. Error bars represent SEM. Scale bar = 20 μ m.

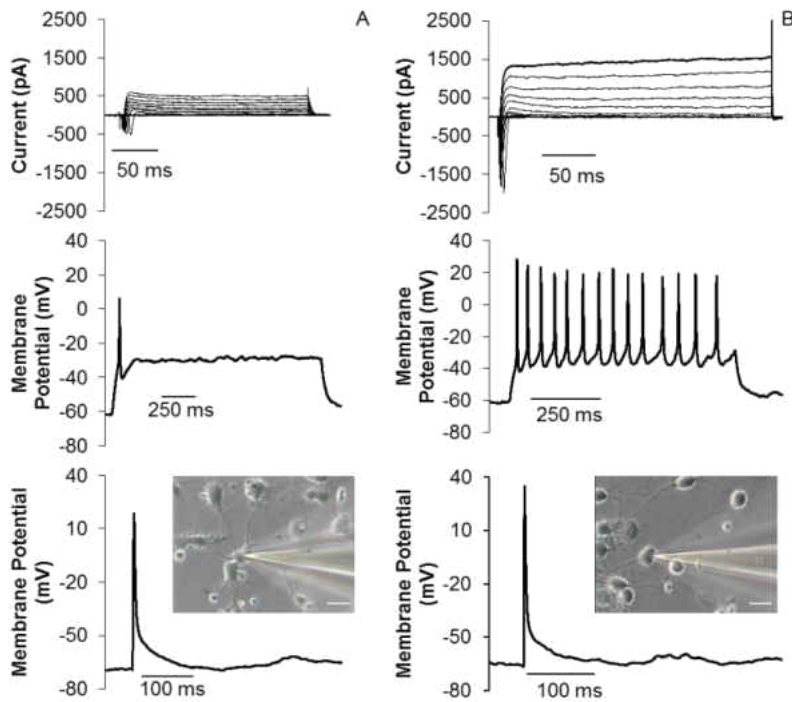


Figure 3-5. Representative electrophysiological recordings of hiPSC-derived neurons. Patch-clamp recordings were taken at 7 (A) and 28 (B) DIV. (Top) Voltage-clamp recording of inward sodium and outward potassium currents (-70 mV holding potential, 10 mV steps). (Middle) Neurons were not likely to fire repeatedly in response to depolarizing current injections at a -70 mV holding potential at 7 DIV versus 28 DIV. (Bottom) A single AP was generated using a 3 ms depolarizing current pulse of 1-2 nA. D. (Inset) Phase contrast image of patched neuron. Scale = 20 μ m.

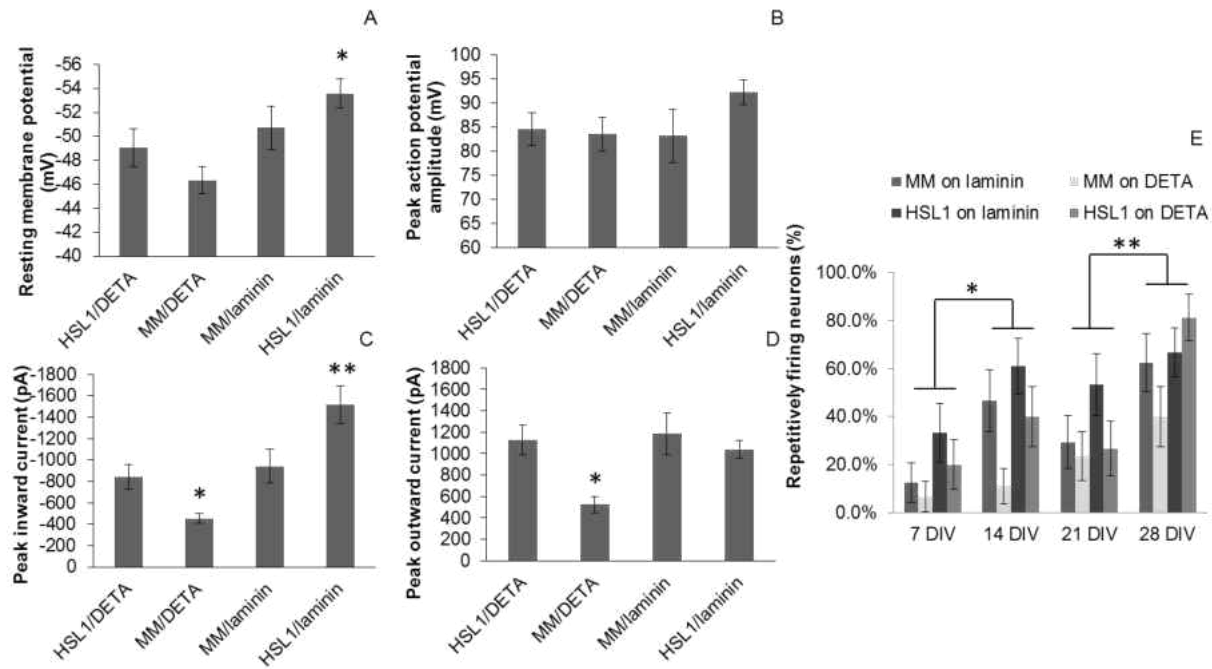


Figure 3-6. Patch-clamp data collected from hiPSC-derived neurons grown in the four different culture conditions. The resting membrane potential (A), AP amplitude (B), peak inward current (C), and peak outward current (D) are represented at 28 DIV. (E) The proportion of cells which repetitively fired APs in response to depolarizing current injections at a -70 mV across all time points evaluated. HSL1/laminin cultures had significantly higher resting membrane potentials (A, *** $p = 0.02$) and peak inward currents (C, ** $p \leq 0.005$). Peak inward (C) and outward currents (D) were significantly lower when grown in MM on DETA (* $p \leq 0.001$ and * $p \leq 0.001$, respectively). Rates of repetitive fire showed a generally increasing trend over time across all conditions (* $p \leq 0.005$) with significant increases across conditions from 7 to 14 DIV and again from 21 to 28 DIV (* $p \leq 0.001$), indicating the improved functional performance of cells over this culture period. Error bars represent SEM.

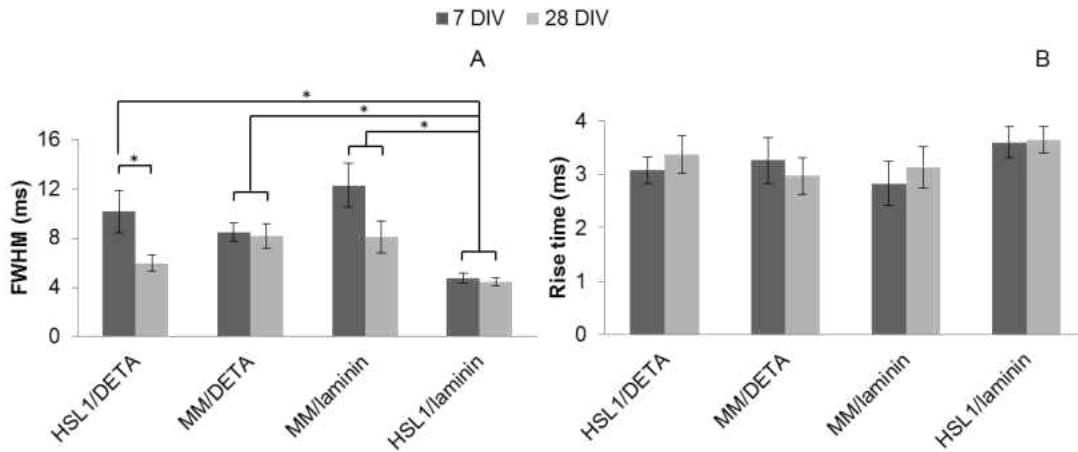
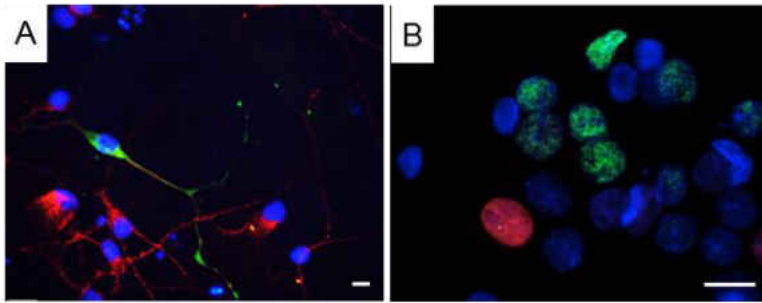


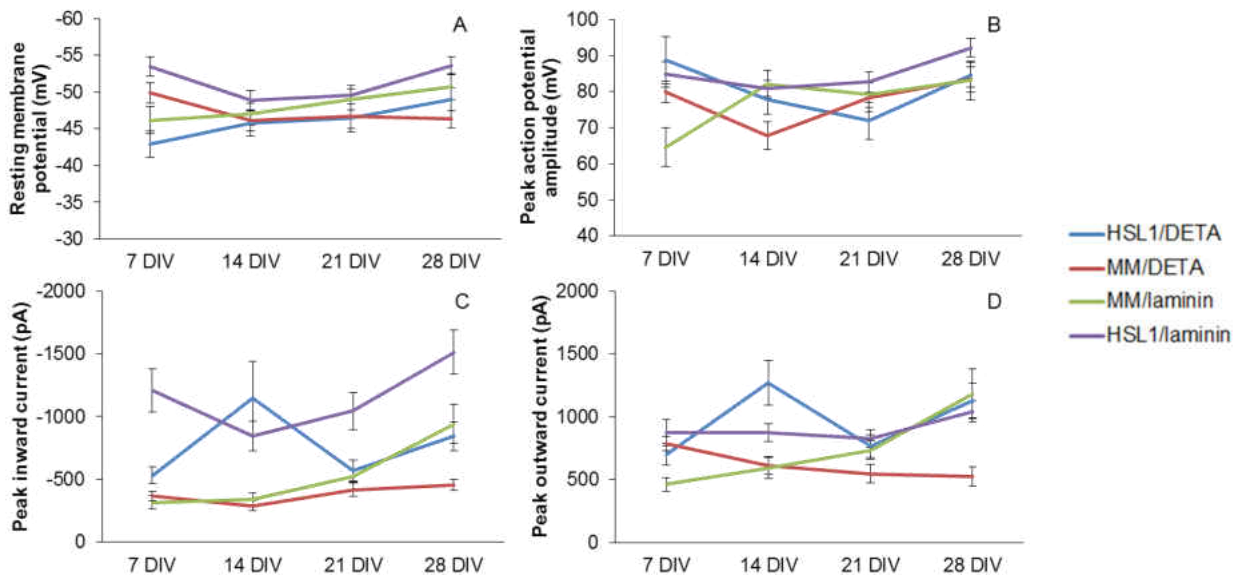
Figure 3-7. Full width half max and rise time comparison of 7 and 28 DIV cultures in various conditions. Values of FWHM (A) and AP rise time (B) were calculated for each condition at both 7 and 28 DIV. Cells cultured in HSL1/DETA showed a significant reduction in AP duration corresponding to a decrease in FWHM from 7 to 28 DIV. This reduction in FWHM resulted in values similar to HSL1/laminin, the condition which exhibited the shortest FWHM time. All cultures grown in MM, regardless of surface, were unable to reach AP duration times similar to those grown in HSL1 at 28 DIV. AP rise times were unaffected by culture medium or surface conditions. *p < 0.05. Error bars represent SEM.

Table 3-1. Composition of HSL1 medium.

| Vendor | Component | Catalog # | Quantity |
|-------------------|-----------------------------|-----------|----------------|
| Invitrogen | Neurobasal®-A | 10888 | 500 mL |
| Invitrogen | B-27® | 17504-044 | 1x |
| Invitrogen | GlutaMAX™ | 35050-061 | 1x |
| Invitrogen | Antibiotic/Antimycotic | 15240-096 | 1% |
| Cell Sciences | BDNF, recombinant human | CRB600B | 20 ng/mL |
| Cell Sciences | NT-3, recombinant human | CRN500B | 20 ng/mL |
| Sigma | Insulin-like Growth Factor | I2656 | 20 ng/mL |
| Fisher Scientific | Adjust osmolarity with NaCl | S671-3 | 297 mOsm final |



Supplemental Figure 3-8. Immunostaining of human and embryonic rat neurons. Only two human iPSC-derived neurons out of all conditions examined stained positive for GFAP (green) (A). No human iPSC-derived neurons positively stained for the marker SATB2, whereas positive control embryonic rat hippocampal cultures stained positive for both SATB2 (red) and CTIP2 (green) (B). Scale bar = 20 μ M.



Supplemental Figure 3-9. Patch-clamp data collected from hiPSC-derived neurons grown in various conditions. The resting membrane potential (A), peak AP amplitude (B), peak inward current (C), and peak outward current (D) are represented across all time points evaluated. Error bars represent SEM.

CHAPTER 4 – PHYSIOLOGICAL A β CONCENTRATIONS PRODUCE A MORE BIOMEMETIC REPRESENTATION OF ALZHEIMER'S DISEASE PHENOTYPE IN CULTURED HUMAN NEURONS

Introduction

Alzheimer's disease (AD) is a worldwide pandemic estimated to have affected 26.6 million people in 2006. By the year 2050, this figure is projected to quadruple without pharmacological intervention [105]. Given the increased rate of diagnosis and the rising expense associated with long-term personal care, the cost of treating AD is estimated to reach \$1 trillion in the USA alone by 2050 [106].

Only five FDA-approved medications are currently on the market. Though these medications are widely prescribed to treat the cognitive symptoms of AD, there is much debate over their effectiveness [93, 107-109]. In spite of the significant progresses in elucidating the biological mechanisms of AD [110, 111], no practical treatments exist which prevent or significantly delay its progression.

Contributing to the dearth of effective medications for treating AD is the lack of robust, biomimetic models that accurately recapitulate the pathophysiology of the condition in human tissue. Without a reliable humanized model, progress in therapy development and testing is seriously hindered. Current animal models, including a wide variety of species [83, 112], poorly represent complex human neurochemistry and neurodegeneration [113]. As of March 2014, more than three dozen drugs have failed in AD clinical trials despite positive pre-clinical data from over two dozen transgenic models [114]. With recent advances in the development of robust, neuronal human

induced pluripotent stem cell (hiPSC) lines [115-119], there is an opportunity to develop a human-based *in vitro* disease model for AD which may lead to better translation of lab research to clinical results.

Amyloid- β is known to be a crucial causative protein in AD development [120, 121]. Disease progression is linked to accumulation of A β and formation of plaques and phosphorylated tau tangles, leading to reduced neuronal activity and eventually cell death. Specifically, low-weight A β oligomers, not monomers [122] or fibrils commonly associated with disease endpoints, have been shown to be the primary pathological species [123-129]. Amyloid beta protein dimers directly isolated from AD patients have been shown to impair synaptic plasticity and memory but not the amyloid plaque cores from which they were derived [123]. In particular, A β 1-42 oligomers have been shown to induce calcium dyshomeostasis by depleting endoplasmic reticulum calcium [130] in rat cultures, were elevated in transgenic mice which had significant learning and memory deficits [131] and correlate strongly with dementia in elderly patients [127, 132-134].

Treatment of cultured neurons with A β has long been used as a means to model AD *in vitro*. However, the fact that we see poor translation of *in vitro* studies to the clinic suggests these models are poor representations of the disease. Studies commonly use non-physiological A β concentrations to achieve neuronal impairment *in vitro* [135-140]. This is problematic because opposing effects have been reported when investigating higher than physiologic concentrations of A β [83]. Furthermore, the high rates of cell death and expression of tau tangles in response to such treatments is representative of

late-stage AD. Targeting therapeutics to treatment of this late-stage phenotype is inappropriate since neurological damage is already severe, and so likely to be irreversible. Moreover, acute treatment with nonphysiologically relevant doses to promote rapid neurodegeneration is fundamentally unrepresentative of AD progression *in vivo*, and so poorly suited to mechanistic studies of early disease states. We hypothesize that chronic exposure of human neurons to a physiologically representative dose of A β will produce an *in vitro* phenotype which more closely represents early-stage AD pathology, and therefore a more appropriate model for evaluating novel AD therapeutics.

Materials and Methods

Cell culture

Human iPSC-derived neurons (Cellular Dynamics International, iCell Neurons NRC-100-010-001) were plated at 700 cells per mm² according to manufacturer's instructions. Cells were plated in maintenance medium (NRM-100-121-001 with NRM-100-031-001) and incubated overnight at 37°C 5% CO₂. Plated cells were changed to Hybrid Systems Laboratory Medium 1 (HSL1) without phenol red as phenol red may interact with amyloidogenic compounds [141]. HSL1 was specifically developed to facilitate the long-term survival and maturation of hippocampal neurons [142] (Berry et al. 2015). Medium was changed every 3-5 days and maintained over 28-30 days *in vitro* (DIV). Chronic treatment of 10 nM A β , a dose close to physiological A β concentrations [143], began at 7 DIV to give cellular networks enough time to establish robust connections (Berry et al 2015). Acute, 48 hr treatments of 10 nM and 5 μ M A β were performed 2 days prior to patch clamp electrophysiology (26-28 DIV).

Surface modification

Cells were plated onto laminin-coated (Sigma, L2020, 3.3 μ g/mL) coverslips which had been treated with the self-assembled monolayer, N-1(3-[trimethoxysilyl]propyl)-diethylenetriamine (DETA, United Chemical Technologies Inc., Bristol, PA, T2910KG). Briefly, plasma-cleaned glass coverslips (Thomas Scientific 1217N81, 18 mm, no. 1.5) were silanized with a 0.1% (v/v) mixture of DETA in freshly distilled toluene (Fisher T2904) as described previously [144]. The DETA-treated glass was heated to just below

the boiling point of toluene (70°C), rinsed with toluene, reheated to 70°C, and then dried in an oven overnight at (100-105°C). Surfaces were validated via contact angle measurement and X-ray photoelectron spectroscopy as described previously [145]. Laminin was added to DETA-treated glass overnight at 4°C. DETA has previously been used for long-term culture of multiple cell types, including neurons [57, 61, 94, 97, 146], and enhances the adsorption of laminin onto the culture surfaces (see Supplemental Figure 4-5).

Amyloid- β oligomer preparation

Amyloid- β oligomers (Bachem, H-1368) were prepared as described previously [147]. Briefly, A β peptide was monomerized using HFIP (Sigma-Aldrich, 105228) and dried overnight. Peptide films were further dehydrated with dry nitrogen and stored under desiccant at -80°C until use. Peptide films were resuspended in dimethylsulphoxide (DMSO) and diluted to 100 μ M in Neurobasal A medium without phenol red (Invitrogen, 12349-015). Peptide suspensions were allowed to oligomerize for 24 hrs at 5°C before use. Preparations of A β ₁₋₄₂ were centrifuged at 14,000 rpm to remove any large fibrils and the supernatant was then diluted in phenol red-free medium for immediate use. The final concentration of DMSO was \leq 0.1%.

Oligomer characterization

A β protein was prepared using a protocol known to produce low-weight oligomers [147]. To confirm the success and quality of our oligomerization protocol, gel electrophoresis of pure A β protein was performed, followed by a coomassie blue stain. Mini-PROTEAN® 10-20% Tris-Tricine Precast Gels (Bio-Rad, 456-3113) were loaded with

the purified A β peptide suspended in Tricine Sample Buffer (Bio-Rad, #161-0739), and electrophoresed for 1-2 hrs at 120 V in Tris-Tricine SDS buffer (Sigma-Aldrich, T1165). Gels were then stained with Coomassie Brilliant Blue (Bio-Rad, 161-0786), and destained (Bio-Rad, Coomassie Brilliant Blue R-250 Destaining Solution 161-0438161-0438) to evaluate low-weight oligomer formation (Supplemental Figure 4-6).

MTT assay

MTT solution (Thiazolyl Blue Tetrazolium Bromide (Sigma, M5655) at 5 mg/mL in PBS) was added to cultures at a 1:5 ratio and incubated for 2-3 hrs. The MTT solution/culture medium was then removed and fresh lysis buffer (1% SDS and 0.57% glacial acetic acid in DMSO) was added to wells, triturated, and transferred to a 96-well plate (Falcon, 3-353070). Cell viability was then assessed using a plate reader (Bio-Tek, KC4 Synergy HT) to detect emission levels at 570 nm and thereby quantify purple formazan byproduct levels in each sample. Emission levels were normalized to background levels achieved when measuring MTT/culture medium solution from wells with no cells plated.

Immunocytochemistry

Cultures were fixed using 4% paraformaldehyde for 20 mins before being rinsed with phosphate-buffered saline (PBS) at 4°C. Cells were then permeabilized for 20 mins with 0.2% Triton X-100 in PBS and incubated at room temperature for 2 hrs in blocking buffer (2.5% donkey serum, 2.5% goat serum, and 0.5% BSA) to prevent non-specific antigen binding. Primary antibodies rabbit monoclonal anti-microtubule associated protein tau (abcam, ab32057, 1:250), and chicken polyclonal anti-beta-III tubulin (Millipore, ab9354, 1:1,000) were diluted in blocking buffer then added to the

permeabilized cultures and maintained overnight at 4°C. Cells were then rinsed four times with PBS and incubated with their respective secondary antibodies diluted in blocking serum: goat anti-chicken Alexa 568 (A11041) and donkey anti-rabbit Alexa 488 (A21206) at 1:200 (Molecular Probes) for 2 hrs at room temperature. After rinsing four times in PBS, cells were mounted with ProLong® antifade reagent (Life Technologies, P36930) onto glass slides. The cells were imaged using a Zeiss LSM 510 confocal microscope. Expression of the respective antibodies was then quantified with ImageJ [148] by measuring the integrated density and normalizing to cell number. Results are expressed relative to values recorded for untreated controls. A minimum of 50 fields of view at 40x magnification were quantified per condition.

Patch-clamp electrophysiology

Electrophysiological properties of hiPSC-derived neurons were investigated after 28-30 DIV. Whole-cell patch clamp recordings were performed on the 37°C heated stage of an upright microscope (Axioscope FS2, Carl Zeiss, Göttingen, Germany). Extracellular recordings were performed in the same medium used for cell culture (+10 mM HEPES buffer), including drug treatments. The intracellular recording solution (140 mM K-gluconate, 4 mM NaCl, 0.5 mM CaCl₂, 1 mM MgCl₂, 1 mM EGTA, 5 mM HEPES acid, 5 mM HEPES base, and 5 mM Na₂ATP) was loaded into borosilicate glass patch pipettes (BF150-86-10; Sutter, Novato, CA) produced with a pipette puller (Sutter, P97). Patch pipettes with a resistance in the range of 6–10 MΩ were used for all recordings. Voltage-clamp and current-clamp experiments were performed with a Multiclamp 700B amplifier (Axon Instruments, Foster City, CA, USA). Signals were filtered at 2 kHz and

digitized at 20 kHz with an Axon Digidata 1322A interface. Offset potentials were nulled before formation of a giga Ω seal and fast and slow capacitance was compensated for in all recordings. Membrane potentials were corrected by subtraction of a 15 mV tip potential, calculated using Axon's pClamp10 software (Axon Instrument, Foster City, CA, USA). To generate a single action potential (AP), a 3 ms depolarizing current pulse of sufficient intensity (1-2 nA) was applied. Inward and outward currents were evoked by a series of 250 ms depolarizing steps from -70 to +170 mV with +10 mV increments. Depolarization-evoked repetitive firing was recorded in current clamp mode. Gap-free recordings of spontaneous activity of patched neurons were performed for up to 5 m while holding the cell membrane at optimal threshold (between -45 and -50 mV). All recordings and analysis were performed using pClamp 10.

Statistical analysis

One way analysis of variance (ANOVA) tests were performed to assess differences between treatments of hiPSC-derived neurons followed by Student-Newman-Keuls Method tests. Post hoc Student-Newman-Keuls Method tests were also performed on data sets that did not have equal variance (resting membrane potential, MTT) but had a normal distribution of data. Data that had equal variance but were not normally distributed were analyzed using ANOVA on ranks, followed by the Dunn's method for multiple comparisons (inward and outward currents, max rep firing, rise time). Square root transformations were performed on the spontaneous firing and maximum repetitive firing data sets to properly condition them for ANOVA analysis. Statistical differences in tau protein staining intensity between each A β treatment and untreated controls were

independently assessed via student's t-test. Each experiment included data collected from at least 3 independent cultures. Data is presented as mean \pm standard error of the mean.

Results

Cell morphology and viability

In all conditions, phase-contrast microscopy revealed cells which appeared healthy and had extensive neuritic outgrowth over the 4 week culture period. Phase images showed similar gross morphology across conditions, with no obvious aberrant morphological changes upon addition of A β (Figure 4-1A). Assessment of cell viability by MTT assay yielded no significant differences between control and treatment with 10 nM A β , both acute and chronically ($p > 0.05$, Figure 4-1B). However, treatment with 5 μ M A β significantly reduced cell viability compared to control cultures ($p = 0.005$). In 5 μ M A β -treated cultures, viability dropped by 35.66% (± 5.75). Viability in acute and chronic 10 nM treated cultures were 103.93% (± 2.83) and 99.07% (± 3.96) respectively compared to untreated controls (Figure 4-1B). These differences were not significant ($p > 0.05$). These results indicate that chronic exposure to a pathological concentration of A β was insufficient to induce significant levels of cell death over a 4-week culture period. Acute A β treatment, with concentrations not representative of levels reported in human tissue, led to significant cell death after just 48 hours in culture.

Electrophysiological function

Representative electrophysiological recordings of control and treated neurons highlight (Figure 4-2A,B,C) the major differences in electrophysiological function quantified in Figure 4-3. The resting membrane potential of cultured neurons was significantly reduced in 5 μ M A β -treated cultures compared to untreated controls ($p = 0.034$, Figure

4-3A). Conversely, no significant difference in resting membrane potential was observed for either acute or chronic 10 nM treatments ($p > 0.05$). Inward sodium and outward potassium currents were significantly reduced in 5 μM $\text{A}\beta$ -treated cultures compared to control ($p < 0.05$) but were not significantly different among control and 10 nM-treated cultures ($p > 0.05$, Figure 4-3B,C).

The maximum number of APs fired during stimulation while holding the membrane potential at -70 mV was calculated for each condition. No significant differences were observed between control and 10 nM treated cultures ($p > 0.05$); however, 5 μM $\text{A}\beta$ -treated cultures were significantly lower than all other conditions ($p < 0.007$, Figure 4-3D). Despite this difference, AP amplitudes were not significantly different between any condition tested ($p = 0.410$, Figure 4-3E). However, while AP amplitude was unaffected $\text{A}\beta$ -treatment, AP waveforms were affected in 5 μM $\text{A}\beta$ -treated cultures as rise time and calculated FWHM values were significantly increased over control and 10 nM treated cultures ($p < 0.05$).

Spontaneous APs were recorded from patch-clamped cells with a gap-free protocol where current was held between -35 and -40 mV (Figure 4-3H). Again, 5 μM $\text{A}\beta$ -treated cultures were significantly hindered in function ($p < 0.001$). Similarly, chronic 10 nM treatment was significantly lower than control and 10 nM acute conditions ($p \leq 0.02$), suggesting impaired functional performance in both 5 μM acute and 10 nM chronic conditions.

Immunocytochemical analysis of tau expression levels

Immunostaining and confocal microscopy highlighted the presence of tau protein in cultured neurons under all examined conditions. Control and A β treated cultures were stained for presence total tau protein as early-stage tauopathies may include not only hyperphosphorylated tau but other toxic oligomers [149, 150]. The anti-tau antibody used detects both phosphorylated and non-phosphorylated tau. Analysis of positive staining intensity revealed increases in tau accumulation in response to A β treatment. Calculation of statistical differences suggested an upregulation of tau expression in 5 μ M treated cultures with a greater than 90% confidence interval ($p = 0.057$). The slight increase in positivity observed in 10 nM treated cultures was more modest, and insufficient to suggest any significant changes in tau expression over the time-frame investigated.

Discussion

A human-based neuronal culture system incorporating an accurate AD pathophysiological phenotype would be of considerable value to future drug development and disease modeling applications. While the availability of patient derived iPSC models of AD are available [151-153], cell line variability may inhibit the widespread applicability of conclusions drawn from specific lines. Commercially available iPSC-derived human cells offer an extremely reproducible alternative for general screening purposes. Study of A β mediated phenotypic responses in cultured wild type neurons offers a widely available platform for generalized assessment of neurodegeneration in human tissues. Therapeutic screens and/or mechanistic studies of AD progression, once tested in a generalized model, could then be advanced to specific patient iPSC lines for continued personalized evaluation. Previous studies have typically used acute, high doses of A β to model AD effects on cells *in vitro*. However, our results indicate that although such treatments induce severe pathological phenotypes rapidly in cultured human neurons, this method may not best recapitulate the AD disease state as it occurs *in vivo*.

As of the submission of this article, we are unaware of any study that has used human iPSCs to characterize the effect of pathophysiological levels of A β *in vitro*. A previous study has used human cell sources to investigate the effect of high (non-physiologic) acute doses on A β -induced cytotoxicity and cell cycle induction [154]. However, assessment of the *functional* response of these cells to physiologically representative

levels of A β over extended culture periods has not been performed. We therefore investigated treatment of hiPSC-derived neurons with low-doses of A β over extended time-courses to evaluate the ability for these cells to mimic the *in vivo* pathophysiology of early AD progression more closely.

AD patients undergo a slow neurodegenerative process which takes years to manifest in a detectable phenotype [155]. In the early-stages of AD pathology, patients exhibit synaptic dysfunction, amyloid beta accumulation in the brain but low concentrations of A β_{1-42} in the cerebral spinal fluid (CSF), a high tau/p-tau ratio in the CSF, and beginning stages of cortical/hippocampal diminishment [156, 157]. This alteration in functional performance precedes significant cell death, which usually only occurs in later stages of AD progression. Acute high doses of A β *in vitro* therefore jump straight to late-stage AD modeling and do little to accurately recapitulate the slow progressive nature of the condition. A model system that more closely mimics the mild cognitive impairment stage of the disease would therefore be more suitable for studies into early AD pathophysiology. Furthermore, such a system would be beneficial for screening compounds for their capacity to prevent disease progression before late-stage cell death occurs.

Our results more closely mirror the *in vivo* effects of A β in human neural tissue at early stages of AD progression. The collected data highlight that chronic treatment of A β at a physiologic dose results in impaired neuronal firing capacities without significant cell death. Acute, high dose A β treatment also produced a reduction in spontaneous activity, but this was coupled with a significant reduction in cell viability, indicating a more rapid

progress toward cell death than is typically seen in AD patients. No significant differences were seen in AP amplitudes when under current clamp, indicating treated cells were capable of firing APs as healthy control cells but only when membrane potentials were artificially maintained. AP waveforms were unaltered by chronic or acute 10 nM treatment, but AP rise time and FWHM were significantly increased when acutely treated with a high dose of A β . These results are supported by previous studies which demonstrate how different A β doses result in significant and conflicting electrophysiological responses in cultured rodent neurons [158, 159]. Furthermore, changes in AP rise time and FWHM in acute high dose A β treated cells indicates a change in sodium conductance and rectifying potassium channel activity in this condition [102]. Such drastic functional changes are poorly representative of AD phenotypes. A recent *in vivo* study examining cortical and thalamic electrophysiology in a rat model of AD demonstrated that the disease state produced a significant reduction in neural activity without alterations in AP waveform metrics [160]. Our presented data correlate with the findings of this study, and support the hypothesis that chronic low dose A β treatment produces functional phenotypes in cultured human neurons that more closely recapitulate AD pathology. Furthermore, these findings confirm that acute high dose A β treatment induces functional phenotypic changes in cultured neurons that are not observed in *in vivo* models of AD.

While we cannot entirely rule out that the functional deficits seen in chronically-treated A β cultures were due to the prepared low-weight oligomers and not aggregated forms derived from the added peptide, it is highly unlikely since such higher-weight oligomers,

if formed, would cause the observed effects as aggregated forms of A β have not been shown to be neurotoxic [123-129]. Furthermore, regular medium changes would reduce the presence of any aggregated species and maintain a consistent physiological level of A β .

Tau is a major structural protein in neurons responsible for stabilizing axonal microtubules, and has been shown to be constitutively expressed in iCell neurons specifically [149]. Neurodegenerative tauopathies, concomitant with AD, include a reduced association of tau with microtubules, the accumulation of intracellular bundles of highly insoluble, straight or paired helical tau filaments, and the hyperphosphorylation of tau and the subsequent formation of neurofibrillary tangles (NFTs) [150]. Moreover, in stages leading up to (and during) the appearance of NFTs, neurotoxic tau oligomers are present and have been shown to contribute to neurodegeneration in drosophila and transgenic mice models of AD [28-31]. As such, the increased presence of tau aggregates in cells is an established hall mark of neuronal degeneration in AD and associated tauopathies.

In this study, immunocytochemical analysis of tau protein in cultured cells showed a significant increase in tau positivity in response to acute high doses of A β . Conversely, neither acute, nor chronic 10 nM A β treatments produced significant increases of tau protein positivity. This result was expected as A β -mediated impairment of electrophysiological function is known to precede accumulation of tau in the brain during early AD progression. These data provide further evidence to support the hypothesis that chronic low-dose A β is more appropriate for modeling early AD stages *in vitro*.

Previous studies have demonstrated that increased presence of A β does not upregulate tau gene expression, but rather promotes the formation of larger tau aggregates through hyperphosphorylation of specific sites. Given this, the observed increase in tau staining positivity detected in these experiments is believed to result from increased aggregation of the protein within cultured cells, thereby increasing the detection of the positive fluorescence signal above background levels.

Taken together these results suggest that acute, non-physiological doses of A β poorly represent early AD phenotype, in terms of modeling electrophysiological function, cell death, and tau aggregation. Chronic, physiological levels of A β more accurately recreate the mild functional impairment of neurons during initial neurodegenerative stages of AD. The stability of these commercial hiPSC-derived neurons over extended time courses, and the more accurate representation of disease phenotype, demonstrate the utility of the described system for modeling early AD progression *in vitro*. As such, this system is highly amenable to studies designed to further our understanding of AD progression and provide a valuable potential tool for therapeutic drug screening.

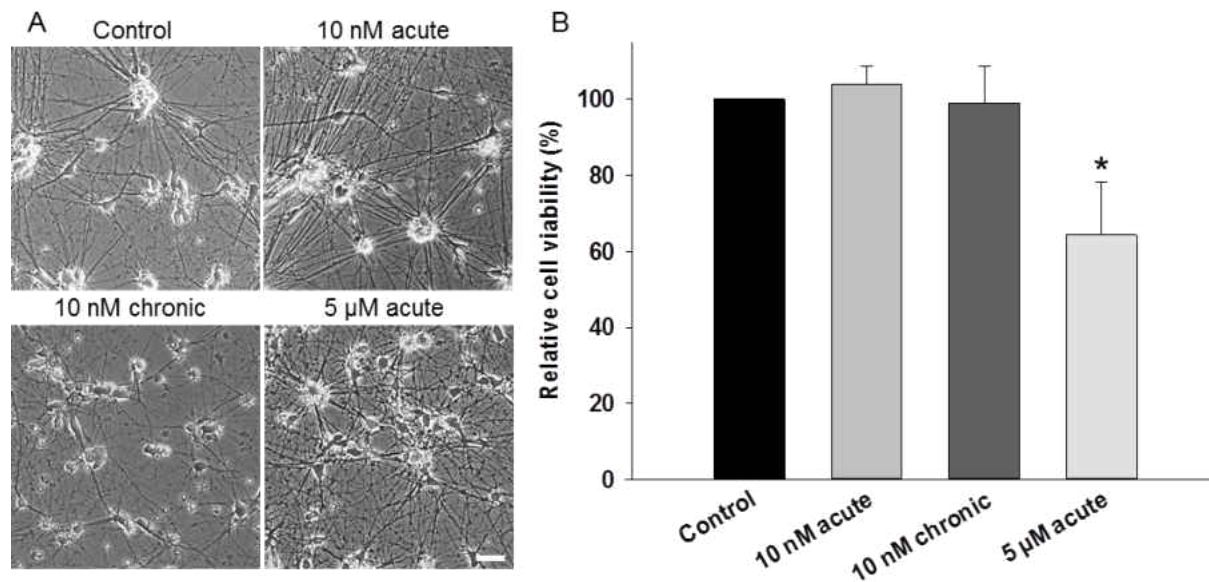


Figure 4-1. Treatment of hiPSC derived neurons with physiological doses of A β does not appear to effect gross cell morphology or viability. A) Representative phase contrast images of hiPSC-derived neurons comparing untreated, chronic, and acute A β treated cells at 30 DIV. Scale = 50 μ m. B) Viability of hiPSC-derived neurons determined by MTT assay at 30 DIV following treatment with A β . Acute 5 μ M treatment significantly reduced cell viability ($P < 0.05$) whereas acute and chronic 10 nM treatments had no significant effect on cell survival.

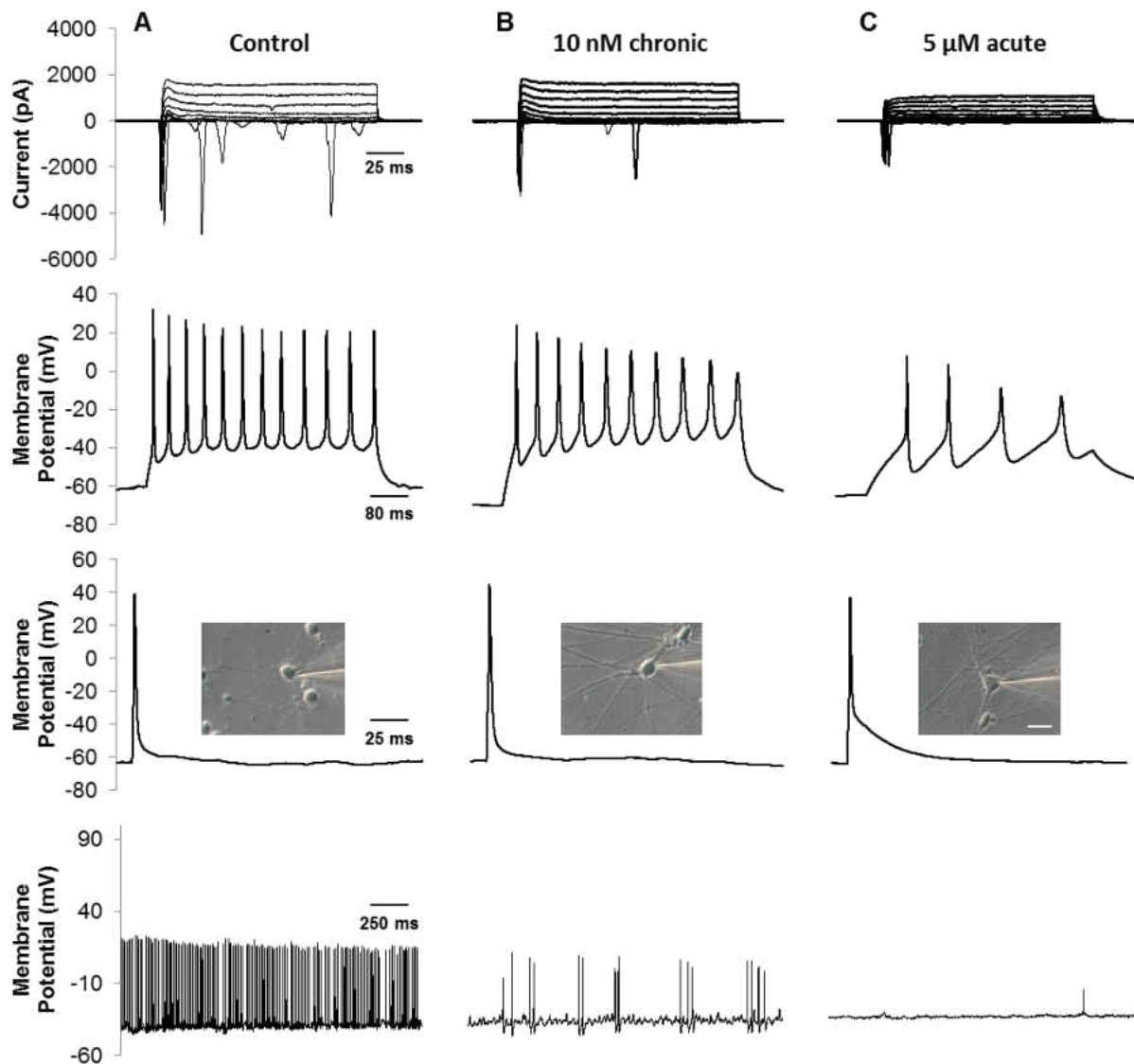


Figure 4-2. Representative electrophysiological recordings of untreated and A β -treated hiPSC-derived neurons. Patch-clamp recordings were taken between 28-30 DIV in control (column A), 10 nM chronic (column B), and 5 μ M acute (column C). Recordings from cells acutely treated with 10 nM A β were also taken but are represented by control data here as there were no significant differences between the two conditions ($p > 0.05$). (Top row) Voltage-clamp recording of inward sodium and outward potassium currents (-70 mV holding potential, 10 mV steps). (Second row) Neurons fired repeatedly in response to depolarizing current injections at a -70 mV holding potential. (Third row) A single AP was generated using a 3 ms depolarizing current pulse of 1-2 nA. (Bottom row) Gap free recordings were performed for up to 5 m to measure spontaneous activity of patched cells. (Inset) Phase contrast image of patched neuron. Scale = 20 μ M.

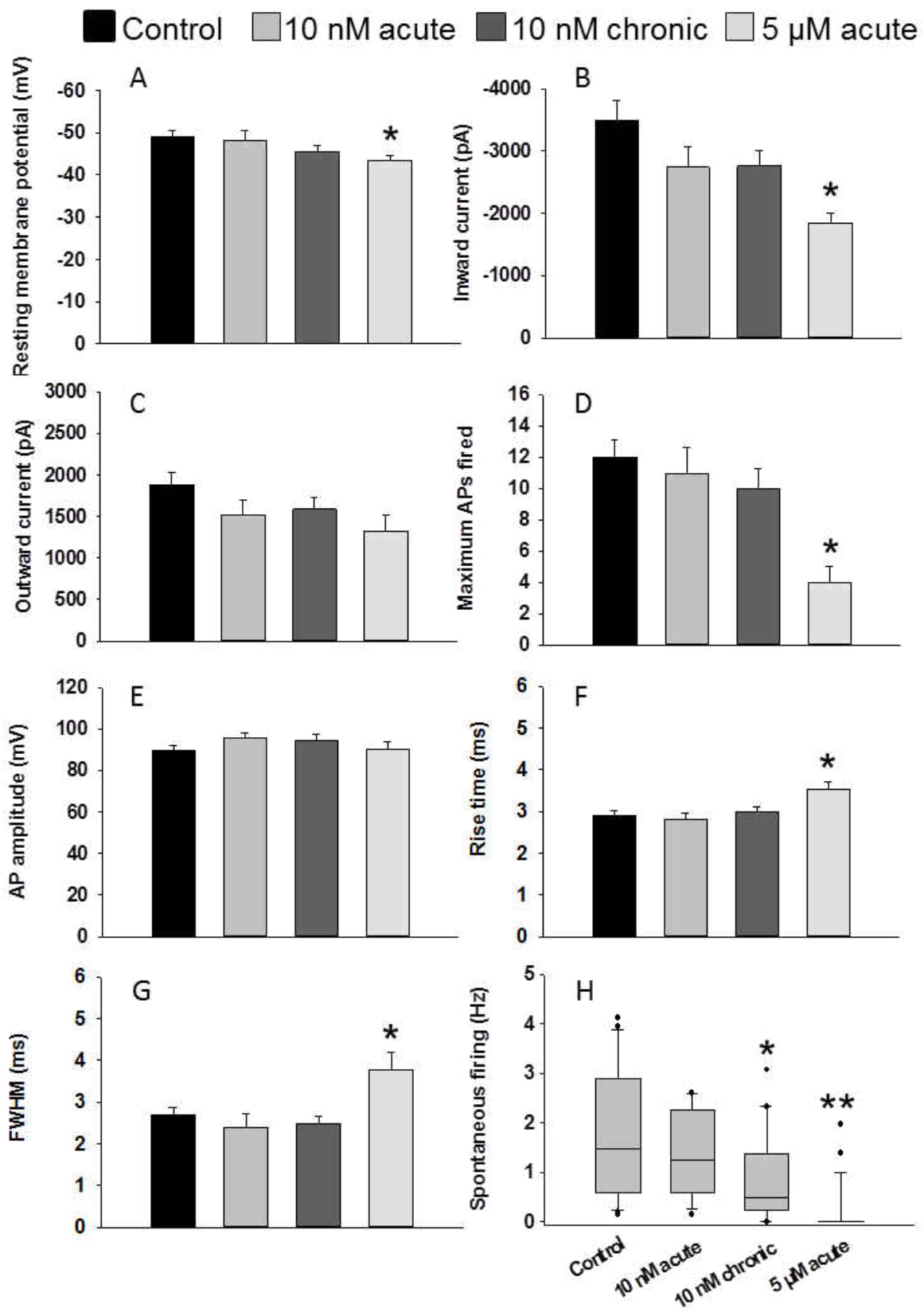


Figure 4-3. Changes in electrophysiological characteristics of hiPSC-derived neurons treated with A β . The resting membrane potential (A), peak inward current (B), peak outward current (C), maximum APs fired in response to depolarizing current injections at -70 mV (D), and peak action AP (E) are represented at 28 DIV. Whereas the resting membrane potential, membrane resistance, peak outward current, and AP amplitude was maintained across all conditions, inward sodium currents and maximum APs fired were significantly reduced in acute, 5 μ M treated cultures ($p < 0.05$). Treatment with 5 μ M of A β resulted in an even more significant drop in spontaneous neural firing activity ($p < 0.01$). Time to peak AP and AP duration, and represented by rise time (F) and FWHM (G) respectively was significantly increased in 5 μ M treatment of A β ($p < 0.05$). 10 nM A β acute treatment did not have a significant effect on spontaneous APs fired during gap-free recordings (H) but chronic 10 nM A β resulted in a significant drop in the spontaneous activity of these cultures ($p < 0.05$). Error bars represent SEM.

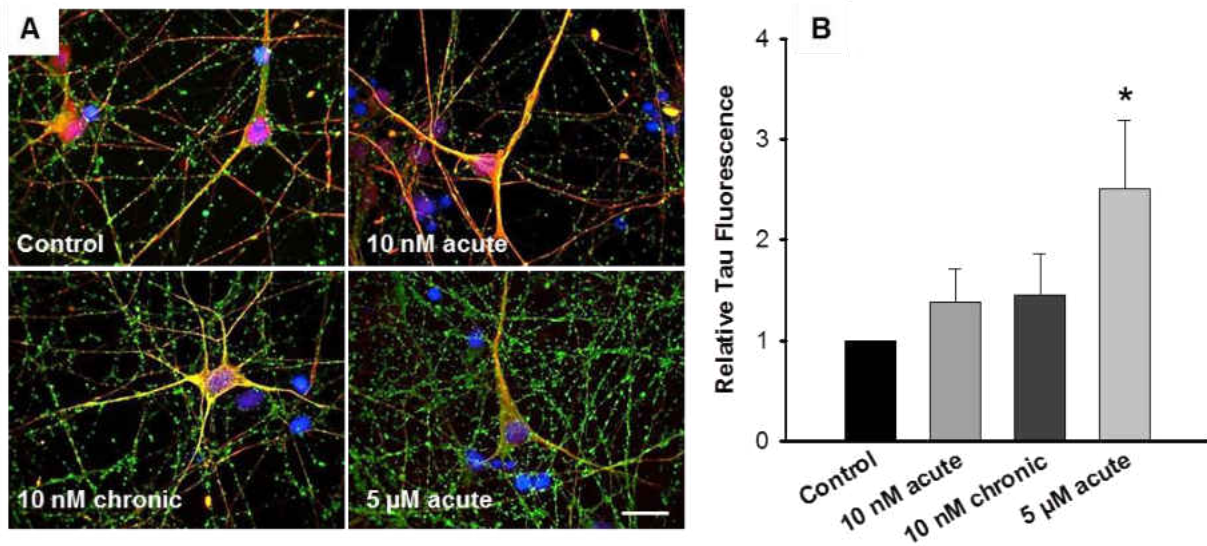
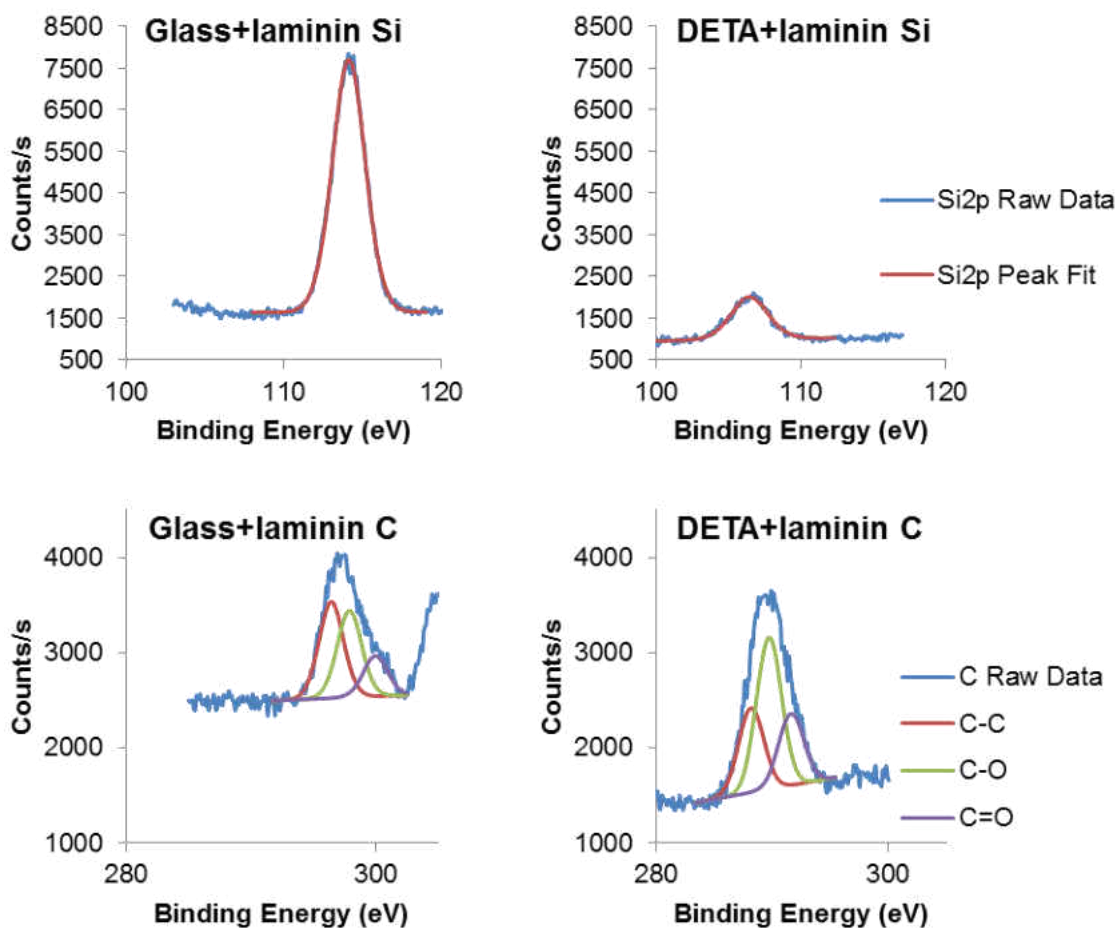


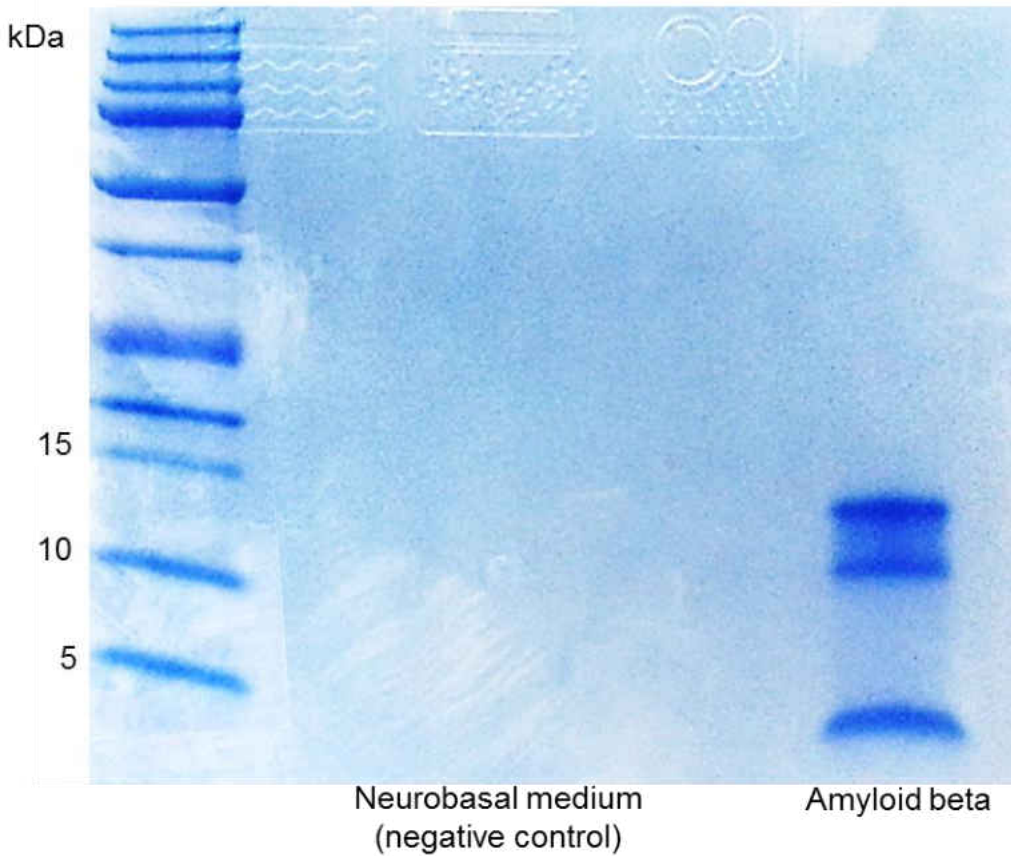
Figure 4-4. Tau protein is upregulated in hiPSC-derived neurons treated with higher-than-physiologic concentrations of A β . (A) Cells were fixed at culture endpoints (28-30 DIV) and stained for beta-III tubulin (red), tau (green), and DAPI (blue). Scale bar = 20 μ m. (B) Image analysis of tau protein intensity was analyzed relative to control tau positive staining while accounting for differences in cell viability ($p = 0.057$).

Table 4-1. HSL1 medium, detailed below, was designed to promote the long-term survival and maturation of hippocampal neurons *in vitro*.

| <i>Vendor</i> | <i>Component</i> | <i>Catalog #</i> | <i>Quantity</i> |
|-------------------|-----------------------------|------------------|-----------------|
| Invitrogen | Neurobasal®-A | 10888 | 500 mL |
| Invitrogen | B-27® | 17504-044 | 1x |
| Invitrogen | GlutaMAX™ | 35050-061 | 1x |
| Invitrogen | Antibiotic/Antimycotic | 15240-096 | 1% |
| Cell Sciences | BDNF, recombinant human | CRB600B | 20 ng/mL |
| Cell Sciences | NT-3, recombinant human | CRN500B | 20 ng/mL |
| Sigma | Insulin-like Growth Factor | I2656 | 20 ng/mL |
| Fisher Scientific | Adjust osmolarity with NaCl | S671-3 | 297 mOsm final |



Supplemental Figure 4-5. XPS analysis of laminin on glass vs. laminin on DETA. XPS analysis of laminin on DETA-modified glass and unmodified glass. The carbonyl peak, which is indicative of protein for these samples, is smaller on glass than on DETA-modified glass relative to the underlying substrate (Si).



Supplemental Figure 4-6. Amyloid beta oligomerization gel electrophoresis and coomassie blue stain. Pure oligomerized samples of A β were run on 10-20% tris-tricine gels and stained to visualize protein bands. Only low molecular weight bands were present.

CHAPTER 5 – FEED-FORWARD NETWORK PATTERNING OF HUMAN IPSC-DERIVED NEURONS; TOWARDS THE DEVELOPMENT OF A LAYERED MODEL OF THE HUMAN CORTEX

Introduction

Translation of drug effects from animal trials to clinical research is often poor, with clinical trials failing in humans after promising results are obtained in animal models [161]. Inaccurate predictions of therapeutic effects in humans during current animal-based drug testing necessitates the development of robust, human-based *in vitro* test beds to improve pre-clinical predictive power. To this end, we are working to model the central nervous system's *in vivo* structure by recapitulating a layered neuronal network using chemical surface patterns to control cell adhesion.

Dynamic changes in synaptic strength are continuously occurring *in vivo* with neurodegeneration occurring when this process breaks down. Cultures maintained on patterned substrates were stimulated using defined electrical protocols in order to induce changes in synaptic strength and thereby produce *in vitro* analogues of phenomena such as long-term potentiation (LTP). Inhibition of LTP is an indicator of serious neurodegenerative diseases, such as Alzheimer's. Current *in vitro* models of LTP are limited to slice cultures from animal tissue sources. This study focuses on the development of a human system whereby LTP can be induced, maintained and altered, with and without drug treatment, as an indicator of network health and viability.

The ability to generate accurate models of ordered mammalian neural tissue has remained limited due to the inherent complexity of the native tissue. To date, ordered

models of the mammalian cortex are few in number, and their capacity to recapitulate the native layered structure is extremely limited. Several groups have demonstrated that ordered neural networks could be established at the single cell level using patterned silane surfaces to control cell adhesion and neuritic development [57, 83, 162]. However, these studies used rodent cells and relied on patch-clamp electrophysiology for functional assessment, limiting their utility for human-based, high throughput applications.

More recently, Tang-Schomer *et al.* generated a 3D neuronal rat model which utilized a layered silk protein-based porous scaffold and gel matrix to recapitulate components of *in vivo* structure and function [163]. However, the presented model was not amenable to high-throughput drug testing or assessment of network circuitry, since functional analysis again relied on patch-clamp electrophysiology.

In 2013, Odawara and colleagues demonstrated an ability to generate a 3-layer neuronal culture system with extensive neuritic growth between the separated cell populations [28]. Using this system, the authors demonstrated that cells grown within gravity oriented collagen matrices generated field potential burst firing behavior that was detectable using a mixture of MEA and calcium imaging analysis. The system was validated as a means to perform drug analysis through assessment of responses to the GABA inhibitor bicuculline and AMPA/kainite receptor antagonist CNQX. Despite this positive data, the model was predominantly validated using rodent cells and only a preliminary assessment of cell survival was performed with human cell types. Moreover, although capable of promoting anisotropic neuritic development, the presented model

was not capable of controlling the direction of this outgrowth (i.e. neurites extended in both directions along a single axis). As such, the ability of this platform to emulate the controlled “feed-forward” networks observed in the hippocampus (dentate gyrus to CA3 to CA1) was limited.

Truly predictive preclinical neuropharmacological studies require long-term, high-throughput investigation in real time, but such analysis is nearly impossible with traditional electrophysiological recording tools. Patch clamp electrophysiology is invasive, usually limited to single cell measurements, and constrained to short-term experiments. Experiments conducted using patch-clamp electrophysiology also requires multiple experimental repeats as coverslips patched are removed from sterile culture environments. Slice cultures are also for short-term use only and cannot be used for long-term, chronic study which is required for measuring network activity and slice culture acquisition required termination perform electrophysiological studies because they can be used to non-invasively detect network-wide synaptic activity and neural connectivity of populations long-term. MEAs are also highly accessible to manipulation, both electrically and environmentally, with the addition of drugs into the media where effects can be measured across entire networks. Use of MEAs comprised of optically transparent materials allows for the application of various imaging techniques. Therefore, MEAs present an excellent tool for building a platform to measure long-term network activity and synaptic architecture *in vitro* including the acquisition of synaptic activity and neural connectivity of individual or populations of neurons in dissociated or patterned cultures.

Chemical patterning of cytophilic and cytophobic SAMs facilitated the establishment of patterned surfaces for the control of cell attachment and neuritic outgrowth [63, 83, 85]. Using this technology, surfaces were patterned to produce neural populations arranged into layers feeding forward to subsequent layers, thereby mimicking the cellular architecture of the *in vivo* tissue. Microelectrode arrays were used to monitor these layered networks for evidence of network connectivity over time. Previous work has characterized the initial establishment of this system, and validated the methodology employed to achieve a functional *in vitro* analogue of the layered neural networks observed in the *in vivo* central nervous system using rat cells [97]. Following the characterization of an appropriate human-based cell source on a controlled, self-assembled monolayer (SAM) surface that can be used to pattern culture substrates (Chapter 2), we aim to reproduce the patterned architecture and take the system a step further by using it to study network responses in reaction to both electrical and chemical stimuli. With the development of an *in vitro* system which can predict clinical drug effects, we hope to improve future medical research and drug development.

Materials and Methods

Human iPSC culture

Human iPSC-derived neurons were obtained from Cellular Dynamics International (iCell Neurons, NRC-100-010-001) and plated according to manufacturer's instructions. Cells were plated in maintenance medium (NRM-100-121-001 with NRM-100-031-001) and incubated overnight at 37°C 5% CO₂ before medium was changed to Hybrid Systems Laboratory Medium 1 (HSL1) and half the medium was changed every 3-5 days.

Astrocyte cultures

Commerically available, human astrocytes were obtained from Lonza (Normal Human Astrocytes, CC-2565) and cultured according to manufacturer's instructions. Astrocytes were also derived from rat pups using a protocol adapted from a previously described method [164]. Briefly, cerebral hemispheres were removed and rinsed with ice-cold Hibernate E (Gibco, A12476-01) Harvested cortex was then cut into smaller sections with scalpels and then transferred to Hibernate E without Ca²⁺ (BrainBits, HE-CA) with papain (2 mg/ml) and incubated at 35°C for 10 minutes with shaking. Cells were rinsed with fresh Hibernate E and mechanically dissociated using a fire-polished Pasteur pipette before plating in culture-ready flasks. Medium was changed after 2 DIV and every other day thereafter. After 7-9 DIV, medium was changed, flasks were closed, and then placed on a rotary shaker at 200 rpm with a 1.5-in. stroke diameter at 37°C for 6 h. Culture medium was discarded and then shaken for another 18 h. After 18 h, medium was changed again and flasks were again shaken until fewer than 10 phase-

dark cells per 100x field of view were observed. This method will remove oligodendrocytes and microglia and leave a nearly pure bed of astrocytes adhered to the surface of the culture flask. Purified astrocytes were dislodged from the culture flasks by incubating at 37°C with trypsin (0.05% trypsin/ EDTA in HBSS, Gibco, 25200). Trypsin inhibitor (trypsin inhibitor, soybean, Gibco, 17075-029) was added at 0.5 mg/ml to deactivate the trypsin once cells were lifting off the substrate. Suspended cells were collected and spun at 500 x g for 5 min and then resuspended in fresh culture medium for plating. Astrocytes were co-cultured with hiPSCs at a ratio of approximately 117 neurons per astrocyte as described previously [165].

Surface preparation

Microelectrode arrays were plasma cleaned for 10 minutes to avoid damage produced during an acid wash. The method used for surface modification was similar to those described previously [166, 167]. Briefly, cleaned glass slips and MEAs were immersed in a 0.1% (v/v) DETA in HPLC-graded or distilled toluene solvent, heated to just below boiling for 30 minutes, and then allowed to cool to room temperature. The surfaces were rinsed in fresh toluene, heated for 30 min as before, and oven dried for 2 hrs to overnight. Patterning was produced via photolithography by exposing the previously prepared DETA monolayer to 45 seconds of ArF laser irradiation (deep UV 193 nm excimer laser from Lambda Physik at a pulse power of 230 mW and a frequency of 10 Hz) through a quartz mask (Bandwidth foundry, Eveleigh, Australia). The ablated region was backfilled with 0.1% tridecafluoro-1,1,2,2-tetrahydrooctyl-1-trichlorosilane (13F) in a

chloroform solution for 5 min, then rinsed in chloroform, and finally oven dried for 15 min.

For quality control, chemically altered surfaces were measured using a Thermo ESCALAB 220i-XL X-Ray photoelectron spectroscopy instrument (XPS) equipped with an aluminum anode and a quartz monochromator. Surface charge compensation was achieved using a low-energy electron flood gun when necessary. Survey and high-resolution scans were recorded for relevant elements on surfaces including Si 2p, C 1s, N 1s, and O 1s (pass energy of 50 eV, step size = 1 eV). The spectrometer was calibrated against the reference binding energies of clean Cu, Ag and Au samples. Peak fitting was performed with Avantage version 3.25 software, provided by Thermo Electron Corporation. In addition, the binding energy (BE) scale was adjusted such that the aliphatic C1s peak appears at 285eV. For surface hydrophobicity/hydrophilicity characterization, a droplet of deionized water (5 μ L) was applied to a surface at three different locations and the average contact angle was taken.

Extracellular MEA recordings

MEAs were obtained from Multichannel systems and consisted of an 8x8 grid of 30 μ m electrodes spaced 200 μ m apart. Data was acquired via the Multichannel Systems 1060B amplifier (Sampling rate, 25 kHz, Bandwidth 8 Hz to 10 kHz) with temperature control set to 37°C. Raw signals were first filtered with a 2nd order Butterworth 300 Hz high-pass filter followed by spike detection over 5 standard deviations of noise. Spontaneous neural activity was checked every other day for five minutes during each experimental session.

Electrical induction of LTP was initiated by applying tetanic stimulus using protocols adapted from Chippalone *et al.* (2008) [168] and Jimbo *et al.* (1999) [169]. Any active channels were first probed for their connectivity by applying a biphasic, rectangular pulse (25 ms at 200 mV followed by 25 ms at -200 mV). A tetanus pulse was then applied (20 bursts at 0.2 Hz each with 11 pulses at an intraburst frequency of 20 Hz) to induce LTP followed by probing as before to compare responses pre- and post- tetanus.

PDMS Microtunnels

Mixed PDMS (SYLGARD 184 silicone elastomer kit, Dow Corning) was slowly poured over a wafer with a SU-8 microtunnel mold and allowed to spread over the whole wafer. The wafer was then moved to an oven for curing (at least 2 h at 70 °C). The cured PDMS microtunnels were carefully cut from the wafer and sterilized before placement onto MEAs.

Results

The design shown in Figure 5-1, based off of previous successful rat neural network establishment [97], consists of a series of four 100 μm -thick lines that were aligned over the MEA electrode grid. These lines act as reservoirs for cellular adhesion and growth. The feed-forward pattern was designed to encourage axonal extension in one direction by utilizing a broad exit from the cell reservoirs to encourage axonal growth, thin lines (2.5 μm) of extension which inhibit cell-body adherence, and a fragmented connection (20 μm gap) leading to succeeding reservoirs which inhibit axons from extending back (feed-back) along the unidirectionally-designed track (see Figure 5-1) [170]. During initial cell culture phase (0 to \sim 4 DIV), cells which land outside the patterned reservoirs will either migrate toward the DETA patterned surface (if they are within a short radius) or, being unable to successfully adhere to the culture surface, will eventually die.

Initial pattern adherence tests were done to narrow down an optimal plating density for MEAs. Human iPSCs were plated at 500, 700, and 1000 cells/ mm^2 on glass coverslips and monitored over the first 4 DIV. Human iPSCs were able to successfully respond to the patterned chemical cues and migrate to the DETA-patterned surfaces over 4 DIV for all densities plated without overwhelming the pattern (Figure 5-2). Likewise, cells were able to successfully conform to the pattern when grown on aligned MEAs (Figure 5-3).

Following the results from this initial pattern test, hiPSCs were plated onto patterned MEAs at 500, 1000, and 2000 cells/ mm^2 to evaluate electrical function at various densities. hiPSCs cultured on both patterned and unpatterned MEAs were checked daily

for activity but either no or sporadic activity on no more than one channel at a time was detected for over 30 DIV.

According to Cellular Dynamics International (CDI), the hiPSCs consisted of a mixed population of GABAergic and glutamatergic neurons at proportions of approximately 60 % and 40 % respectively. We hypothesized that the inhibitory, GABAergic neurons may be dampening the signal of the excitatory, glutamatergic neurons. In order to increase the spontaneous activity of the hiPSCs, various combinations of neurotransmitters/blockers were added to boost electrophysiological maturation of the cultures. Previously, it has been shown that addition of 25 μM of glutamate stimulates recovery of electrical function in cultured adult rat hippocampal neurons with little toxicity [61]. In addition, augmentation of cultures with 0.08, 0.4, 2, 10, 50 μM GABAzine (Sigma, SR-95531) has been shown to increase spontaneous activity on MEAs (CDI, <http://www.cellulardynamics.com/products/neurons.html>). Cultures plated at 500, 850, or 1000 cells/ mm^2 onto MEAs (patterned and unpatterned) and were chronically grown either without any additional compounds or in medium containing 25 μM glutamate, 0.4 μM GABAzine, 25 μM glutamate and 0.4 μM GABAzine, 25 μM glutamate and 20 μM GABAzine, or 25 μM glutamate and 40 μM GABAzine. Cultures grown on MEAs without additional drugs were also acutely treated with increasing concentrations of both glutamate and GABAzine to try to induce electrical activity. No consistent, robust activity was seen on any condition tested. While almost all MEAs had no spontaneous activity, a few displayed spontaneous activity on one channel (out of 63). In order to stimulate electrical activity, these MEAs with active channels were stimulated using a tetanic

pulse. Post stimulation these channels either decreased in activity or did not change their spontaneous firing.

In order to support network formation and increase spontaneous activity of hiPSCs, astrocytes were co-cultured with hiPSCs. Unpatterned, DETA-coated MEAs were treated with laminin following positive results described in Chapter 2 of this dissertation. When co-cultured with hiPSCs, Normal Human Astrocytes (NHA) caused massive clumping of neurons resulting in peeling and eventual cell death. All of the MEAs cultured with the NHA had peeled off within three weeks with no detected electrical activity. Following the unsuccessful culture of NHA with hiPSCs, hiPSCs were co-cultured with purified glia derived from primary rat pups. Primary rat glia had previously been shown to increase the spontaneous activity of the hiPSCs utilized for this study [165]. Additionally, cells were cultured with microtunnels (Figure 5-4) as previously described [171, 172] in a collaboration with Bruce Wheeler's lab. Tunnels were placed in the center of the MEA field, essentially bisecting the electrode area in half. To induce feed-forward architecture, PDMS barriers were placed at one side of the microtunnels for ~3 DIV to allow axonal extension through the microtunnels from only one side. Upon removal, neuritic extensions were observed reaching between the previously separated cell populations. Neurons were able to successfully extend processes through these microtunnels as activity was consistently detected within the microtunnels; however, activity was never detected outside the tunnels. Test pulses (200 mV biphasic square pulse) were performed on active channels within the tunnels of each MEA but no responses were observed in adjacent channels just outside the tunnels. The same

results were observed for MEAs cultures in which no barrier was placed to block entry from one side of the microtunnels.

Discussion

The development of a system that more closely recapitulates or mimics *in vivo* neural architecture would be a useful tool for basic science research and/or high-throughput screening of therapeutic compounds. To this end, we attempted to culture hiPSCs on MEAs that were patterned in a feed-forward manner to provide a layer of control over the cultured neural networks. Results indicate these hiPSCs are able to grow robustly and respond to chemical surface patterning cues (Figures 5-2, 5-3). Previous studies utilizing patch-clamp electrophysiology have shown that these cells are electrically active and functionally mature (Chapters 2,3) [81, 173]. However, consistent, robust activity was not detected with or without patterns when plated at multiple cell densities (from 500 to 2000 cells/mm²), with glutamate addition (25 μM), by addition of various concentrations of GABAazine (0.4 to 40 μM) with or without the presence of glutamate, in response to electrical stimuli, or when co-cultured with NHA. Signals were only detected when amplified by the increased resistance of the microtunnels in the presence of supportive purified rat glia.

Signal detection on MEAs is mediated by a tight cell-electrode attachment, sufficient field potential amplitude, and electrophysiological competency of cultured cells. Consequently, an inability to detect signals suggests a failure of one of these parameters. A lack of electrophysiological competency of these hiPSCs is unlikely given the successful detection of spontaneous activity of these cells previously via patch-clamp. As such, issues with cell attachment or field potential amplitude seem more

likely. Field potential amplitude is affected by cell density and cell maturity. Again, previous patch-clamp data suggests cell maturity is not likely to be a factor in the cultured conditions. The manufacturer's suggested plating protocol for MEAs recommended significantly higher cell densities in small volumes in order to obtain robust field potential recordings. Our plating protocols were limited to lower cell densities as higher densities would overwhelm the surface pattern and result in poor pattern fidelity. However, this disparity in plating procedures may explain the lack of reliably observed activity in maintained cultures. Expanded cell density ranges were being investigated with the inclusion of microtunnels that allowed higher plating densities while still providing a feed-forward architecture.

Human iPSCs cultured on MEAs consistently appeared qualitatively poorer in cell health compared to patterned or unpatterned glass coverslip controls. As such, the MEA substrate may constitute a less amenable environment for promoting the electrophysiological development of these cells. Investigation into alternative MEA platforms may be a viable direction for future research. High-throughput platforms are available from multiple vendors, e.g. Axion Biosystems, and MED64. However, these platforms may not be amenable to photolithography patterning methods due to surface material composition or physical obstruction of the photo mask necessary for surface ablation by built-in culture wells. In these cases, micro-contact printing of laminin or other surface molecules may be utilized.

Alternatively, use of MEAs could be substituted for another method of signal detection. Detection of AP firing can be achieved via a rapid-response voltage-sensitive protein

probe such as ArcLight [174]. Optical signals can be used to non-invasively map action potential propagation in response to drug treatment or external electrical stimulation. This stimulation could come from microelectrodes or by using optogenetically engineered neurons which could be stimulated via laser pulse for point stimulation or LED arrays for multisite stimulation [175]. Directed propagation of APs across designated neuronal architecture could easily be visualized utilizing this method. In addition, optical detection has previously been used to assess LTP in hippocampal slices [176, 177], suggesting the use of this method to analyze more complex brain function *in vitro* is a viable alternative to using MEAs.

In conclusion, the development of an ordered model of the human CNS remains an exciting prospect for improving preclinical analysis methods, and a significant bioengineering challenge. The potential uses for such an *in-vitro* test bed include investigation into neurodegenerative disease, traumatic brain injury, and stroke. Movement toward using a high-throughput *in vitro* system would expand and improve drug testing and basic research capabilities by providing a viable, easily manipulatable alternative to expensive, resource intensive *in vivo* testing. Such a platform would also make drug testing and disease research easier and faster, leading to the more rapid development of drug therapies. However, our work described here and the work of others [28, 57, 83, 162, 163], highlights that further development is needed to enable the reliable generation of biomimetic high throughput neuronal cultures for such applications.

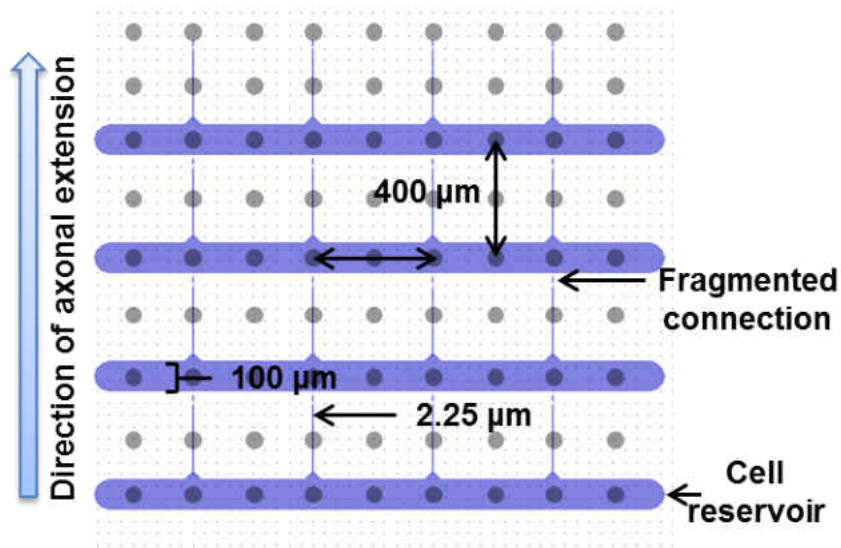


Figure 5-1. Schematic of feed-forward chemical pattern architecture for MEAs. Purple areas correspond to areas with cell-attracting chemical treatment. Small blue dotted background corresponds to chemically treated areas which are not favorable for cell growth. Grey circles indicate positions of microelectrodes (not to scale and not part of pattern). Reservoirs for cellular attachment are 100 μm tall and span the length of the entire microelectrode area. Axonal tracts (thin connecting lines, 2.5 μm wide) direct axonal growth in the indicated direction and extend to within 20 μm of the connecting reservoir where there are breaks to prevent backward axonal growth.

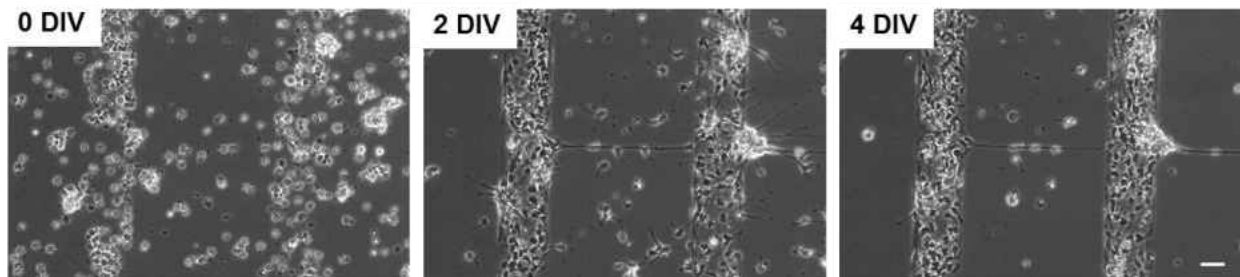


Figure 5-2. Time-lapse phase-contrast images of hiPSCs grown on DETA/13F feed-forward patterns on glass coverslips. Human iPSCs were plated at 1000 cells/ mm^2 onto patterned glass coverslips and monitored over 4 DIV for pattern adherence. Scale = 50 μm .

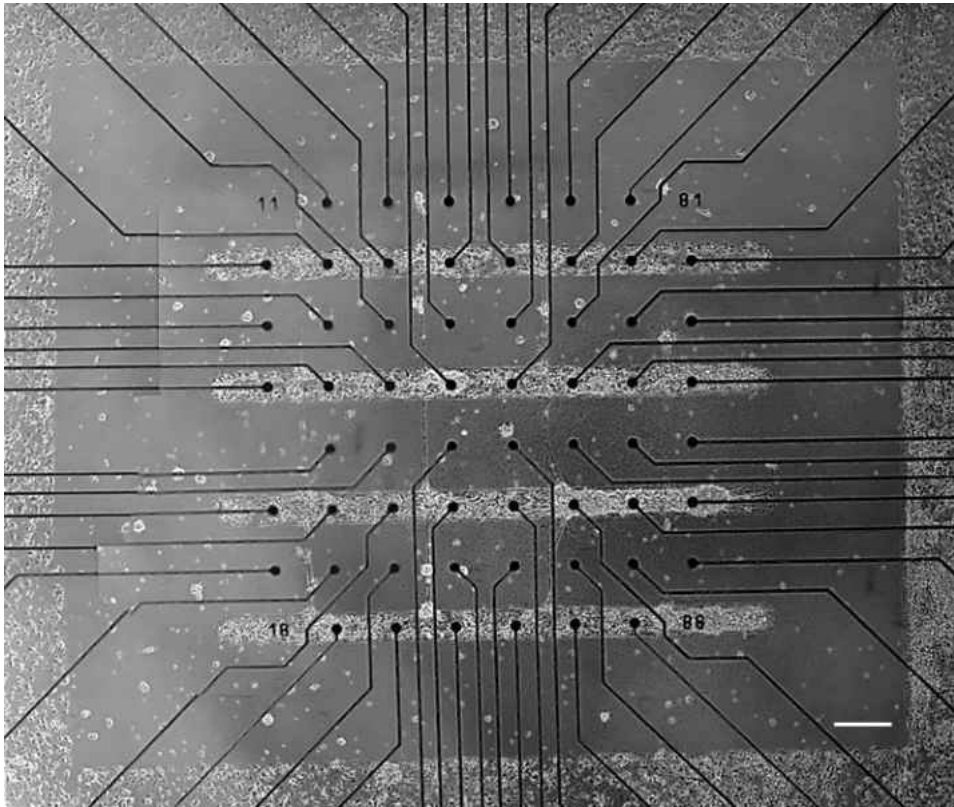


Figure 5-3. Successful patterning of hiPSCs arranged over a MEA at 7 DIV. Cells were plated onto DETA/13F feed-forward patterned MEAs where they exhibited accurate pattern conformity. Scale = 200 μm .

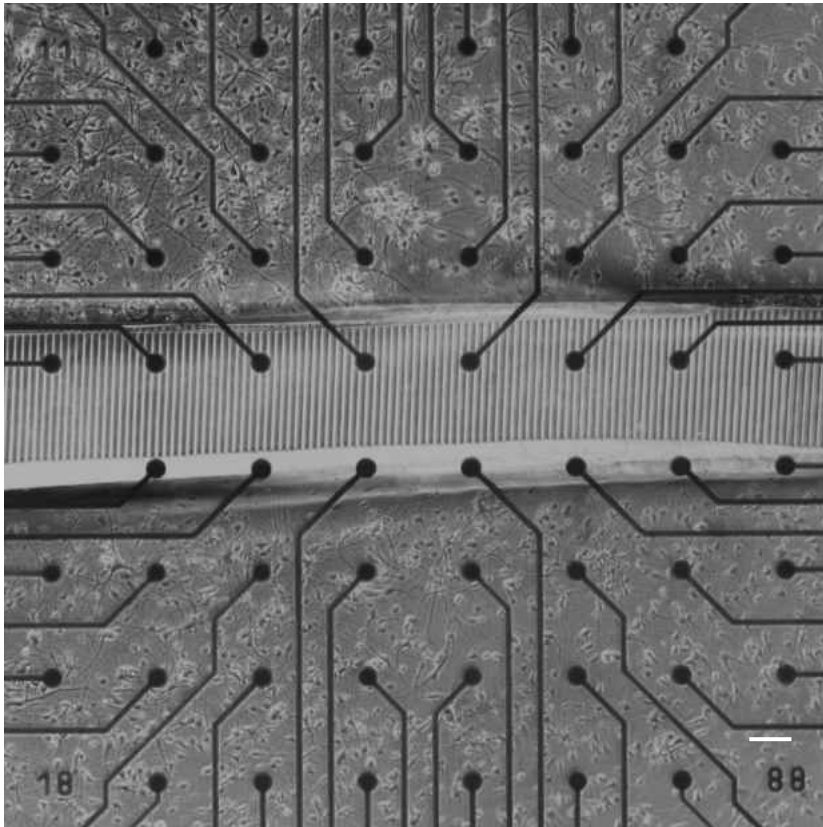


Figure 5-4. PDMS microtunnels on MEAs. Cells were plated on either side of μm by $3\ \mu\text{m}$ microtunnels that bisected the field of electrodes and created two separate culture populations. PDMS barriers (not shown) were also placed on one side of the microtunnels on for some cultures to allow one cell population to extend axons to synapse on the other side for unidirectional flow of APs from one population to the other. Scale = $100\ \mu\text{m}$.

CHAPTER 6 – GENERAL DISCUSSION

Current efforts to build more advanced, biomimetic *in vitro* test beds are limited by the availability of an appropriate cell sources, the ability to accurately recapitulate *in vivo* disease states, and the capacity to engineer microenvironments capable of supporting complex tissue architecture and interactions between cell types.

The selection of an appropriate cell source is vital to gaining accurate predictions of *in vivo* responses. Chapter 2 described significant differences between embryonic and adult rat phenotypes, highlighting the importance of achieving mature endpoints for effective drug screening and disease modeling. The reported findings are of significance given the historical importance of rodent cells for *in vitro* testing, and the continued reliance of investigators on such models for many basic science and applied applications today. Indeed, animal models continue to serve as a standard test system for pre-clinical screening of novel drug compounds. However, the generation of iPSCs offers new possibilities in human tissue modeling and holds the potential for the development of a new standard in pre-clinical drug assessment. As these human cell sources become more readily available, proper vetting across multiple research groups is required to adequately define maturation endpoints and identify suitable time-points for consistent compound evaluation. Chapter 3 highlighted the suitability of one-such commercially-available human neuronal iPSC-derived cell source. These pure populations of neuronal cells displayed typical morphology, expressed correct neuronal markers, were mitotically stable, and could robustly fire APs for over a month in culture.

These cells were also able to thrive on and respond to chemically patterned surfaces, as described in further detail in Chapter 5. Taken together, these results indicate that these commercial hiPSC-derived neurons are suitable candidates for extended *in vitro* studies, and can be applied to chemically-engineered substrates similar to those used in drug-screening platforms [78, 178]. The demonstrated long-term stability of these neuronal cultures also makes assessment of disease progression over longer periods more feasible. Chapter 4 demonstrated the capacity for these cells to be used as a model for early AD progression, whereby physiological, chronic doses of A β produced electrophysiological responses in hiPSC-derived neurons similar to those observed in the neuronal tissue of AD patients *in vivo* [155, 179]. Improvement of current preclinical screening paradigms necessitates the development of models that more closely recapitulate the physiological traits of human diseases. The ability for the developed culture protocol to more closely model AD disease progression therefore represents an important step towards the establishment of more predictive disease models, both for mechanistic studies of pathophysiology and as testbeds for the development of novel therapeutics.

The establishment of a reliable and robust human cell source, with the capacity to recapitulate mature phenotypic behavior and functional responses to A β treatment, will be of considerable value to investigators seeking to model AD progression. However, accurate predictions of neural tissue responses are predicated on the development of more complex and biomimetic neural culture platforms capable of accurately recapitulating CNS behavior. In Chapter 5 we attempted to build a layered, feed-forward

neuronal architecture over MEAs in order to establish a defined network for evaluation of drug responses and/or study of synaptic mechanisms. Human iPSC-derived neurons were able to adhere to and follow chemically patterned cues with high fidelity. However, due to challenges in obtaining spontaneous network activity of the cultured cells on MEAs, we were unable to reproduce results similar to those seen previously using embryonic rat hippocampal neurons using this method [97]. In order to improve the spontaneous activity of cultures, alterations in cell density, surface treatment, medium composition, addition of glutamate and/or GABA_A receptors, and supporting astrocytes from multiple sources were applied. Despite these extensive efforts, spontaneous activity was still rarely detected. Interestingly, when neurons were cultured on MEAs in two small wells divided by a series of microtunnels, robust activity was detected within the microtunnels but never in the wells where the cell bodies were adhered. This result verifies the functionality of the MEAs used, and indicates that analysis of neuronal activity using these cells on MEAs should be possible within a fully-optimized system. It may be that these cultures require maintenance within an enclosed platform (e.g. a microfluidic model) to prevent dissipation of field potential signals and enhanced data capture from underlying electrodes. The integration of an enclosed culture model with MEAs is therefore a viable option for future platform development. Such a model would be in keeping with current efforts towards the development of organ-on-a-chip systems and eventual establishment of multi-organ body-on-a-chip platforms for systemic toxicity screening [8, 77].

In conclusion, the major findings of this thesis are:

1. Embryonic rat neurons take 3-4 weeks in culture to develop a mature profile of AMPA and NMDA ion channel subunits. Therefore, this model system is inappropriate for studying neurodegenerative diseases until the underdeveloped neurons have fully matured in culture.
2. Adult rat neurons have a more advanced ion channel expression profile than embryonic-sourced tissue corresponding with the synaptic machinery implicated in neurodegenerative disease. Adult cultures may therefore serve as a better-suited model for studying complex, advanced-age diseases than embryonic rat cultures.
3. Commercially-sourced human iPSC-derived neurons possess similar characteristics to their *in vivo* counterparts as they display typical neuronal morphology, remain mitotically stable and differentiated for extended periods, express deep-layer marker CTIP2, and are capable of robust electrical function including repetitively firing action potentials. Moreover, their ability to respond to chemical cues makes them an ideal candidate for *in vitro* modeling of complex neural architecture for body-on-a-chip applications.
4. Early AD progression can be modeled *in vitro* using chronic, low-dose treatments of A β , which more closely mimics the *in vivo* effects of A β in human neural tissue at primary stages of AD. Chronic treatment of A β at a physiologic dose results in impaired neuronal firing capacities without significant cell death, as seen *in vivo*.
5. Acute, high dose A β treatment produces a reduction in spontaneous activity, but this is coupled with a significant reduction in cell viability, indicating a more rapid progress

toward cell death than is typically seen in AD patients. Acute, high-dose A β treatments are therefore an inappropriate model of AD.

6. While we were unable to fully-validate the proposed ordered CNS model, despite extensive optimization experiments, the collection of robust firing activity within microtunnels supports the development of spontaneous network activity within these patterned cultures. As such, the proposed platform remains a viable strategy for continued development towards the establishment of a biomimetic model of the human cortex.

Successful development of complex *in vitro* models of the human CNS, employing cell culture protocols developed during this thesis could enable more accurate and predictive drug screening and disease modeling to improve patient well-being and recovery. In order to carry this work forward, future studies should focus on integration of these functional human neurons with bioengineered platforms capable of recreating human neural architectures *in vitro*. In doing so, investigators will improve the biological relevance of these culture systems and enhance their capacity to predict human neural responses to drug treatment or pathological challenge. In addition, the capacity to assess neuronal performance *in situ* will facilitate real-time analysis of cellular development and maturation within these models. Such functionality will greatly improve the overall utility of these models as they will enable continuous assessment of cellular function and maturation rather than the limited perspective obtained via end-point analysis.

Once such integrated platforms are established, continued drive towards more biomimetic tissue culture models for improved *in vitro* modeling should include the integration of supporting cell types, such as astroglia, microglia, and oligodendrocytes, in biologically representative ratios. Recent efforts with co-culture systems [180, 181] indicate that successful maintenance of multiple related cell types is feasible and such complexity is necessary to accurately model human neural tissue *in vitro*.

Finally, the integration of a biomimetic CNS model with other organ-on-a-chip platforms would be advantageous towards the establishment of complex, microfluidic body-on-a-chip systems. Although no-one has yet published more than 4 interconnected organ microenvironments [181], the development of models recapitulating complete human systems is an exciting possibility for future preclinical studies and a current focus of academic, government, and pharmaceutical entities. To that end, investigators seeking to drive the work in this thesis towards body-on-a-chip relevance must consider that inclusion of a suitable blood-brain-barrier (BBB) model is essential if one wishes to accurately model drug, distribution, absorption, and toxicity in neural tissue [182]. As such, the development of a CNS-BBB co-culture system would be a sensible first step towards a more complex multi-organ platform.

As stated previously, neurological disorders are gaining increasing prevalence in developed countries. The need for improved, human models of neural tissue for accurate and effective disease modeling and drug screening has therefore never been greater. The work in this thesis encompasses important steps towards improving cell culture paradigms for more effectively identifying and testing drug targets for new

potential therapeutics. Continued progress in this direction, utilizing the data presented herein, will help improve the translation of benchtop results to bedside treatment, and ultimately improve patient care, wellbeing, and recovery.

REFERENCES

- [1] SSD W, Design LK. The 2012 Statistical Abstract-US Census Bureau. 2011.
- [2] Hebert LE, Scherr PA, Bienias JL, Bennett DA, Evans DA. Alzheimer disease in the us population: Prevalence estimates using the 2000 census. *Arch Neurol.* 2003;60:1119-22.
- [3] Mangialasche F, Solomon A, Winblad B, Mecocci P, Kivipelto M. Alzheimer's disease: clinical trials and drug development. *The Lancet Neurology.* 2010;9:702-16.
- [4] DiMasi JA, Grabowski HG. The cost of biopharmaceutical R&D: is biotech different? *Managerial and Decision Economics.* 2007;28:469-79.
- [5] DiMasi JA, Hansen RW, Grabowski HG. The price of innovation: new estimates of drug development costs. *Journal of Health Economics.* 2003;22:151-85.
- [6] Vernon JA, Golec JH, Dimasi JA. Drug development costs when financial risk is measured using the Fama-French three-factor model. *Health economics.* 2010;19:1002-5.
- [7] Sullivan F. Early Screening, Innovative Solutions to Underline Importance of ADME/Tox Technologies in Successful Drug Development. In: Sullivan F, editor. Considerable Time, Cost Savings to Accrue from Advanced ADME/Tox Technologies 2005.
- [8] Esch MB, Smith A, Prot J-M, Sancho CO, Hickman J, Shuler ML. How Multi-Organ Microdevices Can Help Foster Drug Development. *Advanced drug delivery reviews.* 2014;0:158-69.

- [9] Kola I, Landis J. Can the pharmaceutical industry reduce attrition rates? *Nat Rev Drug Discov.* 2004;3:711-6.
- [10] McGonigle P, Ruggeri B. Animal models of human disease: challenges in enabling translation. *Biochemical pharmacology.* 2014;87:162-71.
- [11] Seok J, Warren HS, Cuenca AG, Mindrinos MN, Baker HV, Xu W, et al. Genomic responses in mouse models poorly mimic human inflammatory diseases. *Proceedings of the National Academy of Sciences.* 2013;110:3507-12.
- [12] Chang R, Liu X, Li S, Li X-J. Transgenic animal models for study of the pathogenesis of Huntington's disease and therapy. *Drug design, development and therapy.* 2015;9:2179.
- [13] Andersen P. Amyotrophic lateral sclerosis associated with mutations in the CuZn superoxide dismutase gene. *Curr Neurol Neurosci Rep.* 2006;6:37-46.
- [14] Rosen DR, Siddique T, Patterson D, Figlewicz DA, Sapp P, Hentati A, et al. Mutations in Cu/Zn superoxide dismutase gene are associated with familial amyotrophic lateral sclerosis. *Nature.* 1993;362:59-62.
- [15] Julien J-P, Kriz J. Transgenic mouse models of amyotrophic lateral sclerosis. *Biochimica et Biophysica Acta (BBA) - Molecular Basis of Disease.* 2006;1762:1013-24.
- [16] Benatar M. Lost in translation: treatment trials in the SOD1 mouse and in human ALS. *Neurobiol Dis.* 2007;26:1-13.
- [17] Zhang D, Luo G, Ding X, Lu C. Preclinical experimental models of drug metabolism and disposition in drug discovery and development. *Acta Pharmaceutica Sinica B.* 2012;2:549-61.

- [18] Wan W, Cao L, Kalionis B, Xia S, Tai X. Applications of Induced Pluripotent Stem Cells in Studying the Neurodegenerative Diseases. *Stem cells international*. 2015;2015:382530.
- [19] Takahashi K, Tanabe K, Ohnuki M, Narita M, Ichisaka T, Tomoda K, et al. Induction of pluripotent stem cells from adult human fibroblasts by defined factors. *Cell*. 2007;131:861-72.
- [20] Cai J, Li W, Su H, Qin D, Yang J, Zhu F, et al. Generation of human induced pluripotent stem cells from umbilical cord matrix and amniotic membrane mesenchymal cells. *J Biol Chem*. 2010;285:11227-34.
- [21] Loh YH, Agarwal S, Park IH, Urbach A, Huo H, Heffner GC, et al. Generation of induced pluripotent stem cells from human blood. *Blood*. 2009;113:5476-9.
- [22] Xue Y, Cai X, Wang L, Liao B, Zhang H, Shan Y, et al. Generating a non-integrating human induced pluripotent stem cell bank from urine-derived cells. *PLoS One*. 2013;8:e70573.
- [23] Zhou T, Benda C, Dunzinger S, Huang Y, Ho JC, Yang J, et al. Generation of human induced pluripotent stem cells from urine samples. *Nat Protoc*. 2012;7:2080-9.
- [24] Malik N, Rao M. A Review of the Methods for Human iPSC Derivation. In: Lakshmiathy U, Vemuri MC, editors. *Pluripotent Stem Cells*: Humana Press; 2013. p. 23-33.
- [25] Jang J, Yoo JE, Lee JA, Lee DR, Kim JY, Huh YJ, et al. Disease-specific induced pluripotent stem cells: a platform for human disease modeling and drug discovery. *Experimental & molecular medicine*. 2012;44:202-13.

- [26] Luo Y, Fan Y, Chen X, Yue L, Yu B, Li Q, et al. Modeling induced pluripotent stem cells from fibroblasts of Duchenne muscular dystrophy patients. *The International journal of neuroscience*. 2014;124:12-21.
- [27] Rajamohan D, Matsa E, Kalra S, Crutchley J, Patel A, George V, et al. Current status of drug screening and disease modelling in human pluripotent stem cells. *Bioessays*. 2013;35:281-98.
- [28] Odawara A, Gotoh M, Suzuki I. A three-dimensional neuronal culture technique that controls the direction of neurite elongation and the position of soma to mimic the layered structure of the brain. *RSC Advances*. 2013;3:23620-30.
- [29] Dennis RG, Dow DE. Excitability of skeletal muscle during development, denervation, and tissue culture. *Tissue engineering*. 2007;13:2395-404.
- [30] Yang X, Pabon L, Murry CE. Engineering Adolescence: Maturation of Human Pluripotent Stem Cell-Derived Cardiomyocytes. *Circulation Research*. 2014;114:511-23.
- [31] Juhas M, Engelmayer GC, Fontanella AN, Palmer GM, Bursac N. Biomimetic engineered muscle with capacity for vascular integration and functional maturation in vivo. *Proceedings of the National Academy of Sciences*. 2014;111:5508-13.
- [32] Holt GR, Softky WR, Koch C, Douglas RJ. Comparison of discharge variability in vitro and in vivo in cat visual cortex neurons. *J Neurophysiol*. 1996;75:1806-14.
- [33] Williams CS, Watson AJM, Sheng H, Helou R, Shao J, DuBois RN. Celecoxib Prevents Tumor Growth in Vivo without Toxicity to Normal Gut: Lack of Correlation between in Vitro and in Vivo Models. *Cancer Research*. 2000;60:6045-51.

- [34] Varghese K, Molnar P, Das M, Bhargava N, Lambert S, Kindy M, et al. A new standard for amyloid Beta toxicity validated by standard and high-throughput electrophysiology. *PLoS one*. 2010;5:8643.
- [35] Chang JC, Brewer GJ, Wheeler BC. Modulation of neural network activity by patterning. *Biosens Bioelectron*. 2001;16:527-33.
- [36] Golan H, Mikenberg K, Greenberger V, Segal M. GABA withdrawal modifies network activity in cultured hippocampal neurons. *Neural Plasticity*. 2000;7:31-42.
- [37] Stead J, Neal C, Meng F, Wang Y, Evans S, Vazquez D, et al. Transcriptional Profiling of the developing rat brain reveals that the most dramatic regional differentiation in gene expression occurs postpartum. *Journal of Neuroscience*. 2006;26:345-53.
- [38] Kamphuis W, Dijk F, O'Brien B. Gene expression of AMPA-type glutamate receptor subunits in rod-type ON bipolar cells of rat retina. *European Journal of Neuroscience*. 2003;18:1085-92.
- [39] Monyer H, Burnashev N, Laurie D, Sakmann B, Seeburg P. Developmental and regional expression in the rat brain and functional properties of four NMDA receptors. *Neuron*. 1994;12:529-40.
- [40] Brewer L, Thibault O, Stanton J, Thibault V, Rogers J, Garci-Ramos G, et al. Increased vulnerability of hippocampal neurons with age in culture: Temporal association with increases in NMDA receptor current, NR2A subunit expression and recruitment of L-type calcium channels. *Brain Research*. 2007;1151:20-31.
- [41] Safronov BV, Wolff M, Vogel W. Axonal expression of sodium channels in rat spinal neurons during postnatal development. *Journal of Physiology*. 1999;524:729-34.

- [42] Beckh S, Noda M, Lubbert H, Numa S. Differential regulation of three sodium channel messenger RNAs in the rat central nervous system during development. *The EMBO Journal*. 1989;8:3611-6.
- [43] Abe K. Neural activity-dependent regulation of gene expression in developing and mature neurons. *Dev Growth Differ*. 2008;50:261-71.
- [44] Cheng B, Furukawa K, O'Keefe JA, Goodman Y, Kihiko M, Fabian T, et al. Basic fibroblast growth factor selectively increases AMPA-receptor subunit GluR1 protein level and differentially modulates Ca²⁺ responses to AMPA and NMDA in hippocampal neurons. *J Neurochem*. 1995;65:2525-36.
- [45] Mattson MP, Kumar KN, Wang H, Cheng B, Michaelis EK. Basic FGF regulates the expression of a functional 71 kDa NMDA receptor protein that mediates calcium influx and neurotoxicity in hippocampal neurons. *J Neurosci*. 1993;13:4575-88.
- [46] Gonzalez-Sulser A, Wang J, Motamedi GK, Avoli M, Vicini S, Dzakpasu R. The 4-aminopyridine *in vitro* epilepsy model analyzed with a perforated multi-electrode array. *Neuropharmacology*. 2011;60:1142-53.
- [47] Wagenaar DA, Madhavan R, Pine J, Potter SM. Controlling bursting in cortical cultures with closed-loop multi-electrode stimulation. *The Journal of Neuroscience*. 2005;25:680-8.
- [48] Edwards D, Das M, Molnar P, Hickman JJ. Addition of glutamate to serum-free culture promotes recovery of electrical activity in adult hippocampal neurons *in vitro*. *Journal of Neuroscience Methods*. 2010;190:155-63.
- [49] Edwards D, Stancescu M, Lambert S, Hickman J. Derivation of a population of stable electrically active neurons from the adult rat brain through manipulation of cdk5 activity. *Journal of Neuroscience*. 2011.

- [50] Lambert M, Barlow A, Chromy B, Edwards C, Freed R. Diffusible, nonfibrillar ligands derived from A beta (1-42) are potent central nervous system neurotoxins. *Proceedings of the National Academy of Sciences of the United States of America*. 1998;95:6448-53.
- [51] Gureviciene I, Ikonen S, Gurevicius K, Sarkaki A, van Groen T. Normal induction but accelerated decay of LTP in APP+PS1 transgenic mice. *Neurobiology of Disease*. 2004;15:188-95.
- [52] Gross G, Rhoades B, Azzazy H, Wu M. The use of neuronal networks on multielectrode arrays as biosensors. *Biosensors and Bioelectronics*. 1995;10:553-67.
- [53] Chiappalone M, Vato A, Tedesco M, Marcoli M, Davide F, Martinoia S. Networks of neurons coupled to microelectrode arrays: a neuronal sensory system for pharmacological applications. *Biosensors and Bioelectronics*. 2003;18:627-34.
- [54] Keefer E, Gramowski A, Stenger D, Pancrazio J, Gross G. Characterization of acute neurotoxic effects of trimethylpropane via neuronal network biosensors. *Biosensors and Bioelectronics*. 2001;16.
- [55] Hofmann F, Bading H. Long-term recordings with microelectrode arrays: Studies of transcription-dependent neuronal plasticity and axonal regeneration. *Journal of Physiology-Paris*. 2006;99:125-32.
- [56] Gross G, Gramowski A, Schiffmann D. Neural network cultures on multielectrode chips: Self-organization of electrically active networks and their uses in neurotoxicology and neuropharmacology. *European Journal of Cell Biology*. 1997;74:36.
- [57] Edwards D, Stancescu M, Molnar P, Hickman J. Two cell networks of adult hippocampal neurons on self-assembled monolayers for the study of neuronal communication *in vitro*. *Biomaterials*. 2011.

- [58] Marom S, Shahaf G. Development, learning and memory in large random networks of cortical neurons: lessons beyond anatomy. *Quarterly Reviews of Biophysics*. 2002;35:63-87.
- [59] Brewer GJ, Torricelli JR, Evege EK, Price PJ. Optimized survival of hippocampal neurons in B27-supplemented Neurobasal, a new serum-free medium combination. *J Neurosci Res*. 1993;35:567-76.
- [60] Schaffner AE, Barker JL, Stenger DA, Hickman JJ. Investigation of the factors necessary for growth of hippocampal neurons in a defined system. *Journal of Neuroscience Methods*. 1995;62:111-9.
- [61] Edwards D, Das M, Molnar P, Hickman JJ. Addition of glutamate to serum-free culture promotes recovery of electrical activity in adult hippocampal neurons in vitro. *Journal of Neuroscience Methods*. 2010;190:155-63.
- [62] Das M, Bhargava N, Gregory C, Riedel L, Molnar P, Hickman JJ. Adult rat spinal cord culture on an organosilane surface in a novel serum-free medium. *In Vitro Cell Dev Biol Anim*. 2005;41:343-8.
- [63] Ravenscroft M, Bateman K, Shaffer K, Schessler H, Jung DR, Schneider TW, et al. Developmental neurobiology implications from fabrication and analysis of hippocampal neuronal networks on patterned silane- modified surfaces. *Journal of American Chemical Society*. 1998;120:12169-77.
- [64] Kamioka H, Maeda E, Jimbo Y, Robinson HP, Kawana A. Spontaneous periodic synchronized bursting during formation of mature patterns of connections in cortical cultures. *Neurosci Lett*. 1996;206:109-12.
- [65] Opitz T, De Lima AD, Voigt T. Spontaneous Development of Synchronous Oscillatory Activity During Maturation of Cortical Networks In Vitro 2002.

- [66] Abrous DN, Koehl M, Le Moal M. Adult Neurogenesis: From Precursors to Network and Physiology. *Physiol Rev.* 2005;85:523-69.
- [67] Liu X, Murray K, Jones E. Switching of NMDA receptor 2A and 2B subunits at thalamic and cortical synapses during early postnatal development. *Journal of Neuroscience.* 2004;24:8885-95.
- [68] Alberdi E, Sánchez-Gómez MV, Cavaliere F, Pérez-Samartín A, Zugaza JL, Trullas R, et al. Amyloid β oligomers induce Ca²⁺ dysregulation and neuronal death through activation of ionotropic glutamate receptors. *Cell calcium.* 2010;47:264-72.
- [69] Texidó L, Martín-Satué M, Alberdi E, Solsona C, Matute C. Amyloid β peptide oligomers directly activate NMDA receptors. *Cell calcium.* 2011;49:184-90.
- [70] Liu J, Chang L, Roselli F, Almeida OF, Gao X, Wang X, et al. Amyloid- β induces caspase-dependent loss of PSD-95 and synaptophysin through NMDA receptors. *Journal of Alzheimer's Disease.* 2010;22:541-56.
- [71] Li S, Jin M, Koeglsperger T, Shepardson NE, Shankar GM, Selkoe DJ. Soluble A β oligomers inhibit long-term potentiation through a mechanism involving excessive activation of extrasynaptic NR2B-containing NMDA receptors. *The Journal of Neuroscience.* 2011;31:6627-38.
- [72] Mucke L, Selkoe DJ. Neurotoxicity of Amyloid β -Protein: Synaptic and Network Dysfunction. *Cold Spring Harbor Perspectives in Medicine.* 2012;2.
- [73] Tang Y-P, Shimizu E, Dube GR, Rampon C, Kerchner GA, Zhuo M, et al. Genetic enhancement of learning and memory in mice. *Nature.* 1999;401:63-9.

- [74] Liu L, Wong TP, Pozza MF, Lingenhoehl K, Wang Y, Sheng M, et al. Role of NMDA Receptor Subtypes in Governing the Direction of Hippocampal Synaptic Plasticity. *Science*. 2004;304:1021-4.
- [75] Isaac JTR, Ashby MC, McBain CJ. The Role of the GluR2 Subunit in AMPA Receptor Function and Synaptic Plasticity. *Neuron*. 2007;54:859-71.
- [76] Kim C-H, Chung HJ, Lee H-K, Huganir RL. Interaction of the AMPA receptor subunit GluR2/3 with PDZ domains regulates hippocampal long-term depression. *Proceedings of the National Academy of Sciences*. 2001;98:11725-30.
- [77] Sung JH, Esch MB, Prot J-M, Long CJ, Smith A, Hickman JJ, et al. Microfabricated mammalian organ systems and their integration into models of whole animals and humans. *Lab on a Chip*. 2013;13:1201-12.
- [78] Smith AS, Long CJ, Berry BJ, McAleer C, Stancescu M, Molnar P, et al. Microphysiological systems and low-cost microfluidic platform with analytics. *Stem cell research & therapy*. 2013;4 Suppl 1:S9.
- [79] Huh D, Torisawa Y-s, Hamilton GA, Kim HJ, Ingber DE. Microengineered physiological biomimicry: Organs-on-Chips. *Lab on a Chip*. 2012;12:2156-64.
- [80] Ghaemmaghami AM, Hancock MJ, Harrington H, Kaji H, Khademhosseini A. Biomimetic tissues on a chip for drug discovery. *Drug Discovery Today*. 2012;17:173-81.
- [81] Haythornthwaite A, Stoelzle S, Hasler A, Kiss A, Mosbacher J, George M, et al. Characterizing Human Ion Channels in Induced Pluripotent Stem Cell-Derived Neurons. *Journal of Biomolecular Screening*. 2012;17:1264-72.

[82] Wilson K, Stancescu M, Das M, Rumsey J, Hickman J. Direct patterning of coplanar polyethylene glycol alkylsilane monolayers by deep-ultraviolet photolithography as a general method for high fidelity, long-term cell patterning and culture. *Journal of Vacuum Science & Technology B*. 2011;29:-.

[83] Edwards D, Stancescu M, Molnar P, Hickman JJ. Two Cell Circuits of Oriented Adult Hippocampal Neurons on Self-Assembled Monolayers for Use in the Study of Neuronal Communication in a Defined System. *ACS Chemical Neuroscience*. 2013;4:1174-82.

[84] Schaffner AE, Barker JL, Stenger DA, Hickman JJ. Investigation of the factors necessary for growth of hippocampal neurons in a defined system. *Journal of Neuroscience Methods*. 1995;62:111-9.

[85] Hickman JJ, Bhatia SK, Quong JN, Shoen P, Stenger DA, Pike CJ, et al. Rational pattern design for in vitro cellular networks using surface photochemistry. *Journal of Vacuum Science & Technology A: Vacuum, Surfaces, and Films*. 1994;12:607-16.

[86] El-Ali J, Sorger PK, Jensen KF. Cells on chips. *Nature*. 2006;442:403-11.

[87] Stenger DA, Hickman JJ, Bateman KE, Ravenscroft MS, Ma W, Pancrazio JJ, et al. Microlithographic determination of axonal/dendritic polarity in cultured hippocampal neurons. *Journal of Neuroscience Methods*. 1998;82:167-73.

[88] Ravenscroft MS, Bateman KE, Shaffer KM, Schessler HM, Jung DR, Schneider TW, et al. Developmental neurobiology implications from fabrication and analysis of hippocampal neuronal networks on patterned silane-modified surfaces. *Journal of the American Chemical Society*. 1998;120:12169-77.

- [89] Liu Q-Y, Coulombe M, Dumm J, Shaffer KM, Schaffner AE, Barker JL, et al. Synaptic connectivity in hippocampal neuronal networks cultured on micropatterned surfaces. *Developmental Brain Research*. 2000;120:223-31.
- [90] Abe K, Chida N, Nishiyama N, Saito H. Spermine promotes the survival of primary cultured brain neurons. *Brain Research*. 1993;605:322-6.
- [91] Kaeberlein M. Spermidine surprise for a long life. *Nat Cell Biol*. 2009;11:1277-8.
- [92] Eisenberg T, Knauer H, Schauer A, Buttner S, Ruckenstuhl C, Carmona-Gutierrez D, et al. Induction of autophagy by spermidine promotes longevity. *Nat Cell Biol*. 2009;11:1305-14.
- [93] Zhou FM, Hablitz JJ. Layer I neurons of rat neocortex. I. Action potential and repetitive firing properties. *Journal of Neurophysiology*. 1996;76:651-67.
- [94] Das M, Molnar P, Devaraj H, Poeta M, Hickman JJ. Electrophysiological and morphological characterization of rat embryonic motoneurons in a defined system. *Biotechnology Progress*. 2003;19:1756-61.
- [95] Luckenbill-Edds L. Laminin and the mechanism of neuronal outgrowth. *Brain Research Reviews*. 1997;23:1-27.
- [96] Powell SK, Kleinman HK. Neuronal laminins and their cellular receptors. *The International Journal of Biochemistry & Cell Biology*. 1997;29:401-14.
- [97] Natarajan A, DeMarse TB, Molnar P, Hickman JJ. Engineered In Vitro Feed-Forward Networks. *Journal of Biotechnology & Biomaterials*. 2013;3.

- [98] Brewer GJ, Boehler MD, Leondopoulos S, Pan L, Alagapan S, DeMarse T, et al. Toward a self-wired active reconstruction of the hippocampal trisynaptic loop: DG-CA3. *Frontiers in Neural Circuits*. 2013;7.
- [99] Liu Z, Ren G, Zhang T, Yang Z. Action potential changes associated with the inhibitory effects on voltage-gated sodium current of hippocampal CA1 neurons by silver nanoparticles. *Toxicology*. 2009;264:179-84.
- [100] Altemus K, Lavenex P, Ishizuka N, Amaral D. Morphological characteristics and electrophysiological properties of CA1 pyramidal neurons in macaque monkeys. *Neuroscience*. 2005;136:741-56.
- [101] Bilkey DK, Schwartzkroin PA. Variation in electrophysiology and morphology of hippocampal CA3 pyramidal cells. *Brain Research*. 1990;514:77-83.
- [102] Picken Bahrey HL, Moody WJ. Early Development of Voltage-Gated Ion Currents and Firing Properties in Neurons of the Mouse Cerebral Cortex 2003.
- [103] Shruti S, Clem RL, Barth AL. A seizure-induced gain-of-function in BK channels is associated with elevated firing activity in neocortical pyramidal neurons. *Neurobiology of Disease*. 2008;30:323-30.
- [104] Castro PA, Pleasure SJ, Baraban SC. Hippocampal heterotopia with molecular and electrophysiological properties of neocortical neurons. *Neuroscience*. 2002;114:961-72.
- [105] Tang-Schomer MD, Davies P, Graziano D, Thurber AE, Kaplan DL. Neural circuits with long-distance axon tracts for determining functional connectivity. *Journal of Neuroscience Methods*.

- [106] Feldman DH, Thinschmidt JS, Peel AL, Papke RL, Reier PJ. Differentiation of Ionic Currents in CNS Progenitor Cells: Dependence upon Substrate Attachment and Epidermal Growth Factor. *Experimental Neurology*. 1996;140:206-17.
- [107] Ding Q, Vaynman S, Akhavan M, Ying Z, Gomez-Pinilla F. Insulin-like growth factor I interfaces with brain-derived neurotrophic factor-mediated synaptic plasticity to modulate aspects of exercise-induced cognitive function. *Neuroscience*. 2006;140:823-33.
- [108] Clark P. Cell behaviour on micropatterned surfaces. *Biosensors and Bioelectronics*. 1994;9:657-61.
- [109] Clark P, Britland S, Connolly P. Growth cone guidance and neuron morphology on micropatterned laminin surfaces. *Journal of Cell Science*. 1993;105:203-12.
- [110] Merkle FT, Alvarez-Buylla A. Neural stem cells in mammalian development. *Current Opinion in Cell Biology*. 2006;18:704-9.
- [111] Deisseroth K, Singla S, Toda H, Monje M, Palmer TD, Malenka RC. Excitation-Neurogenesis Coupling in Adult Neural Stem/Progenitor Cells. *Neuron*. 2004;42:535-52.
- [112] Lochter A, Schachner M. Tenascin and extracellular matrix glycoproteins: from promotion to polarization of neurite growth in vitro. *The Journal of Neuroscience*. 1993;13:3986-4000.
- [113] Leng J, Jiang L, Chen H, Zhang X. Brain-derived neurotrophic factor and electrophysiological properties of voltage-gated ion channels during neuronal stem cell development. *Brain Research*. 2009;1272:14-24.

- [114] Cohen AS, Coussens CM, Raymond CR, Abraham WC. Long-Lasting Increase in Cellular Excitability Associated With the Priming of LTP Induction in Rat Hippocampus. *Journal of Neurophysiology*. 1999;82:3139-48.
- [115] Lein PJ, Banker GA, Higgins D. Laminin selectively enhances axonal growth and accelerates the development of polarity by hippocampal neurons in culture. *Developmental Brain Research*. 1992;69:191-7.
- [116] Miner JH, Cunningham J, Sanes JR. Roles for Laminin in Embryogenesis: Exencephaly, Syndactyly, and Placentopathy in Mice Lacking the Laminin $\alpha 5$ Chain. *The Journal of Cell Biology*. 1998;143:1713-23.
- [117] Liesi P, Dahl D, Vaheri A. Laminin is produced by early rat astrocytes in primary culture. *The Journal of Cell Biology*. 1983;96:920-4.
- [118] Chiu AY, Espinosa De Los Monteros A, Cole RA, Loera S, De Vellis J. Laminin and s-laminin are produced and released by astrocytes, schwann cells, and schwannomas in culture. *Glia*. 1991;4:11-24.
- [119] Cornbrooks CJ, Carey DJ, McDonald JA, Timpl R, Bunge RP. In vivo and in vitro observations on laminin production by Schwann cells. *Proceedings of the National Academy of Sciences*. 1983;80:3850-4.
- [120] Shankar GM, Li S, Mehta TH, Garcia-Munoz A, Shepardson NE, Smith I, et al. Amyloid β -Protein Dimers Isolated Directly from Alzheimer Brains Impair Synaptic Plasticity and Memory. *Nature medicine*. 2008;14:837-42.
- [121] Tu S, Okamoto S-i, Lipton SA, Xu H. Oligomeric A β -induced synaptic dysfunction in Alzheimer's disease. *Molecular Neurodegeneration*. 2014;9:48.

- [122] Giuffrida ML, Caraci F, Pignataro B, Cataldo S, De Bona P, Bruno V, et al. β -Amyloid Monomers Are Neuroprotective. *The Journal of Neuroscience*. 2009;29:10582-7.
- [123] Shankar GM, Li S, Mehta TH, Garcia-Munoz A, Shepardson NE, Smith I, et al. Amyloid- β protein dimers isolated directly from Alzheimer's brains impair synaptic plasticity and memory. *Nat Med*. 2008;14:837-42.
- [124] McGowan E, Pickford F, Kim J, Onstead L, Eriksen J, Yu C, et al. A β 42 Is Essential for Parenchymal and Vascular Amyloid Deposition in Mice. *Neuron*. 2005;47:191-9.
- [125] Caughey B, Peter T, Lansbury J. PROTOFIBRILS, PORES, FIBRILS, AND NEURODEGENERATION: Separating the Responsible Protein Aggregates from The Innocent Bystanders. *Annual Review of Neuroscience*. 2003;26:267-98.
- [126] Glabe CG. Common mechanisms of amyloid oligomer pathogenesis in degenerative disease. *Neurobiology of Aging*. 2006;27:570-5.
- [127] Dahlgren KN, Manelli AM, Stine WB, Baker LK, Krafft GA, LaDu MJ. Oligomeric and Fibrillar Species of Amyloid- β Peptides Differentially Affect Neuronal Viability. *Journal of Biological Chemistry*. 2002;277:32046-53.
- [128] Gong Y, Chang L, Viola KL, Lacor PN, Lambert MP, Finch CE, et al. Alzheimer's disease-affected brain: Presence of oligomeric A β ligands (ADDLs) suggests a molecular basis for reversible memory loss. *Proceedings of the National Academy of Sciences*. 2003;100:10417-22.
- [129] Klyubin I, Betts V, Welzel AT, Blennow K, Zetterberg H, Wallin A, et al. Amyloid β Protein Dimer-Containing Human CSF Disrupts Synaptic Plasticity: Prevention by Systemic Passive Immunization. *The Journal of Neuroscience*. 2008;28:4231-7.

[130] Resende R, Ferreira E, Pereira C, Resende de Oliveira C. Neurotoxic effect of oligomeric and fibrillar species of amyloid-beta peptide 1-42: Involvement of endoplasmic reticulum calcium release in oligomer-induced cell death. *Neuroscience*. 2008;155:725-37.

[131] Hsiao K, Chapman P, Nilsen S, Eckman C, Harigaya Y, Younkin S, et al. Correlative memory deficits, A β elevation, and amyloid plaques in transgenic mice. *Science*. 1996;274:99-103.

[132] Mayeux R, Tang M-X, Jacobs DM, Manly J, Bell K, Merchant C, et al. Plasma amyloid β -peptide 1-42 and incipient Alzheimer's disease. *Annals of Neurology*. 1999;46:412-6.

[133] Lambert MP, Barlow AK, Chromy BA, Edwards C, Freed R, Liosatos M, et al. Diffusible, nonfibrillar ligands derived from A β 1-42 are potent central nervous system neurotoxins. *Proceedings of the National Academy of Sciences*. 1998;95:6448-53.

[134] Selkoe DJ. Soluble oligomers of the amyloid β -protein impair synaptic plasticity and behavior. *Behavioural Brain Research*. 2008;192:106-13.

[135] Choi YJ, Chae S, Kim JH, Barald KF, Park JY, Lee S-H. Neurotoxic amyloid beta oligomeric assemblies recreated in microfluidic platform with interstitial level of slow flow. *Sci Rep*. 2013;3.

[136] Izzo NJ, Staniszewski A, To L, Fa M, Teich AF, Saeed F, et al. Alzheimer's Therapeutics Targeting Amyloid Beta 1-42 Oligomers I: Abeta 42 Oligomer Binding to Specific Neuronal Receptors Is Displaced by Drug Candidates That Improve Cognitive Deficits. *PLoS ONE*. 2014;9:e111898.

- [137] Deshpande A, Mina E, Glabe C, Busciglio J. Different Conformations of Amyloid β Induce Neurotoxicity by Distinct Mechanisms in Human Cortical Neurons. *The Journal of Neuroscience*. 2006;26:6011-8.
- [138] Carriba P, Jimenez S, Navarro V, Moreno-Gonzalez I, Barneda-Zahonero B, Moubarak RS, et al. Amyloid- β reduces the expression of neuronal FAIM-L, thereby shifting the inflammatory response mediated by TNF α from neuronal protection to death. *Cell Death Dis*. 2015;6:e1639.
- [139] Minter MR, Main BS, Brody KM, Zhang M, Taylor JM, Crack PJ. Soluble amyloid triggers a myeloid differentiation factor 88 and interferon regulatory factor 7 dependent neuronal type-1 interferon response in vitro. *Journal of neuroinflammation*. 2015;12:71.
- [140] Sheikh AM, Michikawa M, Kim SU, Nagai A. Lysophosphatidylcholine increases the neurotoxicity of Alzheimer's amyloid β 1-42 peptide: Role of oligomer formation. *Neuroscience*. 2015;292:159-69.
- [141] Chinestra P, Diabira D, Urban NN, Barrionuevo G, Ben-Ari Y. Major differences between long-term potentiation and ACPD-induced slow onset potentiation in hippocampus. *Neuroscience Letters*. 1994;182:177-80.
- [142] Bortolotto ZA, Collingridge GL. On the mechanism of long-term potentiation induced by (1S,3R)-1-aminocyclopentane-1,3-dicarboxylic acid (ACPD) in rat hippocampal slices. *Neuropharmacology*. 1995;34:1003-14.
- [143] Cirrito JR, May PC, O'Dell MA, Taylor JW, Parsadanian M, Cramer JW, et al. In vivo assessment of brain interstitial fluid with microdialysis reveals plaque-associated changes in amyloid-beta metabolism and half-life. *The Journal of neuroscience : the official journal of the Society for Neuroscience*. 2003;23:8844-53.

- [144] Riedel G, Reymann KG. Metabotropic glutamate receptors in hippocampal long-term potentiation and learning and memory. *Acta Physiologica Scandinavica*. 1996;157:1-19.
- [145] McGuinness N, Anwyl R, Rowan M. The effects of trans-ACPD on long-term potentiation in the rat hippocampal slice. *NeuroReport*. 1991;2:688-90.
- [146] Das M, Bhargava N, Gregory C, Riedel L, Molnar P, Hickman JJ. Adult rat spinal cord culture on an organosilane surface in a novel serum-free medium. *In Vitro Cellular & Developmental Biology-Animal*. 2005;41:343-8.
- [147] Klein WL. A beta toxicity in Alzheimer's disease: globular oligomers (ADDLs) as new vaccine and drug targets. *Neurochemistry International*. 2002;41:345-52.
- [148] Li T, Jiang L, Chen H, Zhang X. Characterization of Excitability and Voltage-gated Ion Channels of Neural Progenitor Cells in Rat Hippocampus. *Journal of Molecular Neuroscience*. 2008;35:289-95.
- [149] Chai X, Dage JL, Citron M. Constitutive secretion of tau protein by an unconventional mechanism. *Neurobiology of Disease*. 2012;48:356-66.
- [150] Bloom GS, Ren K, Glabe CG. Cultured cell and transgenic mouse models for tau pathology linked to β -amyloid. *Biochimica et Biophysica Acta (BBA) - Molecular Basis of Disease*. 2005;1739:116-24.
- [151] Sproul AA, Jacob S, Pre D, Kim SH, Nestor MW, Navarro-Sobrinho M, et al. Characterization and molecular profiling of PSEN1 familial Alzheimer's disease iPSC-derived neural progenitors. *PLoS ONE*. 2014;9:e84547.

- [152] Israel MA, Yuan SH, Bardy C, Reyna SM, Mu Y, Herrera C, et al. Probing sporadic and familial Alzheimer's disease using induced pluripotent stem cells. *Nature*. 2012;482:216-20.
- [153] Hossini AM, Megges M, Prigione A, Lichtner B, Toliat MR, Wruck W, et al. Induced pluripotent stem cell-derived neuronal cells from a sporadic Alzheimer's disease donor as a model for investigating AD-associated gene regulatory networks. *BMC Genomics*. 2015;16:84.
- [154] Biella G, Di Febo F, Goffredo D, Moiana A, Taglietti V, Conti L, et al. Differentiating embryonic stem-derived neural stem cells show a maturation-dependent pattern of voltage-gated sodium current expression and graded action potentials. *Neuroscience*. 2007;149:38-52.
- [155] Mufson EJ, Mahady L, Waters D, Counts SE, Perez SE, DeKosky ST, et al. Hippocampal plasticity during the progression of Alzheimer's disease. *Neuroscience*.
- [156] Sperling R, Mormino E, Johnson K. The evolution of preclinical Alzheimer's disease: Implications for prevention trials. *Neuron*. 2014;84:608-22.
- [157] Sperling RA, Aisen PS, Beckett LA, Bennett DA, Craft S, Fagan AM, et al. Toward defining the preclinical stages of Alzheimer's disease: Recommendations from the National Institute on Aging-Alzheimer's Association workgroups on diagnostic guidelines for Alzheimer's disease. *Alzheimer's & Dementia*. 2011;7:280-92.
- [158] Wang Y, Zhang G, Zhou H, Barakat A, Querfurth H. Opposite Effects of Low and High Doses of A β ₄₂ on Electrical Network and Neuronal Excitability in the Rat Prefrontal Cortex. *PLoS ONE*. 2009;4:e8366.

- [159] Varghese K, Molnar P, Das M, Bhargava N, Lambert S, Kindy MS, et al. A New Target for Amyloid Beta Toxicity Validated by Standard and High-Throughput Electrophysiology. *PLoS ONE*.5:e8643.
- [160] Sanganahalli BG, Herman P, Behar KL, Blumenfeld H, Rothman DL, Hyder F. Functional MRI and neural responses in a rat model of Alzheimer's disease. *NeuroImage*. 2013;79:404-11.
- [161] Cavanaugh SE, Pippin JJ, Barnard ND. Animal models of Alzheimer disease: historical pitfalls and a path forward. *Altx*. 2014;31:279-302.
- [162] Kwiat M, Elnathan R, Pevzner A, Peretz A, Barak B, Peretz H, et al. Highly Ordered Large-Scale Neuronal Networks of Individual Cells – Toward Single Cell to 3D Nanowire Intracellular Interfaces. *ACS Applied Materials & Interfaces*. 2012;4:3542-9.
- [163] Tang-Schomer MD, White JD, Tien LW, Schmitt LI, Valentin TM, Graziano DJ, et al. Bioengineered functional brain-like cortical tissue. *Proceedings of the National Academy of Sciences*. 2014;111:13811-6.
- [164] Cole R, de Vellis J. Preparation of astrocyte, oligodendrocyte, and microglia cultures from primary rat cerebral cultures. *Protocols for neural cell culture*: Springer; 2001. p. 117-27.
- [165] Odawara A, Saitoh Y, Alhebshi AH, Gotoh M, Suzuki I. Long-term electrophysiological activity and pharmacological response of a human induced pluripotent stem cell-derived neuron and astrocyte co-culture. *Biochem Biophys Res Commun*. 2014;443:1176-81.
- [166] Das M, Bhargava N, Gregory C, Riedel L, Molnar P, Hickman JJ. Adult rat spinal cord culture on an organosilane surface in a novel serum-free medium. *In Vitro Cellular & Developmental Biology - Animal*. 2005;41:343-8.

- [167] Das M, Wilson K, Molnar P, Hickman JJ. Differentiation of skeletal muscle and integration of myotubes with silicon microstructures using serum-free medium and a synthetic silane substrate. *Nature Protocols*. 2007;2:1795-801.
- [168] Berdondini L, Chippalone M, van der Wal PD, Imfeld K, de Rooij NF, Koudelka-Hep M, et al. A microelectrode array (MEA) integrated with clustering structures for investigating in vitro neurodynamics in confined interconnected sub-populations of neurons. *Sensors and Actuators B-Chemical*. 2006;114:530-41.
- [169] Jimbo Y, Robinson HPC, Kawana A. Strengthening of synchronized activity by tetanic stimulation in cortical cultures: Application of planar electrode arrays. *IEEE Transactions on Biomedical Engineering*. 1998;45:1297-304.
- [170] Stenger DA, Hickman JJ, Bateman KE, Ravenscroft MS, Ma W, Pancrazio JJ, et al. Microlithographic determination of axonal/dendritic polarity in cultured hippocampal neurons. *J Neurosci Methods*. 1998;82:167-73.
- [171] Dworak BJ, Wheeler BC. Novel MEA platform with PDMS microtunnels enables the detection of action potential propagation from isolated axons in culture. *Lab Chip*. 2009;9:404-10.
- [172] Liangbin P, Sankaraleengam A, Eric F, Gregory JB, Bruce CW. Propagation of action potential activity in a predefined microtunnel neural network. *Journal of Neural Engineering*. 2011;8:046031.
- [173] Xu X, Lei Y, Luo J, Wang J, Zhang S, Yang X-J, et al. Prevention of β -amyloid induced toxicity in human iPS cell-derived neurons by inhibition of Cyclin-dependent kinases and associated cell cycle events. *Stem Cell Research*. 2013;10:213-27.

- [174] Han Z, Jin L, Platasa J, Cohen LB, Baker BJ, Pieribone VA. Fluorescent Protein Voltage Probes Derived from ArcLight that Respond to Membrane Voltage Changes with Fast Kinetics. *PLoS ONE*. 2013;8:e81295.
- [175] Fenno L, Yizhar O, Deisseroth K. The Development and Application of Optogenetics. *Annual Review of Neuroscience*. 2011;34:389-412.
- [176] Momose-Sato Y, Sato K, Arai Y, Yazawa I, Mochida H, Kamino K. Evaluation of Voltage-Sensitive Dyes for Long-Term Recording of Neural Activity in the Hippocampus. *J Membrane Biol*. 1999;172:145-57.
- [177] Ohta M, Saito T, Saito K, Kurasaki M, Hosokawa T. Effect of Trichloroethylene on Spatiotemporal Pattern of LTP in Mouse Hippocampal Slices. *International Journal of Neuroscience*. 2001;111:257-71.
- [178] Park TH, Shuler ML. Integration of cell culture and microfabrication technology. *Biotechnology Progress*. 2003;19:243-53.
- [179] Selkoe DJ. Alzheimer's disease is a synaptic failure. *Science*. 2002;298:789-91.
- [180] Materne EM, Ramme AP, Terrasso AP, Serra M, Alves PM, Brito C, et al. A multi-organ chip co-culture of neurospheres and liver equivalents for long-term substance testing. *Journal of biotechnology*. 2015;205:36-46.
- [181] Maschmeyer I, Lorenz AK, Schimek K, Hasenberg T, Ramme AP, Hubner J, et al. A four-organ-chip for interconnected long-term co-culture of human intestine, liver, skin and kidney equivalents. *Lab Chip*. 2015;15:2688-99.
- [182] Tourovskaia A, Fauver M, Kramer G, Simonson S, Neumann T. Tissue-engineered microenvironment systems for modeling human vasculature. *Experimental biology and medicine (Maywood, NJ)*. 2014;239:1264-71.

